8-2016

Modeling, Control, and Impact Analysis of The Next Generation Transportation System

Feng Zhu
Purdue University

Graduate School Form
30 Updated 12/26/2015

PURDUE UNIVERSITY
GRADUATE SCHOOL
Thesis/Dissertation Acceptance

This is to certify that the thesis/dissertation prepared

By Feng Zhu

Entitled

MODELING, CONTROL, AND IMPACT ANALYSIS OF THE NEXT GENERATION TRANSPORTATION SYSTEM

For the degree of Doctor of Philosophy

Is approved by the final examining committee:

Satish V. Ukkusuri Chair	Fred Mannering
Hubo Cai	Xiaojun Lin
Andrew Liu	

To the best of my knowledge and as understood by the student in the Thesis/Dissertation Agreement, Publication Delay, and Certification Disclaimer (Graduate School Form 32), this thesis/dissertation adheres to the provisions of Purdue University's "Policy of Integrity in Research" and the use of copyright material.

Approved by Major Professor(s): Satish V. Ukkusuri

Approved by: Dulcy M. Abraham 6/15/2016

Head of the Departmental Graduate Program Date

MODELING, CONTROL, AND IMPACT ANALYSIS OF THE NEXT GENERATION TRANSPORTATION SYSTEM

A Dissertation

Submitted to the Faculty

of

Purdue University

by

Feng Zhu

In Partial Fulfillment of the

Requirements for the Degree

of

Doctor of Philosophy

August 2016

Purdue University

West Lafayette, Indiana

To my father

ACKNOWLEDGMENTS

First and foremost, I would like to give my sincere respect and greatest gratitude to my mentor, Prof. Satish V. Ukkusuri. I owe my deepest gratitude to Prof. Ukkusuri, a respectable, responsible and resourceful scholar, who has enlightened me not only in my graduate study with his experienced learning and his insightful ideas in the field of transportation, but also in my future career with his responsible attitude towards research and work. I truly appreciate his impressive patience and kindness with me. This thesis would not have been possible without his continuous guidance and support throughout my PhD study at Purdue.

Secondly, I would like to express my heartfelt gratitude to my PhD advisory committee members: Prof. Fred Mannering, Prof. Hubo Cai, Prof. Andrew Liu, and Prof. Xiaojun Lin. Their constructive and valuable comments have greatly helped to improve the quality of this dissertation.

My gratitude also goes to all the ITE members of Purdue, and the colleagues in the Interdisciplinary Transportation Modeling and Analytics Laboratory at Purdue. Especially I am obliged to Xianyuan Zhan, Xinwu Qian, Arif Sadri, Wenbo Zhang, Tho Le, and Hemant Gehlot. I enjoyed the atmosphere of the research group. Lots of my research contributions will not be possible without the exchanging of ideas, inspiring discussion, and valuable suggestions and comments from all the group members.

Finally, I would like to give my special thanks to all my family members, my father Fuchao Zhu, my mother Lingfei Zhou, my sister Ying Zhu, for their thoughtfulness and encouragement all along from the very beginning of my postgraduate study. Especially, I am so blessed to have my love Juan Du to be always on my side during the precious days at Purdue.

TABLE OF CONTENTS

Page

Page

Page

LIST OF TABLES

LIST OF FIGURES

ABSTRACT

Zhu, Feng PhD, Purdue University, August 2016. Modeling, Control, and Impact Analysis of The Next Generation Transportation System. Major Professor: Satish V. Ukkusuri.

This dissertation aims to develop a systematic tool designated for connected and autonomous vehicles, integrating the simulation of traffic dynamics, traffic control strategies, and impact analysis at the network level.

The first part of the dissertation is devoted to the traffic flow modeling of connected vehicles. This task is the foundation step for transportation planning, optimized network design, efficient traffic control strategies, etc, of the next generation transportation system. Chapter 2 proposes a cell-based simulation approach to model the proactive driving behavior of connected vehicles. Firstly, a state variable of connected vehicle is introduced to track the trajectory of connected vehicles. Then the exit flow of cells containing connected vehicles is adjusted to simulate the proactive driving behavior, such that the traffic light is green when the connected vehicle arrives at the signalized intersection. Extensive numerical simulation results consistently show that the presence of connected vehicles contributes significantly to the smoothing of traffic flow and vehicular emission reductions in the network. Chapter 3 proposes an optimal estimation approach to calibrate connected vehicles' car-following behavior in a mixed traffic environment. Particularly, the state-space system dynamics is captured by the simplified car-following model with disturbances, where the trajectory of non-connected vehicles are considered as unknown states and the trajectory of connected vehicles are considered as measurements with errors. Objective of the reformulation is to obtain an optimal estimation of states and model parameters simultaneously. It is shown that the customized state-space model is identifiable

with the mild assumption that the disturbance covariance of the state update process is diagonal. Then a modified Expectation-Maximization (EM) algorithm based on Kalman smoother is developed to solve the optimal estimation problem.

The second part of the dissertation is on traffic control strategies. This task drives the next generation transportation system to a better performance state in terms of safety, mobility, travel time saving, vehicular emission reduction, etc. Chapter 4 develops a novel reinforcement learning algorithm for the challenging coordinated signal control problem. Traffic signals are modeled as intelligent agents interacting with the stochastic traffic environment. The model is built on the framework of coordinated reinforcement learning. The Junction Tree Algorithm based reinforcement learning is proposed to obtain an exact inference of the best joint actions for all the coordinated intersections. The algorithm is implemented and tested with a network containing 18 signalized intersections from a microscopic traffic simulator. Chapter 5 develops a novel linear programming formulation for autonomous intersection control (LPAIC) accounting for traffic dynamics within a connected vehicle environment. Firstly, a lane based bi-level optimization model is introduced to propagate traffic flows in the network. Then the bi-level optimization model is transformed to the linear programming formulation by relaxing the nonlinear constraints with a set of linear inequalities. One special feature of the LPAIC formulation is that the entries of the constraint matrix has only values in {-1, 0, 1}. Moreover, it is proved that the constraint matrix is totally unimodular, the optimal solution exists and contains only integer values. Further, it shows that traffic flows from different lanes pass through the conflict points of the intersection safely and there are no holding flows in the solution. Three numerical case studies are conducted to demonstrate the properties and effectiveness of the LPAIC formulation to solve autonomous intersection control.

The third part of the dissertation moves on to the impact analysis of connected vehicles and autonomous vehicles at the network level. This task assesses the positive and negative impacts of the system and provides guidance on transportation planning, traffic control, transportation budget spending, etc. In this part, the impact of

different penetration rates of connected vehicle and autonomous vehicles is revealed on the network efficiency of a transportation system. Chapter 6 sets out to model an efficient and fair transportation system accounting for both departure time choice and route choice of a general multi OD network within a dynamic traffic assignment environment. Firstly, a bi-level optimization formulation is introduced based on the link-based traffic flow model. The upper level of the formulation minimizes the total system travel time, whereas the lower level captures traffic flow propagation and the user equilibrium constraint. Then the bi-level formulation is relaxed to a linear programming formulation that produces a lower bound of an efficient and fair system state. An efficient iterative algorithm is proposed to obtain the exact solution. It is shown that the number of iterations is bounded, and the output traffic flow solution is efficient and fair. Finally, two numerical cases (including a single OD network and a multi-OD network) are conducted to demonstrate the performance of the algorithm. The results consistently show that the travel time of different departure rates of the same OD pair are identical and the algorithm converges within two iterations across all test scenarios.

1. INTRODUCTION

Intelligent transportation systems (ITS) are embracing an unprecedented era featuring the practical application of automation and communication technologies. The conceptual application products include connected vehicles, connected corridors, autonomous vehicles (also known as self-driving vehicles or driver-less vehicles), autonomous highways, autonomous freights, autonomous parking lots, and autonomous intersection managements, etc. In this dissertation, we refer to this new era of ITS as the next generation transportation system.

1.1 Background

Inter-vehicle communications (IVC) system is the first step towards this next generation transportation system and has received tremendous interests from academics, industries, and government agencies. Connected vehicle (CV) technology grows rapidly since its inception owing to the development of wireless communication technology, especially the Dedicated Short Range Communications (DSRC) technology. DSRC has great potential in the area of ITS, as it facilitates the wireless exchange of information between vehicles (i.e., Vehicle-to-Vehicle, V2V), as well as between vehicles and roadside infrastructure (i.e., Vehicle-to-Infrastructure, V2I), as demonstrated in Figure 1.1. In Europe, IVC is known as Car to Car (C2C) and Car to X (C2X) technology. Though CV has not been implemented in the real world transportation system yet, many auto companies (e.g. Mercedes-Benz, BMW, Ford, etc.) are expending significant efforts to produce vehicles with communication features. In addition, many test beds are ongoing in US, Europe, and Japan. Furthermore, the U.S. DOT National Highway Traffic Safety Administration [1] plans to mandate IVC technology on every single vehicle by 2016.

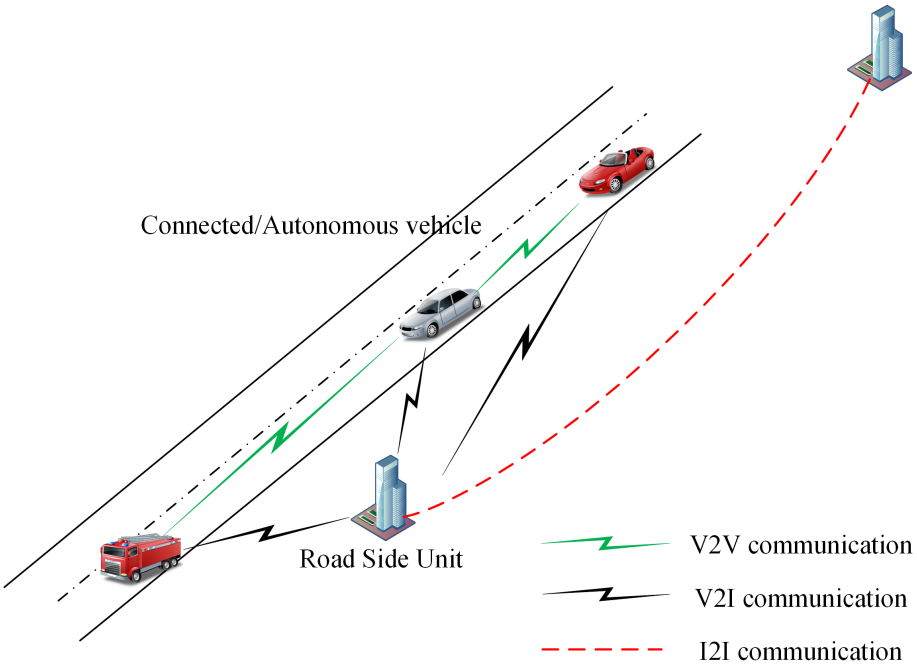

Fig. 1.1. Inter-vehicle communications (IVC) system demonstration

The realization of autonomous vehicle in the real world is not in the distant future as well. The realization is an international pursuit. In 1977, the pioneering computerized driver-less car was designed by Tsukuba Mechanical Engineering Lab, Japan. Starting at 1987, the Eureka PROMETHEUS Project (PROgraMme for a European Traffic of Highest Efficiency and Unprecedented Safety) initiated the research of driver-less cars in Europe. As part of the project, Dickmanns' team developed the VaMP Mercedes sedan and drove on multi-lane highway in Paris in 1993, and the ARGO team drove their Lancia Thema testbed car in Italy with 94% of the time in autonomous mode in 1996. In US, the DARPA (Defense Advanced Research Projects Agency) Grand Challenge organized the first long distance (150 miles in California's Mojave desert) autonomous driving competition in 2004. In the competition, none of the autonomous vehicles finished the trip. However, five autonomous vehicle successfully completed the course in 2005. The third Grand Challenge in 2007, known as Urban Challenge, has set up more complicated rules including obeying real world

traffic regulations, dealing with blocked routes and obstacles, merging into traffic, etc, and the course was in an urban area environment. Six teams finally finished the course. Later in 2008, some of the team leaders of the Urban Challenge joined the driver-less car project in Google. In 2014 June, Google debuted the conceptual driver-less car and claims to launch driver-less cars to the public before 2019. Many vehicle manufacturers are also publicly committed to producing autonomous vehicles in the near future. E.g. Nissan plans to sell autonomous vehicles in 2018, Volvo claims to bring crash-free autonomous vehicle to the public in 2020, etc, Moreover, as predicted from various publications [2], traffic lights will be eliminated and 75% of vehicles will be autonomous vehicles by the year 2040.

Currently it is encouraging that some states in the US have passed the legislature allowing autonomous vehicles to drive legally on public roads. In 2013, NHTSA issued a preliminary statement of policy concerning the autonomous vehicle. Different levels of autonomous vehicle development are presented in the statement [3], as shown in Table 1.1. As of 2014 May, California, Nevada, Florida, Michigan, and Washington DC have enacted the legislation to allow the licensing of autonomous vehicles. A more detailed map showing the current status of the autonomous vehicle legislation is presented in Figure 1.2.

1.2 Motivations

The connected vehicle (CV) and autonomous vehicle (AV) technology have the potential to greatly improve the transportation system in terms of safety, efficiency, and sustainability. According to the U.S. Department of Transportation's (DOT) Research and Innovative Technology Administration [4], the CV technology will potentially reduce 81% of all-vehicle target crashes, 83% of all light-vehicle target crashes, and 72% of all heavy-truck target crashes annually. It will also improve the congestion problem in US which consumes up to 4.2 billion hours and 2.8 billion gallons of fuel annually. Note these numbers would also apply to autonomous vehicles as

Table 1.1.
Development levels of autonomous vehicles [3]

Level 1 Function-specific Automation	Automation of specific control functions, such as cruise control, lane guidance and automated parallel parking. Drivers are fully engaged and responsible for overall vehicle control (hands on the steering wheel and foot on the pedal at all times).
Level 2 - Combined Function Automation	Automation of multiple and integrated control functions, such as adaptive cruise control with lane centering. Drivers are responsible for monitoring the roadway and are expected to be available for control at all times, but under certain conditions can disengaged from vehicle operation (hands off the steering wheel and foot off pedal simultaneously).
Level 3 - Limited Self-Driving Automation	Drivers can cede all safety-critical functions under certain conditions and rely on the vehicle to monitor for changes in those conditions that will require transition back to driver control. Drivers are not expected to constantly monitor the roadway.
Level 4 - Full Self-Driving Automation	Vehicles can perform all driving functions and monitor roadway conditions for an entire trip, and so may operate with occupants who cannot drive and without human occupants.

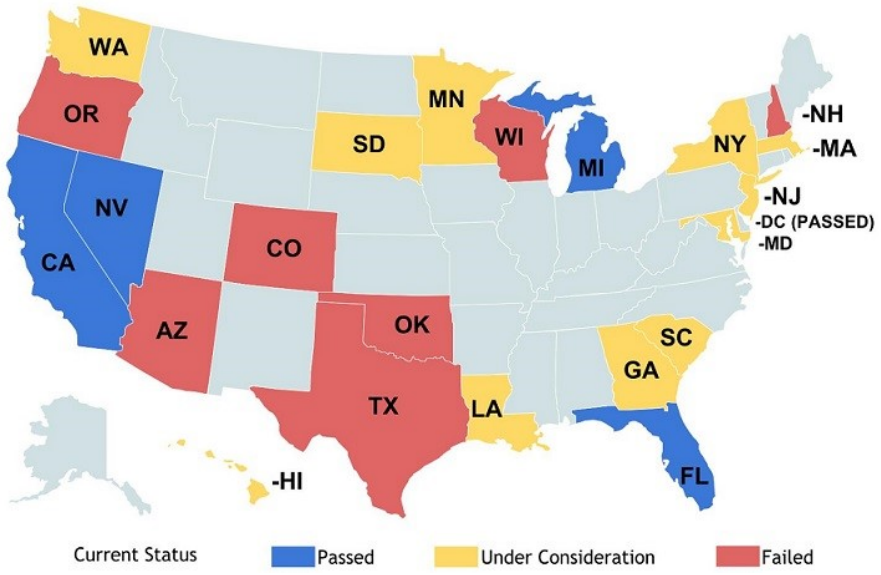

Fig. 1.2. Autonomous vehicle legislature in US as of May 2014 (CIS 2014)

autonomous vehicles are the more advanced and autonomous version of connected vehicles.

The rapid development of connected vehicles and autonomous vehicles also brings new challenges to the area of traffic flow modeling, traffic control strategies, and network impact analysis.

1.2.1 Traffic flow modeling

There is limited literature on traffic flow simulation with connected vehicles and autonomous vehicles, or the integration of traffic flow simulation and network telecommunication simulation. Towards this end, one approach is to develop a trace-based mobility model and then insert the trace to the network telecommunication simulation. The trace-based mobility model can be based on either real-world observations or traffic flow simulator. E.g., [5] constructed the trace-based mobility model by using the GPS taxi data. [6] generated the trace data by running the traffic simulator

VISSIM [7]. One major limitation of the trace-based mobility model is that the traffic simulation and network communication simulation are independent, i.e., there is no interaction between these two simulations. Addressing this issue, [8] developed a coupled simulation platform integrating the network simulator OMNET++ [9] and traffic simulator SUMO [10], which allows dynamic interaction between both simulators. [11] studied the impact of penetration rate of connected vehicle on the stability of traffic flow and road capacity. In the modeling framework, the inter-vehicle communication is modeled by a VANET simulator named JiST/SWANS [12], and the traffic flow is modeled by cellular automaton. It is found that the traffic efficiency is improved even for a 5% penetration rate of connected vehicles. However, the improvement is based on connected vehicles' willingness to adjust acceleration and speed under certain circumstances. It does not consider the impact from the cooperation between connected vehicles.

1.2.2 Traffic control strategies

Connected vehicle is a new and reliable source to provide traffic flow information to the signal controller, as a complement to the traditional flow detection techniques. The telecommunication technology enables the coordination between vehicles and infrastructures that eventually contributes to more efficient traffic signal control strategies. For example, distributed controllers can be installed in the intersection. Through wireless communication, the controller has accesses to the traversing information (e.g., queue length, average speed, delay) of the connected vehicles approaching the intersection. Based on the information, the controller runs inherent algorithms and outputs the best timing plan for a better operation of the intersection. Moreover, by means of Infrastructure to Infrastructure (I2I) communication, the signal controllers share information in the network level and take the best joint decisions. The road side equipments (RSE) assist the coordination of the signal controllers. The technology to enable I2I can be either dedicated short range communications (DSRC)

or cellular networks. In the deployment stage of connected vehicles, traffic flows are mixed with non-connected (not equipped with wireless communication device) vehicles and the connected vehicles. The signal controller only accesses the traversing information (e.g., speed, location, arrival time) of connected vehicles and then estimates the traffic state of the intersection. Dependent on the penetration rate of connected vehicles, the accuracy of the traffic state estimation varies. [13] confirmed in simulation runs that the average delay of the intersection is significantly decreased even with a low penetration rate (20%) of connected vehicles. The improvement due to connected vehicles is much higher with unexpected demands [14].

1.2.3 Traffic impact analysis

The technology of autonomous vehicles has great potential to push the road traffic accidents to the minimum rate, because (1) autonomous vehicles are controlled by computers, (2) autonomous vehicles do not possess human errors (e.g, alcohol-driving, fatigue-driving), and (3) disabled people, seniors, and children are free and safe to drive. [15] investigated a total of 5,471 crashes data from 2005 to 2007 and found that 93% of crashes were attributed to human factors. Particularly, about 41% were recognition errors, about 34% were decision errors. Moreover, according to [16], in 2012, there were 10,322 fatalities considered as alcohol-impaired-driving crash (it comprises of 31% of total traffic fatalities for the year), and there were a total of 1,168 children age 14 and younger killed in motor vehicle traffic crashes. It is foreseeable that in the transportation system with mass autonomous vehicles, human-error driven accidents will significantly reduce.

It is also foreseeable that autonomous vehicles will alleviate traffic congestion due to shorter headways, better route choice, speed harmonization, and coordinated traffic platoon. However, the relationship between traffic congestion and road safety is a debated issue. [17] investigated the relationships between the single- and multi-vehicle accident rates and traffic flow (in terms of the hourly flow instead of the

average daily traffic) and found that the relationship could be fitted with the power law function. [17] further studied the relationship by dividing traffic flow into free-flow and congested-flow conditions. It was discovered that the total accident rate and the hourly flow follows the U-shaped curve for the free-flow condition, and accident rate is sharply increased with hourly flow for the congested-flow condition. [18] found that separate predictive model should be developed for single- and multi-vehicle crashes and solely using traffic flow may not capture accurately the characteristics of crashes, other explanatory covariates such as traffic volume, vehicle density, and V/C ratio should also be incorporated. [19] introduced a congestion index to represent the level of traffic congestion to investigate the effect of congestion on road accidents. Results from various model specifications have shown that congestion has on impact on the occurrence of accidents. [20] studied the impact of freeway traffic oscillation on traffic safety. It is found that speed variation is a significant variable on crash rates. The possibility of one crash increases by about 8% with an additional unit increase in the standard deviation of speed.

In all, these three subjects (i.e., traffic flow modeling, traffic control strategies, and traffic impact analysis) are highly correlated and play a crucial role in the realization of the safest, most efficient, and most sustainable transportation system. On the one hand, traffic flow modeling is the foundation step and the building block for traffic control strategies and traffic impact analysis. On the other hand, traffic impact analysis assesses the performance of traffic control strategies and provides guidance for improvement. Traffic impact analysis and control strategies are highly relying on the accurate simulation of traffic flows regarding connected vehicles and autonomous vehicles. Inversely, the implementation of traffic control will exert impacts on the traffic flows in the network. Only the integration of these three parts forms the systematic tool for the assessment and improvement of the next generation transportation system. Currently, there are barely sufficient studies addressing these up-to-date issues hence providing strong driving forces for the research topics of this dissertation.

1.3 Overall contributions

This dissertation aims to develop a systematic tool designated for connected and autonomous vehicles, integrating the simulation of traffic dynamics, traffic control strategies, and impact analysis at the network level of the next generation transportation system. Figure 1.3 presents the overall picture of the dissertation.

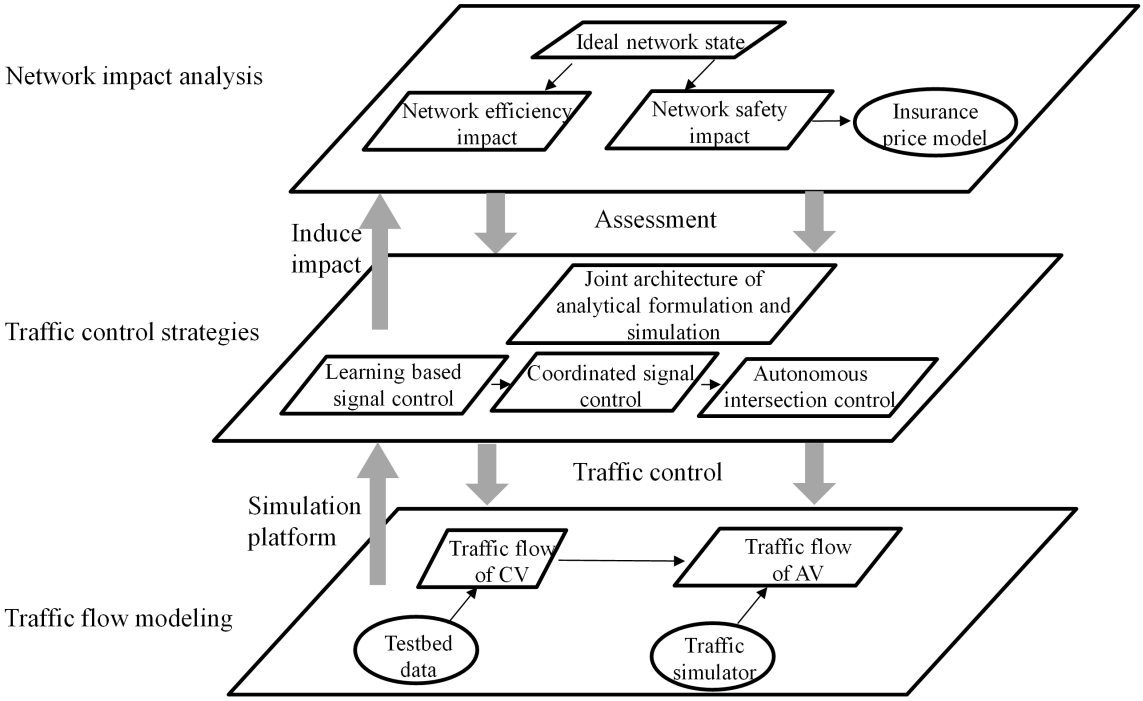

Fig. 1.3. Overall picture of the dissertation

The first part of the dissertation is devoted to the traffic flow modeling of the connected vehicles and autonomous vehicles. This task is the foundation step for transportation planning, optimized network design, efficient traffic control strategies, etc, for the next generation transportation system. Specific contributions include:

- Heterogeneous driving behaviors are considered to capture the traffic flow oscillation in the microscopic traffic simulation including the timid, neutral, aggressive, and connected vehicle driving behavior.

- Based on the empirical data of connected vehicles from the Michigan testbed, we develop the linear regression model for the relationship between spatial headway and speed for the connected vehicle.

- Extensive simulation tests have been conducted to analyze the mobility benefits of connected vehicle under different penetration rates and demand scenarios.

The second part contributes to proposing efficient traffic control strategies to better off the next generation transportation system. This task pushes the next generation transportation system to a better performance state in terms of traffic safety, travel time saving, vehicular emission reduction, etc. Specific contributions include:

- Examining the performance of the learning based signal control under the mixed connected vehicle environment.

- Extending the junction tree algorithm (JTA) to obtain the best joint actions for the entire traffic network.

- Proposing a linear programming formulation accounting for both autonomous intersection control and system optimal based dynamic traffic assignment.

The third part moves on to the impact analysis of connected vehicles and autonomous vehicles at the network level. This task assesses the positive and negative impacts of the system and provides guidance on transportation planning, traffic control, transportation budget spending, etc. Specific contributions include:

- Revealing the impact of different penetration rates of connected vehicle and autonomous vehicles on the network efficiency and mobility of the transportation system.

- Formulating the ideal network state problem and proposes solution algorithms of the problem.

1.4 Organization of the dissertation

The overall dissertation is consisting of three parts. Part I (Chapter 2 and Chapter 3)is on traffic flow modeling. Specifically, Chapter 2 is devoted to proposing a cell-based simulation approach to model the proactive driving behavior of connected vehicles. Chapter 3 proposes an optimal estimation approach to calibrate connected vehicles' car-following behavior in a mixed traffic environment. Part II (Chapter 4 and Chapter 5) is on traffic control strategies. Specifically, Chapter 4 develops a novel reinforcement learning algorithm based on Junction Tree Algorithm for the challenging coordinated signal control problem. Chapter 5 develops a novel linear programming formulation for autonomous intersection control accounting for traffic dynamics within a connected vehicle environment. Part III (Chapter 6) is on impact analysis. Specifically, Chapter 6 sets out to model an efficient and fair transportation system accounting for both departure time choice and route choice of a general multi OD network within a dynamic traffic assignment environment. Finally, Chapter 7 concludes the dissertation and discusses the interesting future research directions.

Along with this work, the following research has been submitted or published in peer-reviewed journals, conference proceedings, and presented at conferences, all listed below.

Peer-Review Journal Papers

1. **Zhu, F.**, & Ukkusuri S.V. 2016. Efficient and fair system states in dynamic transportation networks (submitted to Transportation Research Part B).

2. **Zhu, F.**, & Ukkusuri S.V. 2016. On modeling the proactive driving behavior of connected vehicles: a cell-based simulation approach (submitted to Journal of Advanced Transportation).

3. Aziza, H.M., **Zhu, F.**, & Ukkusuri S.V. 2013. Learning Approaches Based Traffic Signal Control Algorithms with Neighborhood Information Sharing: An Application for Sustainable Mobility (submitted to Journal of Intelligent Transportation Systems, passed second round review).

4. **Zhu, F.**, & Ukkusuri S.V. 2016. An optimal estimation approach for the calibration of the car-following behavior of connected vehicles in a mixed traffic environment. Accepted for publication in IEEE Transactions on Intelligent Transportation Systems.

5. **Zhu, F.**, & Ukkusuri S.V. 2015. A linear programming formulation for autonomous intersection control within a dynamic traffic assignment and connected vehicle environment. *Transportation Research Part C: Emerging Technologies*, 55, pp. 363-378.

6. **Zhu, F.**, Aziza, H.M., Qian X., & Ukkusuri S.V. 2015. A junction-tree based learning algorithm to optimize network wide traffic control: a coordinated multi-agent framework. *Transportation Research Part C: Emerging Technologies*, 58, pp. 487-501

7. **Zhu, F.**, & Ukkusuri S.V. 2015. A reinforcement learning approach for distance-based dynamic tolling in the stochastic network environment. *Journal of Advanced Transportation*, 49(2), pp. 247-266.

8. Zhan, X., Ukkusuri S.V., & **Zhu, F.** 2014. Inferring urban land use using large-scale social media check-in data. *Networks and Spatial Economics*, 14, pp. 647-667.

9. **Zhu, F.**, & Ukkusuri S.V. 2014. Accounting for dynamic speed limit control problems in the stochastic traffic environment: a reinforcement learning approach. *Transportation Research Part C: Emerging Technologies*, 41, pp. 30-47.

10. **Zhu, F.**, & Ukkusuri S.V. 2013. A cell based dynamic system optimum model with non-holding back flows. *Transportation Research Part C: Emerging Technologies*, 36, pp. 367-380.

11. **Zhu, F.**, Lo, H.K. & Lin, H.-Z. 2013. Delay and emissions modelling for signalised intersections. *Transportmetrica B: Transport Dynamics*, 1(2), pp. 111-135.

Working Papers

1. **Zhu, F.**, & Ukkusuri S.V. 2016. Information provision optimization in network equilibrium with generalized route choice inertia.

2. **Zhu, F.**, & Ukkusuri S.V. 2015. An Efficient Equivalent of Cell Transmission Model for Traffic Systems.

3. **Zhu, F.**, & Ukkusuri S.V. 2015. On Dynamic Information Propagation through Inter-Vehicle Communications.

4. **Zhu, F.**, & Ukkusuri S.V. 2015. On Learning based Intersection Signal Control with Partial Information from Connected Vehicles.

5. **Zhu, F.**, & Ukkusuri S.V. 2015. Accounting for Traffic Oscillation under the Mixed Connected Vehicle Environment in Microscopic Traffic Simulation.

Peer-review Conference Papers

1. **Zhu, F.**, & Ukkusuri, S.V. 2016. On modeling the proactive driving behavior of connected vehicles: a cell-based simulation approach. To appear in Proceedings of the 95th Transportation Research Board Meeting, Washington D.C.

2. **Zhu, F.**, & Ukkusuri, S.V. 2015. On Dynamic Information Propagation through Inter-Vehicle Communications. In Proceedings of the 94th Transportation Research Board Meeting, Washington D.C.

3. **Zhu, F.**, & Ukkusuri, S.V. 2015. Accounting for Traffic Oscillation under the Mixed Connected Vehicle Environment in Microscopic Traffic Simulation. In Proceedings of the 94th Transportation Research Board Meeting, Washington D.C.

4. **Zhu, F.**, & Ukkusuri, S.V. 2015. A linear programming formulation for autonomous intersection control within a dynamic traffic assignment and connected vehicle environment. In Proceedings of the 94th Transportation Research Board Meeting, Washington D.C.

5. **Zhu, F.**, Aziza, H.M., Qian, X., & Ukkusuri, S.V. 2014. Junction tree-based reinforcement learning algorithm for coordinated multiagent systems to solve network-level signal control. In Proceedings of the 93rd Transportation Research Board Meeting, Washington D.C.

6. **Zhu, F.**, & Ukkusuri, S.V. 2013. A non-holding back linear programming model for system optimum dynamic traffic assignment problem. In Proceedings of the 92nd Transportation Research Board Meeting, Washington D.C.

7. Aziz, H.M., **Zhu, F.**, & Ukkusuri, S.V. 2013. Reinforcement learning-based signal control using r-markov average reward technique accounting for neigh-

borhood congestion information sharing. In Proceedings of the 92nd Transportation Research Board Meeting, Washington D.C.

Part I: Traffic Flow Modeling

2. MODELING THE PROACTIVE DRIVING BEHAVIOR OF CONNECTED VEHICLES

With the communication characteristics, connected vehicles are able to pro-actively change speed to adapt to the prevailing traffic condition. Even in the mixed traffic environment, connected vehicles may function as leading vehicles, hence influencing the driving pattern of following non-connected vehicles. This chapter proposes a cell-based simulation approach to model the proactive driving behavior of connected vehicles. Firstly, a state variable of connected vehicles is introduced to track the trajectory of connected vehicles. Then the exit flow of cells containing connected vehicles is adjusted to simulate the proactive driving behavior, such that the traffic light is green when the connected vehicle arrives at the signalized intersection. The second part of the chapter conducts numerical tests to examine the effect of the proactive driving behavior of connected vehicles. Extensive test results consistently show that the presence of connected vehicles contributes significantly to the smoothing of traffic flow and vehicular emission reductions in the network.

2.1 Introduction

Intelligent transportation systems (ITS) are embracing an unprecedented era featuring the application of communication and automation technologies, particularly, connected vehicles (vehicles equipped with wireless communication devices) and automated vehicles (also known as self-driving or driver-less vehicles). This next generation ITS is not in the distant future, as the U.S. National Highway Traffic Safety Administration (NHTSA) planed to mandate connected vehicle technology by 2016, and Google debuted the conceptual driver-less "bubble" car in 2014 and claimed to launch driver-less cars before 2019. Tremendous interests are attracted to connected

and automated vehicles due to the huge benefits they are able to bring. According to the U.S. Research and Innovative Technology Administration (2014), connected vehicle technology will potentially reduce 81% of all-vehicle target crashes and vastly improve the congestion problem in US which consumes up to 4.2 billion hours and 2.8 billion gallons of fuel annually. In this study, we focus on the mobility benefits, especially, the speed stability, of connected vehicles and leave out the discussion of automated vehicles, though the methodology may also applies to automated vehicles as well.

The emerging connected vehicle technology brings new challenges to the research of traffic flow modeling. In traditional traffic flow modeling, vehicles travel at free flow speed unless the spacial headway (inter-vehicle distance) is within a certain range (e.g., 125 meters), where vehicles will follow the leading vehicle to maintain a safe and short distance. Typically in the literature of car following modeling, the spacial headway is a function of the driver's reaction time and the speed of the leading vehicle [21, 22, 23, 24], and the following vehicle's movement is dependent on the leading vehicle's movement. We consider this kind of car following behavior as *passive driving behavior*. Almost all of the traditional car following models belong to this category. The passive car following behavior is typical in the present world mainly due to the lack of information on the prevailing traffic condition (e.g., status of traffic light in the downstream intersection). One typical case is that vehicles travel at free flow speed before reaching the signalized intersection (red traffic light) then stop till the light turns to green, as demonstrated later in Figure 2.1 (a-1).

However, connected vehicles may behave differently from non-connected vehicles due to the unique communication characteristics. Particularly, connected vehicles are able to communicate with other connected vehicles (V2V communication) through the vehicle ad-hoc network (VANET) or communicate directly with the infrastructure (V2I communication), such that connected vehicles are more informed about the traffic condition downstream (e.g., the timing plans of the downstream intersection). With the prevailing traffic information, connected vehicles are able to adjust the

driving speed accordingly rather than blindly adjust speed based on the speed change of the leading vehicle. In other words, connected vehicles change speed pro-actively and is independent of the speed change of the leading vehicle. We consider this kind of driving behavior as *proactive driving behavior*.

The proactive driving behavior of connected vehicles contributes significantly to the smoothing of traffic flow in the transportation network. Even in the mixed connected vehicle environment, connected vehicles may function as the leading vehicle to influence the driving behavior of following non-connected vehicles. This chapter applies the meso-scopic cell transmission model as the underlying traffic flow model. Firstly, we introduce the state variable of connected vehicles akin to every cell at every time step in order to track the trajectory of individual connected vehicles. Then the exit flow of cells containing connected vehicles is adjusted to account for the proactive driving behavior of connected vehicles. With the adjusted exit flow, connected vehicles reach the signalized intersection before the traffic light turns red. The second part of the chapter conducts extensive numerical tests to examine the effect of the proactive driving behavior of connected vehicles.

The rest of the chapter is structured as below. Section 2.2 is devoted to the recent literature on the mobility benefit analysis of connected vehicle and an motivation example of this study. Section 2.3 introduces the cell transmission model and related changes needed to account for the proactive speed adjustment behavior of connected vehicles. Section 2.4 conducts two numerical case studies including a signalized intersection and the Manhattan downtown network. Followed by Section 2.5 with some concluding remarks and future research directions.

2.2 Related work

Proactive speed adjustment shares similarity with the notion of speed harmonization. Speed harmonization is also known as variable speed limit control [25, 26]. It

is an effective traffic management technique that adjusts the speed limit of the road segment to account for the dynamic change of traffic demand, road construction condition, work zone, and weather condition. The objective of speed harmonization is to smooth the traffic flow towards a more uniform speed.

The recent advance of connected vehicles offers useful technologies in detection and acquisition of high fidelity data that can be used for speed harmonization[26, 27]. Empirical studies have shown the effectiveness of variable speed limit control in smoothing traffic flow and reducing traffic breakdowns [28, 29]. [30] develop an on-line algorithm for variable speed limit control in highway work zone operations. [31] formulate the integrated variable speed limit control and ramp metering problem as a constrained discrete-time optimal control problem. [32] integrate variable speed limit control and ramp metering as a coordination control problem. A model predictive control approach is applied to solve the problem. The numerical case study shows that significant travel time reduction (15%) is gained compared to non-control case. [27] formulate the dynamic speed limit problem as a Markov decision process problem and applied an on-line reinforcement learning algorithm to solve the problem.

Note that the notion of proactive speed adjustment is different from speed harmonization (or variable speed limit control) in the way that proactive speed adjustment requires the vehicle to be informed about the prevailing traffic condition. Hence proactive speed adjustment is associated only with connected vehicles. By contrast, speed limit control is usually applied to a certain road segment, and is effective to both connected and non-connected vehicles.

Though we consider that only connected vehicles are able to pro-actively change speed, the influence of the proactive speed adjustment is not limited to connected vehicles. Because connected vehicles may act as leading vehicles (especially on the single lane roadways in the real world) in the traffic flow propagation, the following non-connected vehicles will exert a similar speed pattern as the leading connected vehicle (as shown later in the demonstration example). In such a way, the influence of the proactive driving behavior of connected vehicles may expand to the whole net-

work. Recently, [33] introduce the influential subspace of connected vehicles within which the connected vehicle is able to influence the macroscopic state of traffic flow to a desired state. However, the analysis is based on a macroscopic traffic flow model using a time-space diagram. The analytical solution is also limited to a single link case.

Motivation example: the potential of a single connected vehicle

Consider the case of a signalized intersection (or a traffic accident) as shown in Figure 2.1. Assuming that the third vehicle (highlighted in red in the figure) is a connected vehicle. Here we consider two scenarios for the purpose of comparison: (a-1) the connected vehicle does not adjust speed pro-actively (i.e., no different from non-connected vehicles); (a-2) the connected vehicle adjusts speed pro-actively. As shown in Figure 2.1 (a-1), all vehicles firstly travel at free flow speed, next stop in front of the intersection due to red traffic light, and then discharge when the light turns to green. In other words, all vehicles passively follow the stop-and-go process of the first vehicle (leading vehicle). On the contrary, in Figure 2.1 (a-2), the third vehicle (connected vehicle) does not blindly follow the second vehicle's trajectory. Away from the intersection about 200 meters, it is aware of the status of traffic light. It pro-actively adjusts the speed such that it arrives at the intersection exactly when the traffic light turns on green. In such a way, the third vehicle avoids the stop-and-go process of the second vehicle. The following vehicles also avoids the stop-and-go process as they are following the third vehicle. Figure 2.1 (b) further presents the speed distribution corresponding to the two types of traffic in Figure 2.1 (a). It is clearly shown that the low speed (0$\sim$2.5 m/s) density of traffic pattern (b-2) is significantly less than that of traffic pattern (b-1).

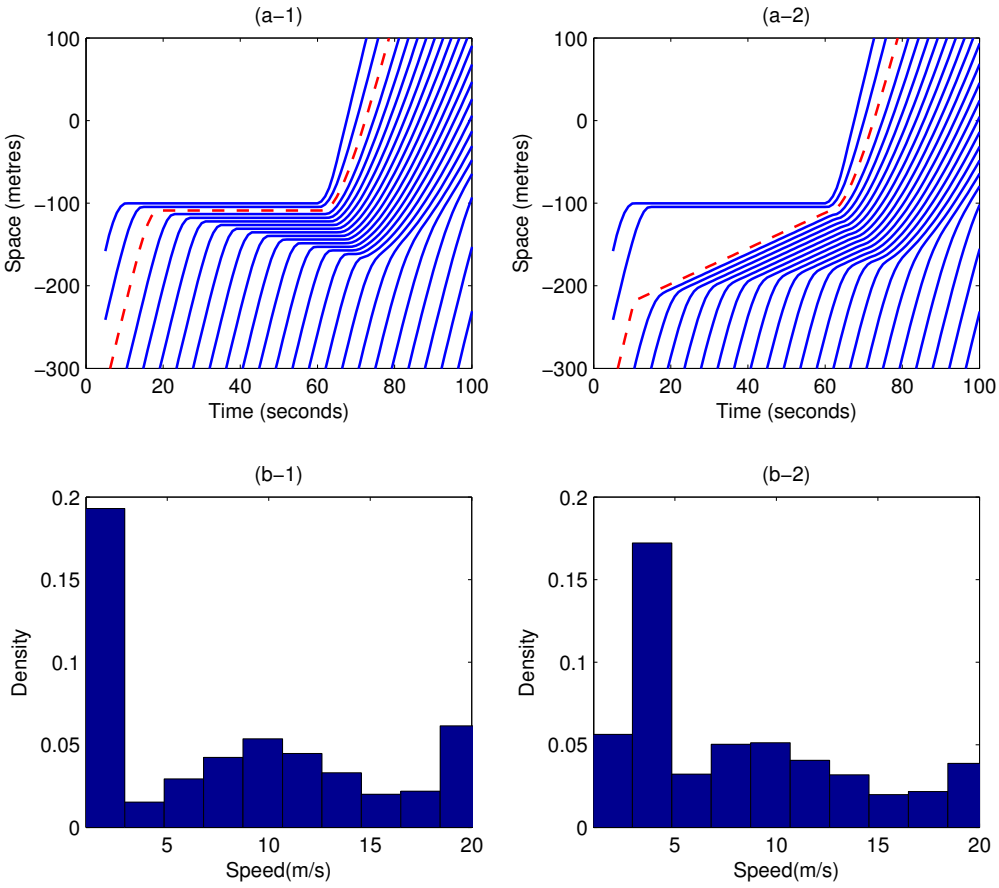

Fig. 2.1. Trajectory of (a-1) passive car following behavior, (a-2) proactive driving behavior; Speed distribution of (b-1) passive car following behavior, (b-2) proactive driving behavior

Notations:

Sets:		
$\mathbf{C}$	:	Set of all cells
$\mathbf{C}_R$	:	Set of origin cells
$\mathbf{C}_S$	:	Set of destination cells
$\mathbf{C}_O$	:	Set of ordinary cells
$\mathbf{C}_D$	:	Set of diverging cells
$\mathbf{C}_M$	:	Set of merging cells
$\mathbf{C}_T$	:	Set of signalized cells
$\mathbf{\Gamma}^{-1}(i)$	:	Set of predecessors of cell i
$\mathbf{\Gamma}(i)$	:	Set of successors of cell i
Parameters:		
W	:	Shock wave speed
V	:	Free-flow speed
S	:	Saturation flow rate
L	:	Length of a cell
T	:	Total time steps
d_J	:	Jam density
N_i^t	:	Maximum number of vehicles allowable in cell i at time t
D_i^t	:	Fixed mean demand input of cell i at time t
Variables:		
Q_i^t	:	Inflow or outflow capacity of cell i at time t
d_i^t	:	Demand input of cell i at time t
p_i^t	:	Probability for the demand or capacity of cell i
x_i^t	:	Cell occupancy (number of vehicles) of cell i at time t
$f_{i,j}^t$	:	Flow from cell i to j at time t
G_i^t	:	Traffic light status of cell i at time t
k_i^t	:	Density of cell i at time t
v_i^t	:	Speed of cell i at time t
CV_i^t	:	The state of connected vehicles of cell i at time t

2.3 Methodology

2.3.1 Assumptions

To begin with, the assumptions in our modeling framework are:

1. The signalized intersection is installed with wireless communication devices. Connected vehicles are able to communicate with the signalized intersection within the transmission range. In the contest of this study, we consider that connected vehicles are aware of the timing plan of the intersection when the distance is within the transmission range.

2. Once the connected vehicle is aware of the traffic light status of the downstream intersection, it will pro-actively adjust speed to arrive at the intersection when the traffic light is green.

3. We utilize the cell transmission model (CTM) to propagate traffic flow. CTM is a meso-scopic traffic flow model that assumes a piecewise linear relationship between traffic flow and density. A series of homogeneous cells are used to represent the road network and time is discretized into time steps. Moreover, we have not considered the lane changing behavior. For more details, please refer to [34, 35].

2.3.2 Cell transmission model

It is noted that in the literature of traffic flow modeling, there are macroscopic link-based models [27, 36, 37, 38] that are more efficient than CTM [34, 35]. However, they are not readily applicable for this study due to the specialty of this study as below. 1) Link-based models propagates traffic flow on an aggregation level where the macroscopic concept (e.g., flow, density, average speed) is applied. In this study, we want to explicitly track the trajectory of individual connected vehicles. 2) Link based models focus on the accumulative traffic flow at the boundaries of the link. In

this study, we want to model connected vehicles' capability of changing speed at any point of the link, hence we care more about the traffic flow dynamics within the link.

CTM provides a convergent approximation to a simplified version of the LWR hydrodynamic model [39, 40], whereby the fundamental diagram of traffic flow and density is assumed to be a piecewise linear function. CTM is one of the widely used network loading models due to its simplicity and capability of covering the whole range of traffic dynamics including queue formation, dissipation, and kinematic wave. Among the wealth of literature, CTM has been used for various dynamic problems in the last decade, including the dynamic user optimal problem [41, 42], dynamic network analysis [43, 44], traffic control management [45, 46, 47, 48], and so on.

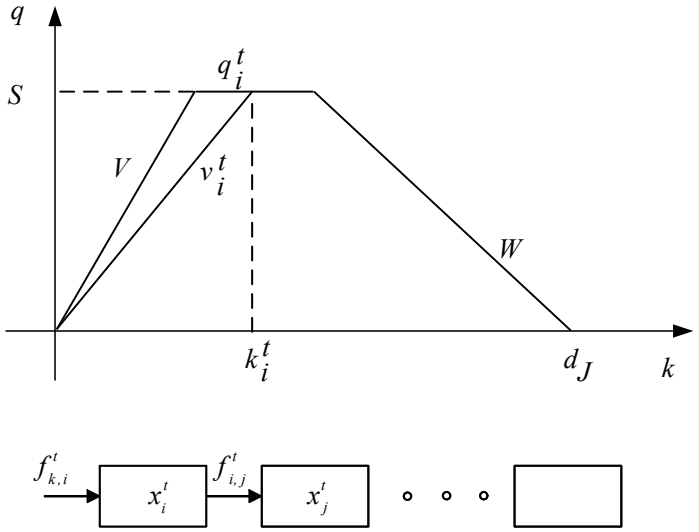

Fig. 2.2. Flow propagation of the cell transmission model

CTM discretizes the road network with a series of homogeneous cells, as shown in Figure 2.2. The length of each cell L is set to be the distance traveled by the free-flow speed V in one time step ξ, i.e., $L = V\xi$. CTM approximates the LWR [39, 40] process by the following set of recursive equations:

Source cells:

$$x_i^t = d_i^{t-1} + x_i^{t-1} - f_{i,j}^{t-1}, \forall i \in \mathbf{C}_R, j \in \mathbf{\Gamma}(i) \tag{2.1}$$

Sink cells:

$$x_i^t = x_i^{t-1} + f_{k,i}^{t-1}, \forall i \in \mathbf{C}_S, k \in \mathbf{\Gamma}^{-1}(i) \tag{2.2}$$

Ordinary/Merging/Diverging cells:

$$x_i^t = x_i^{t-1} + \sum_{k \in \mathbf{\Gamma}^{-1}(i)} f_{k,i}^{t-1} - \sum_{j \in \mathbf{\Gamma}(i)} f_{i,j}^{t-1}, \forall i \in \mathbf{C}_{O,M,D} \tag{2.3}$$

Ordinary cell connectors:

$$f_{i,j}^t = \min\left(x_i^t, Q_i^t, Q_j^t, \frac{W}{V}\left(N_j^t - x_j^t\right)\right), \forall i \in \mathbf{C}_O, j \in \mathbf{\Gamma}(i) \tag{2.4}$$

Diverging cell connectors:

$$f_{i,j}^t = \min\left(\rho_i^t x_i^t, Q_i^t, Q_j^t, \frac{W}{V}\left(N_j^t - x_j^t\right)\right), \forall i \in \mathbf{C}_D, j \in \mathbf{\Gamma}(i) \tag{2.5}$$

where ρ_i^t is an exogenous parameter denoting the proportion of traffic flow diverted to cell i at time t.

Merging cell connectors:

$$f_{i,j}^t = \min\left(x_i^t, Q_i^t, Q_j^t, \frac{W}{V}\rho_i^t\left(N_j^t - x_j^t\right)\right), \forall i \in \mathbf{C}_M, j \in \mathbf{\Gamma}(i) \tag{2.6}$$

In order to capture the uncertainty from traffic demand, we have:

$$d_i^t = p_i^t D_i^t \tag{2.7}$$

Note that D_i^t is a fixed value, representing the predefined demand; and p_i^t denotes a random value within (0, 1) which is generated by certain probability distribution. Based on empirical data, the typical probability distributions of p_i^t include multivariate normal distribution, log-normal distribution, and multivariate log-normal distribution [49, 50, 51, 52]. A similar idea to describe the stochastic traffic network environment with CTM is also discussed in [53].

For signalized intersection, the exit flow is saturation flow rate at green traffic light, and zero at red traffic light. Thus we have:

$$Q_i^t = \begin{cases} S\xi & \text{if } G_i^t = 1 \\ 0 & \text{if } G_i^t = 0 \end{cases} \tag{2.8}$$

where $i \in \mathbf{C}_G$, S is a fixed value, representing the saturation flow, and G_i^t denotes the traffic light status of the signalized cell i at time t. Moreover, $G_i^t = 1$ indicates the green traffic light, while $G_i^t = 0$ indicates the red traffic light.

With the density or cell occupancy determined, the mean speed at the cell level can be derived. Firstly, note that $k_i^t = \frac{x_i^t}{L}$, thus according to the piece-wise fundamental diagram as shown in Figure 2.2, we obtain the associated flow as: $q_i^t = \min\left(k_i^t V, Q_i^t, (d_J - k_i^t)W\right)$. Thus according to the fundamental relationship between flow, density, and speed, we get:

$$v_i^t = \frac{q_i^t}{k_i^t} = \min\left(V, \frac{1}{x_i^t} Q_i^t L, \left(\frac{1}{x_i^t} L d_J - 1\right) W\right), i \in \mathbf{C} \tag{2.9}$$

2.3.3 Tracking the trajectory of connected vehicles

In this study, connected vehicles are generated randomly according to the penetration rate (a preset parameter). However, CTM is originally developed as an efficient meso-scale traffic flow simulation model, where traffic flow is not considered at the individual vehicle level. Thus the probability of a initial source cell containing connected vehicles (i.e., $CV_i^t = 1$) is determined by:

$$\mathbf{P}(CV_i^t = 1) = 1 - (1 - Z)^{d_i^t}, i \in \mathbf{C}_R \tag{2.10}$$

where Z represents the penetration rate of connected vehicles.

As noted in the motivation example, even one single connected vehicle may exert significant impact on the traffic flow profile of the whole network. Hence in this section, we extend CTM to make it capable of tracking the trajectory of connected vehicles. For this purpose, we introduce a state variable of connected vehicles, $CV_i^t, i \in C, t \in [0, T]$, to describe the existence of connected vehicle in cell i at time t, where $CV_i^t > 0$ indicates that there is connected vehicle inside cell i at time t, while $CV_i^t = 0$ indicates the otherwise.

Figure 2.3 demonstrates tracking the trajectory of connected vehicles. The parameter setting of this example comes from Section 2.4.2. Figure 2.3 is only for

demonstration purpose, the proactive speed adjustment of connected vehicles is not implemented yet. From Figure 2.3, the trajectories of connected vehicles are clearly and accurately captured.

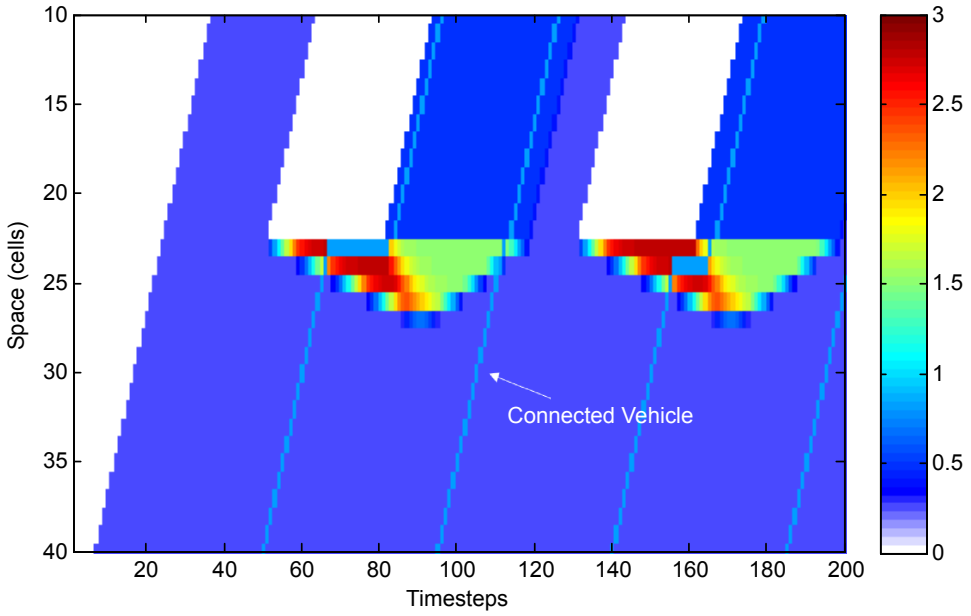

Fig. 2.3. Demonstration of tracking the trajectory of connected vehicles

2.3.4 Accounting for the proactive speed adjustment of connected vehicles

Note that CTM discretizes space into homogeneous cells of the same size. The size of a cell is dependent on the free flow speed and the size of the time step. As indicated in the fundamental diagram of CTM, the flow-density relationship is approximated by a piece-wise linear model (Figure 2.2). In non-congested traffic condition, traffic flow propagates from one cell to another in the free-flow speed (lies on the left side of the fundamental diagram). However, connected vehicles will not travel blindly at free-flow speed at non-congested situation but adjust speed pro-actively to avoid

the stop-and-go pattern at the downstream intersection. Hence, there is a need to modify the flow propagation from the original CTM to account for the proactive driving behavior of connected vehicles. Consider the process of a connected vehicle traversing through a series of cells, the CV states of cells will change chronologically. Hence, we relate the CV state of cells with the trajectory of connected vehicles as below.

For demonstration purpose, as shown in Figure 2.4, consider a general cell i that belongs to a general signalized link. In CTM, this link is discretized into $1...i...n$ cells, where n denotes the ending cell (also the signalized cell) of the link. Further, the value of $(n-i)$ represents the minimum time steps for the traffic flow at cell i to reach the end of the link (i.e., to reach the signalized cell). Let point O represent time t, and point A represent the arrival time of traffic at cell i reaching the intersection. Thus $OA = n - i$. Moreover, let R^t (i.e., point B) denotes the ending time of red traffic light of cell n within the cycle covering time t. Then $OB = R^t - t$ represents the needed time for vehicles in cell i at time t (i.e., x_i^t) to reach the intersection. It is clear that if OB$\leq$OA, the traffic of x_i^t will travel through the intersection freely as the traffic light is green (as shown in Figure 2.4 (a)), otherwise x_i^t will stop in front of the intersection till point B (i.e., time R^t), as presented in Figure 2.4 (b).

Assuming that cell i at time t contains connected vehicles, i.e., $CV_i^t = 1$, and the distance from cell i to n is within transmission range such that the connected vehicle is aware of R^t. In the case of OB>OA (i.e., $R_i^t - t > n_i - i$), the connected vehicle need to adjust speed (particularly, slow down) to reach the ending cell at point B. To simulate this proactive driving behavior, we retain the vehicles in cell i for $\lfloor \frac{OB}{OA} \rfloor$ time steps, where $\lfloor \frac{OB}{OA} \rfloor$ indicates the rounding down integer of $\frac{OB}{OA}$. Specifically in the implementation, at time t, if $0 < CV_i^t < \frac{OB}{OA}$, we update CV_i^{t+1} as $CV_i^t + 1$ in time step $t+1$, and restrict the exit flow to be zero (so as to retain the traffic in cell i). This process continues till $CV_i^t \geq \frac{OB}{OA}$. Then CV_i^{t+1} is updated to be zero, the restriction on the exit flow of cell i is released, and CV_j^{t+1} is updated to be one, where $j \in \Gamma(i)$. In summary, the CV state is updated in a recursive way as shown in

Pseudocode 1 (note that $\frac{OB}{OA} = \frac{R^t - t}{n - i}$). The traffic density patterns in the presence of connected vehicles in Figures 2.5, 2.6, and 2.7 have confirmed that connected vehicles reach the intersection at the end of red traffic light.

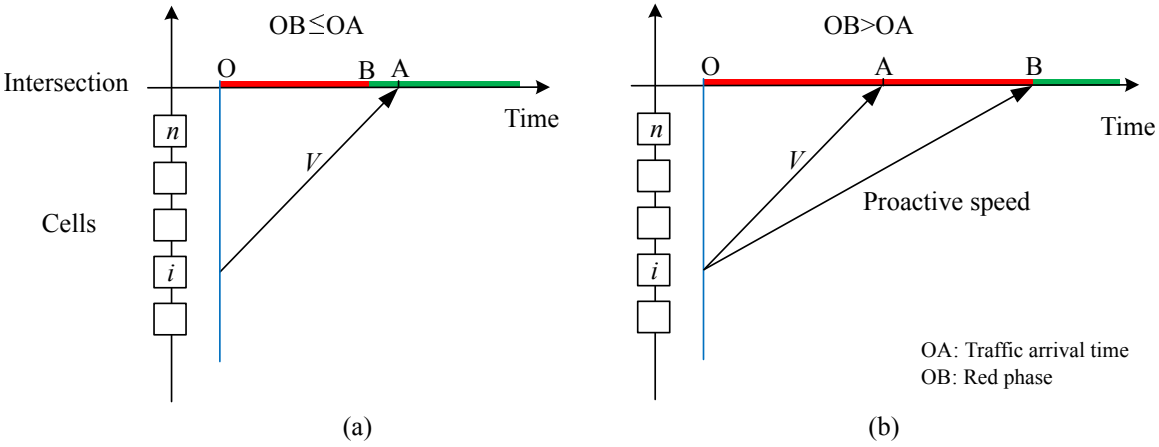

Fig. 2.4. Proactive driving behavior of connected vehicles

2.4 Numerical case studies

2.4.1 Vehicular emissions estimation

To evaluate the environmental impact of the proactive driving behavior of connected vehicles, we apply the approach of vehicle specific power (VSP) developed by [54] to estimate different types of vehicular emissions. It is worthwhile to note that there is a vast literature on vehicular emission estimation. We choose the VSP approach due to its convenience in estimating emission rates based on second-by-second speed profile. Other emission modeling approaches are similarly applicable.

In the VSP approach [54], firstly, VSP is determined based on the second-by-second speed profile for a typical light-duty vehicle as below:

$$VSP = v[1.1a + 9.81sin(arctan(grade)) + 0.132] + 0.000302v^3 \tag{2.11}$$

for $i \in \mathbf{C}_R$ **do**
  Update CV_i^t according to (2.10);
end
while $i \in \mathbf{C}/\{\mathbf{C}_R \cup \mathbf{C}_S\}$ **do**
  $j \in \Gamma(i)$;
  if $0 < CV_i^t < \dfrac{R^t - t}{n - i}$ **then**
    $CV_i^{t+1} = CV_i^t + 1$;
    $f_{i,j}^t = 0$;
  end
  else if $0 < CV_i^t < \dfrac{R^t - t}{n - i}$ **then**
    $CV_i^{t+1} = 0$;
    $CV_j^{t+1} = 1$;
  end
  if $0 < CV_i^t$ *and* $f_{i,j}^t \geq 0$ **then**
  end
  update: $i = j$;
end

Pseudocode 1: The updating process of connected vehicle state and exit flow adjustment

Table 2.1.
VSP modes [54, 55]

VSP mode	Definition(kW/ton)
1	VSP<-2
2	-2≤VSP<0
3	0≤VSP<1
4	1≤VSP<4
5	4≤VSP<7
6	7≤VSP<10
7	10≤VSP<13
8	13≤VSP<16
9	16≤VSP<19
10	19≤VSP<23
11	23≤VSP<28
12	28≤VSP<33
13	33≤VSP<39
14	39<VSP

where VSP denotes the vehicle specific power (kW/metric ton); v denotes vehicle speed (m/s); a denotes acceleration or deceleration (m/s2); and grade is terrain gradient (±%).

Depending on the value, the second-by-second VSP is categorized into fourteen discrete modes as defined in Table 2.1 [54, 55]. Each VSP mode is corresponding to a different type of fuel use and emission rate. [56] measures the energy consumption and pollutant emissions of a EURO IV gasoline passenger car (1.4 L VW Polo 1.4 16V) and develops the normalized average emission rates for CO_2, CO, NO_x and HC by VSP mode as showed in Table 2.2.

Table 2.2.
Normalized average emission rates for CO_2, CO, NO_x and HC by VSP mode [56]

VSP mode	CO_2(g/s)	CO(mg/s)	NO_x(mg/s)	HC(mg/s)
1	0.21	0.03	1.29	0.14
2	0.61	0.07	2.62	0.11
3	0.73	0.14	3.38	0.11
4	1.5	0.25	6.05	0.17
5	2.34	0.29	9.36	0.2
6	3.29	0.69	12.53	0.23
7	4.2	0.58	15.48	0.24
8	4.94	0.64	17.82	0.23
9	5.57	0.61	21.32	0.24
10	6.26	1.01	32.53	0.28
$\geq$11	7.4	1.15	55.75	0.37

2.4.2 Test case 1: a single link

The first test case is a single link with a signalized intersection at the end of the link. The purpose of conducting this test case is to demonstrate that the customized CTM is capable of accounting for the proactive driving behavior of connected vehicles, as well as to examine the mobility benefit that an isolated intersection is able to gain with varied penetration rates of connected vehicles.

The length of the link is 300 meters. Free flow speed is set at 50 kph. The duration of the simulation is 600 s with the time step of one second. Hence the cell discretization of the road is around 13.9 meters. The communication transmission range is set at 200 meters, i.e., the connected vehicle is aware of the timing of traffic lights when it is within 200 meters of the intersection. Details of the other parameters are presented in Table 2.3.

Table 2.3.
Parameter settings of test case 1

Jam density	200	veh/km
Free flow speed	50	km/h
Transmission range	200	meters
Shockwave speed over free flow speed ratio	0.4	
Saturation flow rate	1800	veh/hour
Cycle time	80	seconds
Red phase	40	seconds
Time step	1	second
Duration	600	seconds

In the experiment design, we consider three types of demands: 300 vph (light), 600 vph (medium), and 1200 vph (heavy). The demand inputs are generated according to the lognormal probability distribution with the deviation percentage of 0.20. Note that the saturation flow rate is 1800 vph, and the green time is half of the cycle time.

Thus the capacity of the intersection is 900 vph, and the demand case of 1200 vph will expect over-saturation in the intersection. Figures 2.5, 2.6, and 2.7 present the traffic density profile of the link under different penetration rates of connected vehicles and under different demand scenarios. From the three figures, we have observed the following results:

1. Connected vehicles will pro-actively adjust speed such that when the connected vehicle arrives at the intersection the traffic light turns to green. This pattern is especially clearly demonstrated in the case of low penetration rate of connected vehicles (as shown in Figure 2.5, case of 10%, 50% CV; Figure 2.6, case of 50% CV; Figure 2.7, case of 10%, 50% CV).

2. The stopped traffic significantly reduces with the presence of connected vehicles. Especially in the low and medium demand scenario, even if there are only a couple of connected vehicles (as for the case of 10% CV), the traffic density profile of the link are substantially different from the non-CV case (as shown in Figure 2.5, case of 10% CV; Figure 2.6, case of 10% CV).

3. As expected, over-saturation occurs in the heavy demand scenario (as shown in Figure 2.7). Though stopped traffic also reduces with the presence of connected vehicles, the reduction is not as significant as in the case of low and medium demand. Moreover, a new queue forms up at the end of the transmission range (Figure 2.7, case of 100% CV).

To further quantify the mobility benefits of connected vehicles in terms of speed stability, we consider the weighted average speed and the weighted speed deviation for the speeds that are within the range of (0∼30 kph) as the performance measures (30 kph is just a tentative threshold parameter). Particularly, we firstly compute the speed of every cell at every time step, then subtract the set of speeds that are within the range of (0∼30 kph), then compute the weighted mean and deviation of the speed set with respect to the density of the cell. Table 2.4 presents the weighted

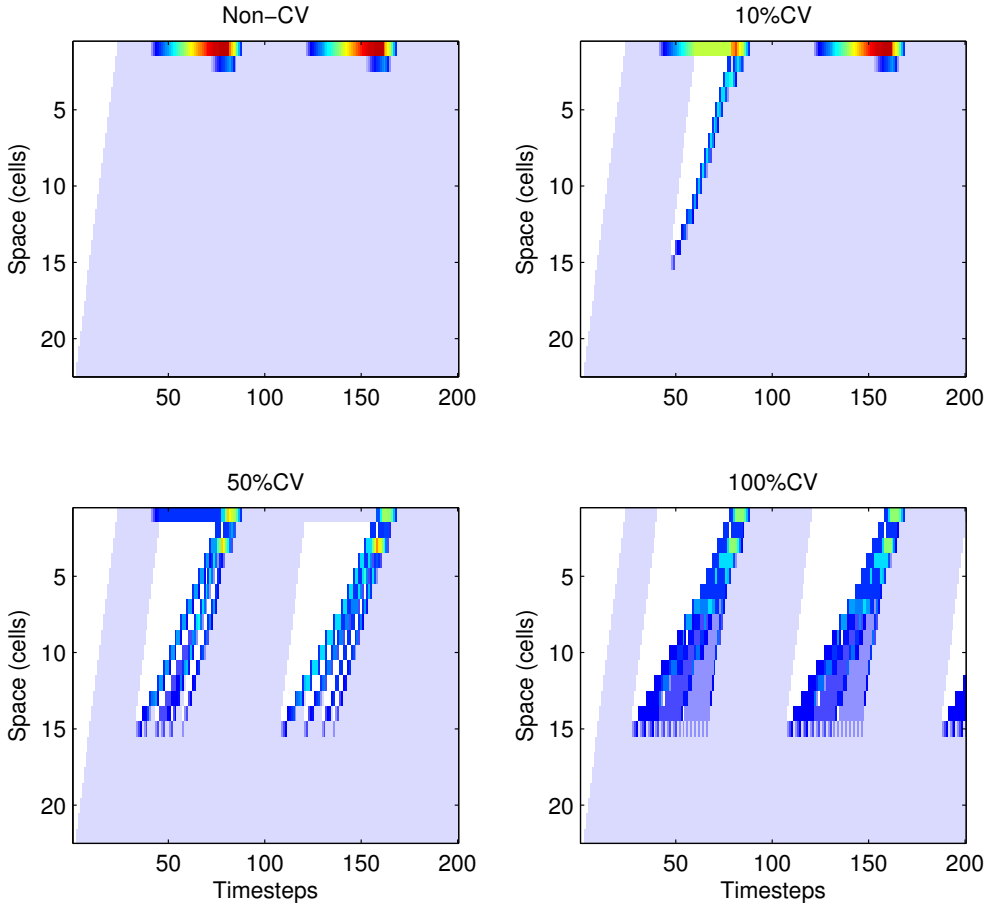

Fig. 2.5. Density demonstration of different connected vehicle penetrations for light demand scenario

mean and deviation of the speed profile of the link under different demand scenarios and penetration rates of connected vehicles. From Table 2.4, we see that:

1. The presence of connected vehicles significantly contributes to increasing the average speed of the link. Even with only 10 % connected vehicles, the average speed improves at least 15.34%, and with 30% connected vehicles, the improvement is at least 27.85%.

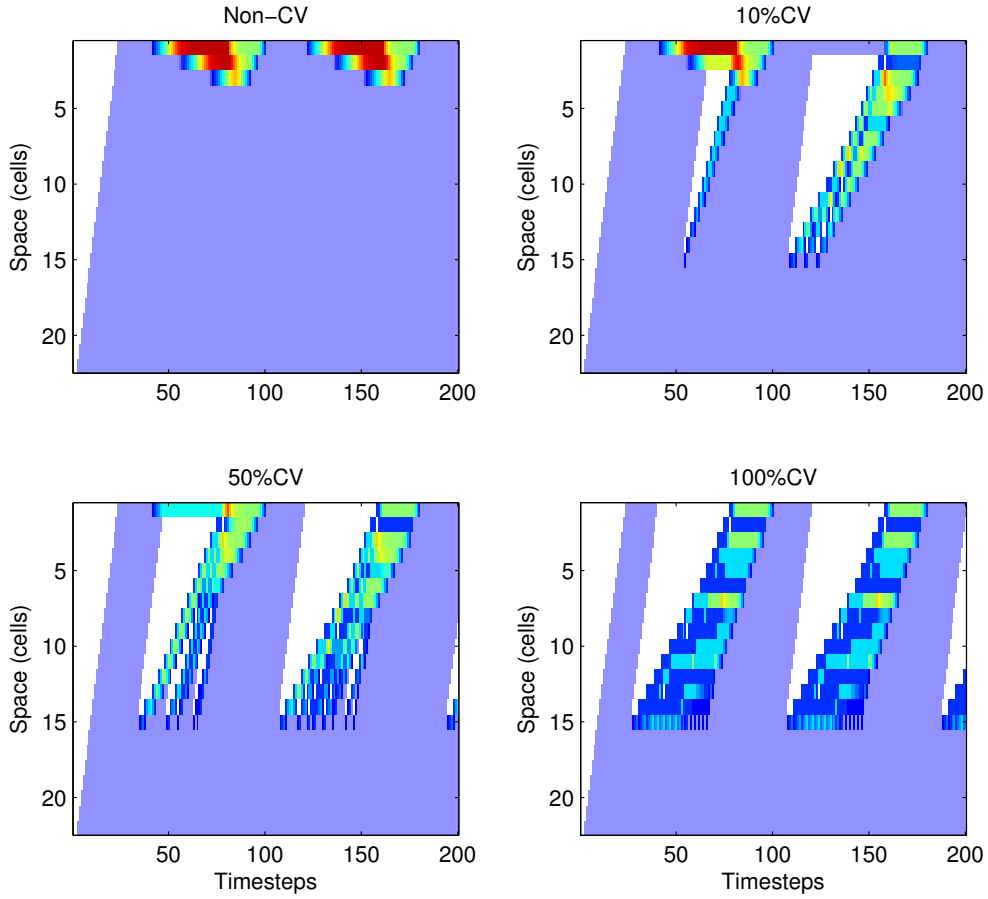

Fig. 2.6. Density demonstration of different connected vehicle penetrations for medium demand scenario

2. The marginal improvement of average speed decreases with the penetration rate of connected vehicles. In other words, the rate of improvement slows down with the penetration rate. Especially, 50% of connected vehicles seems to be a critical point. The average speed increases rapidly (slowly) with the penetration rate before (after) 50% of connected vehicles. This observation may offer valuable insights to designing the most efficient and cost-effective deployment of connected vehicles.

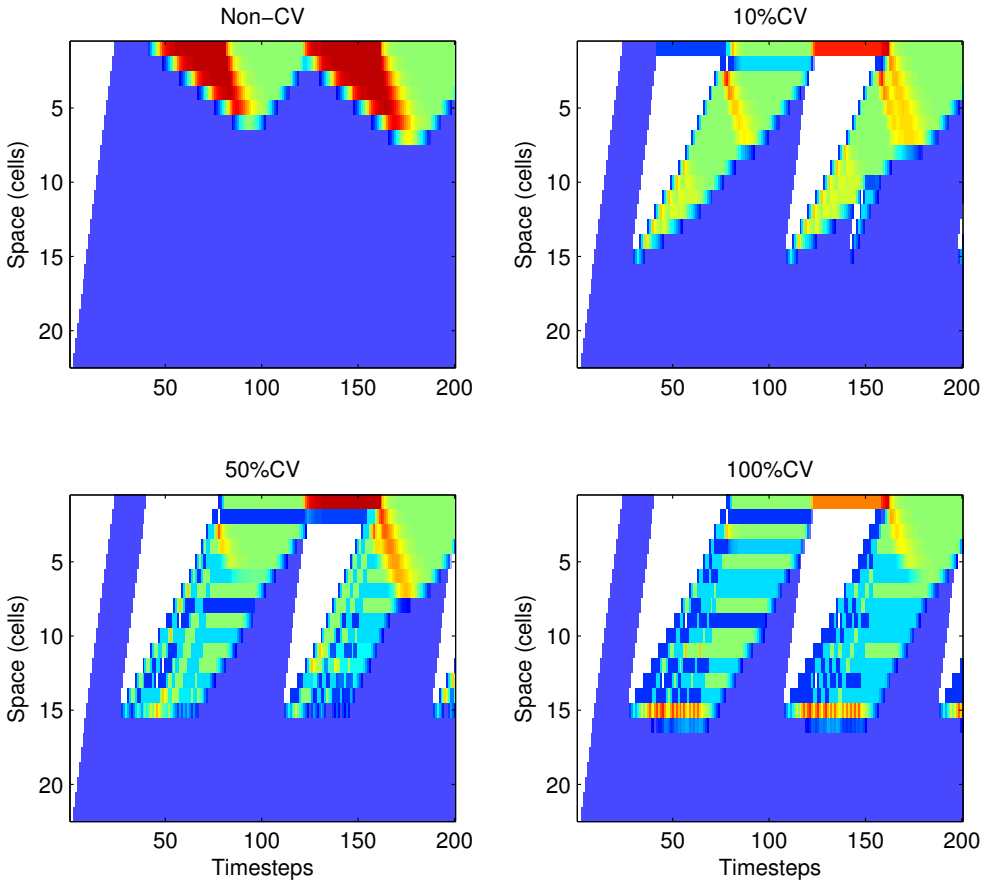

Fig. 2.7. Density demonstration of different connected vehicle penetrations for heavy demand scenario

3. Though there is not a consistent pattern for the deviation of the average speed, it is seen that the deviation is within a narrow range.

2.4.3 Test case 2: Manhattan downtown network

The Manhattan downtown network is a real world network as shown in Figure 2.10. We firstly obtain the shape-file for the Manhattan network, then extract the network configuration information (e.g., the length of links, the direction of links,

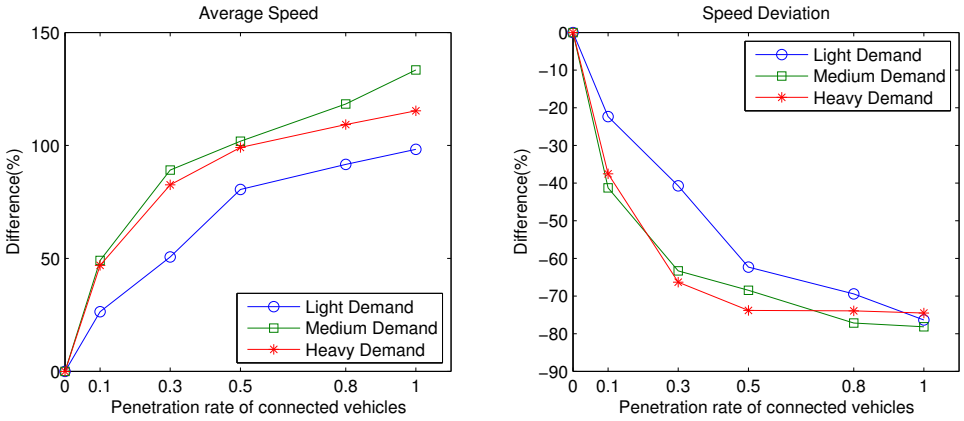

Fig. 2.8. Comparison of speed under different connected vehicle penetrations and demands

the link-node incidence, and origin/destination nodes) and feed it into the Matlab code of the CTM model. For the Manhattan road network, there are 340 links, and the total length of the entire network is 26,252 m. The specific configurations of the network (e.g. the length of each link) are skipped here as they are the same as that in the real world. Other parameter settings are the same as test case 1, unless specified otherwise.

Similar to test case 1, we consider the weighted average speed and speed deviation for the speeds that are within (0∼30 kph) as the performance measures to quantify the mobility benefits of connected vehicles. Table 2.5 presents the weighted mean and deviation of the speed profile of the whole network under different demand scenarios and penetration rates of connected vehicles. The following results can be observed from Table 2.5:

1. It is easily seen that connected vehicles contribute significantly to improving the average speed of the network. Relatively, the improvement of the low demand scenario is the worst. However, even under the low demand case, the average speed increases from 13.7 kph to 18.49 kph with 10% connected vehicles, and to 22.30 kph with 100% connected vehicles.

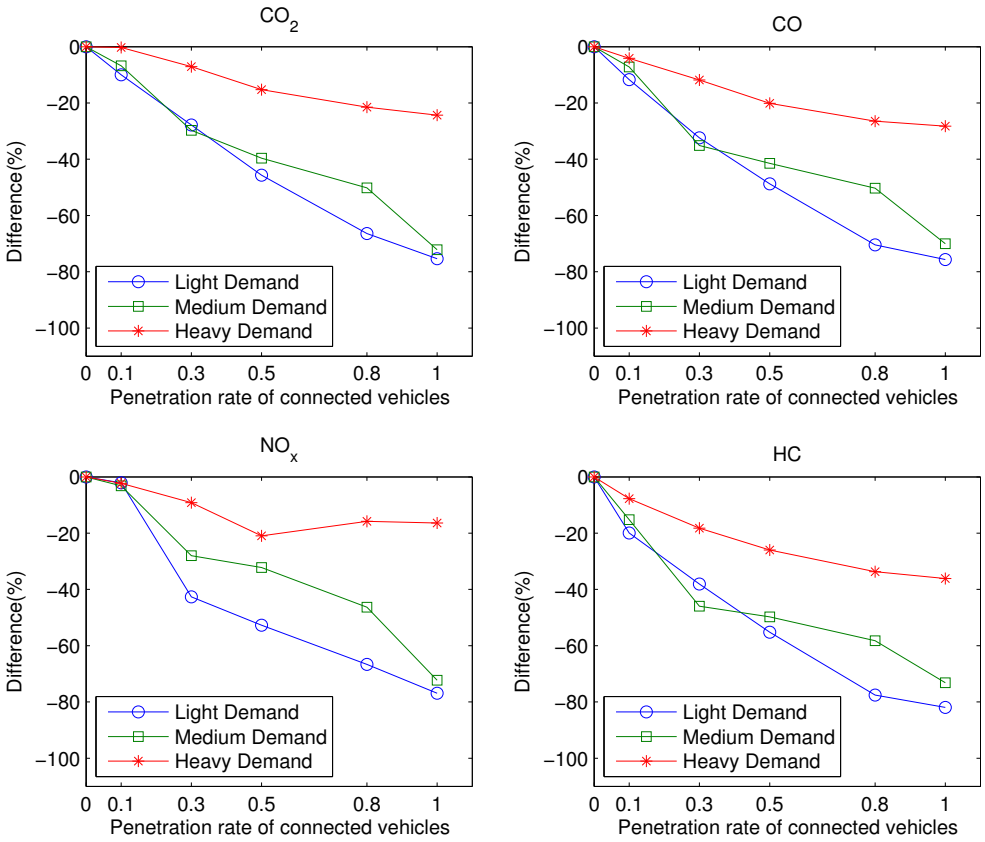

Fig. 2.9. Comparison of emissions under different connected vehicle penetrations and demands

2. Similar to test case 1, the marginal improvement of average speed slows down with the penetration rate. In this test network, 30% of connected vehicles seems to be the critical point instead of 50%. The average speed increases slowly after the penetration rate of 30%. In the deployment of connected vehicles, 30% may be the most cost-effective penetration rates of connected vehicles.

3. The speed deviation increases with the penetration rate of connected vehicles under the medium and heavy demand cases. For the 900 vph demand case, the increase of speed deviation goes up to 48.12% with 30% connected vehicles.

Table 2.4.
Comparison of the average speed ($\leq$ 30 kph) and emissions of test case 1

Demand (vph)		Speed (kph)	Deviation (%)	CO_2 (g)	CO (mg)	NO_x (mg)	HC (mg)
300	Non-CV(Base)	10.06	0.85	561	97	2391	69
	10% CV	11.53	0.75	552	95	2341	67
	30% CV	15.95	0.58	330	54	1372	33
	50% CV	18.07	0.30	268	42	1131	22
	80% CV	18.75	0.28	206	32	797	17
	100% CV	19.95	0.20	138	24	553	12
600	Non-CV(Base)	8.87	0.98	1598	279	6846	197
	10% CV	10.83	0.75	1551	273	6628	185
	30% CV	16.61	0.42	1190	204	4930	126
	50% CV	17.52	0.32	1136	191	4640	117
	80% CV	18.84	0.23	887	147	3676	88
	100% CV	20.71	0.21	445	83	1899	53
900	Non-CV(Base)	9.52	0.85	3181	567	13834	407
	10% CV	13.18	0.60	3130	548	13519	387
	30% CV	17.34	0.32	2952	494	12566	329
	50% CV	19.61	0.23	2531	425	10932	274
	80% CV	19.83	0.22	2623	436	11647	271
	100% CV	20.32	0.22	2455	414	11564	256

How connected vehicles' proactive driving behavior will impact the deviation of speed in the network is an interesting topic. However, it is not the focus of this chapter, hence is left to future research.

Fig. 2.10. Test case 2: Manhattan downtown network

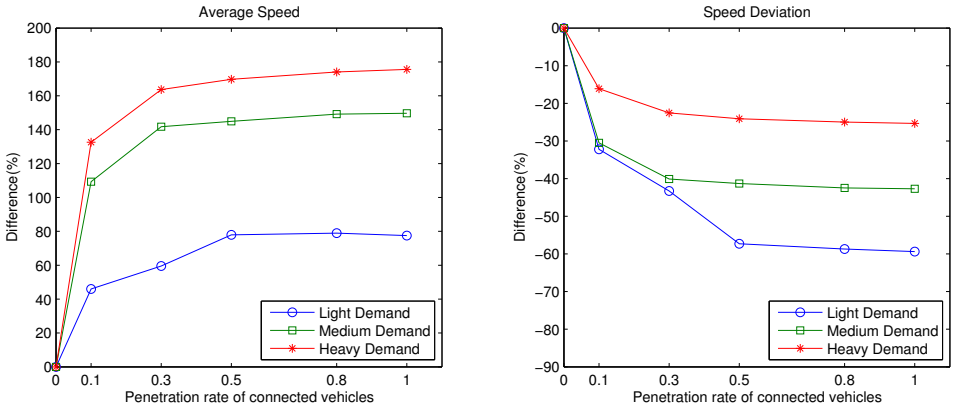

Fig. 2.11. Comparison of speed under different connected vehicle penetrations and demands

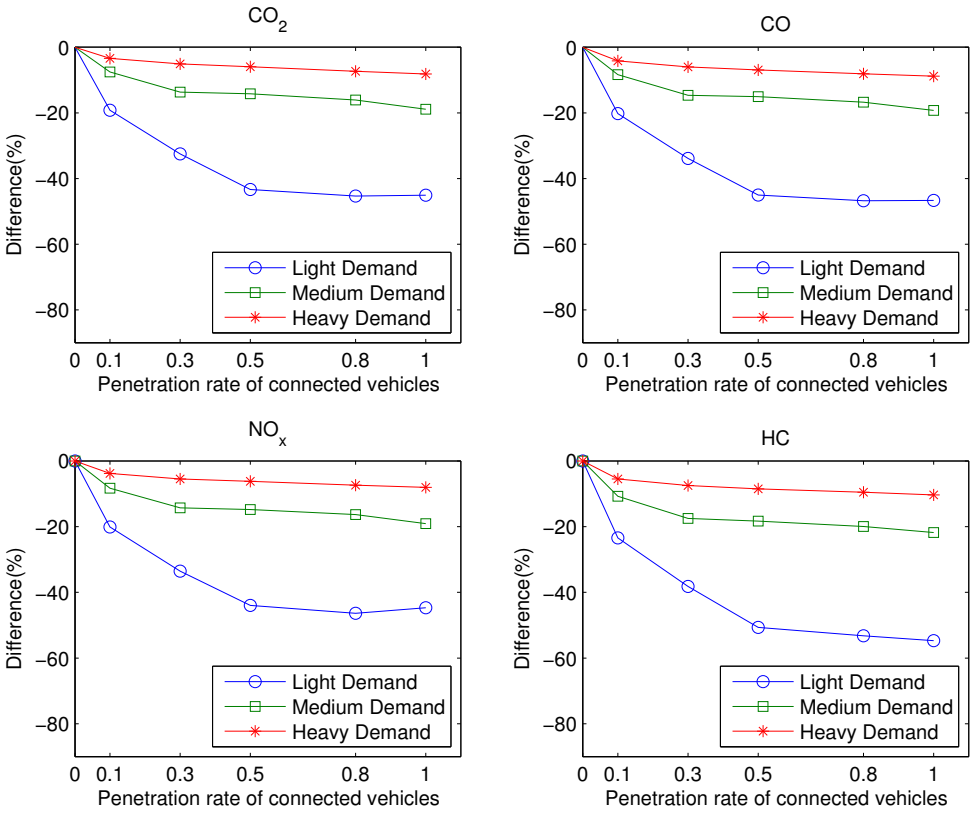

Fig. 2.12. Comparison of emissions under different connected vehicle penetrations and demands

Table 2.5.
Comparison of the average speed ($\leq$ 30 kph) and emissions of test case 2

Demand (vph)		Speed (kph)	Deviation (%)	CO_2 (g)	CO (mg)	NO_x (mg)	HC (mg)
300	Non-CV(Base)	11.94	0.77	12556	2139	53617	1533
	10% CV	17.42	0.52	10145	1706	42832	1173
	30% CV	19.05	0.44	8478	1415	35624	947
	50% CV	21.24	0.33	7114	1176	30030	756
	80% CV	21.36	0.32	6863	1139	28751	717
	100% CV	21.19	0.31	6897	1141	29644	694
600	Non-CV(Base)	6.31	1.12	55956	10253	250678	7777
	10% CV	13.21	0.78	51734	9398	229851	6939
	30% CV	15.26	0.67	48292	8752	214839	6415
	50% CV	15.46	0.66	48028	8710	213651	6351
	80% CV	15.73	0.64	46955	8536	209683	6226
	100% CV	15.76	0.64	45395	8278	202819	6081
900	Non-CV(Base)	4.18	1.21	158942	29963	726002	23182
	10% CV	9.71	1.02	153563	28712	698390	21909
	30% CV	11.01	0.94	150828	28160	686208	21446
	50% CV	11.26	0.92	149484	27894	681015	21205
	80% CV	11.44	0.91	147314	27539	672289	20970
	100% CV	11.50	0.91	145961	27316	667483	20787

2.5 Conclusions

The advent of connected vehicles brings new challenges to the research of traffic flow modeling. Due to the unique communication characteristics, connected vehicles are capable of adjusting speed pro-actively to account for the prevailing traffic conditions. This proactive driving behavior contributes significantly to the smoothing of traffic flow in the transportation network. Even in the mixed connected vehicle environment, connected vehicles may function as the leading vehicle to influence the driving behavior of the following non-connected vehicles, resulting the change of the flow pattern of entire network. This chapter firstly modifies the cell-based mesoscopic traffic flow model to track the trajectory of individual connected vehicles, then

adjusts the exit flow of the cells along the trajectory of connected vehicles to account for the proactive driving behavior. Particularly, it is shown that connected vehicles will pro-actively adjust speed to arrive at the signalized intersection when the traffic light is green. The second part of the chapter conducts two numerical tests including an intersection case and the Manhattan downtown network. To quantify the mobility benefits of connected vehicles, the mean and deviation for the speeds that are within the range of (0∼30kph) are considered as the performance measures. The mean and deviation of speed are weighted with respect to the cell density. For the purpose of comparison, we design multiple test scenarios by varying the demand levels and the penetration rates of connected vehicles. The results clearly and consistently show that the presence of connected vehicles contributes significantly to improving the average speed of the traffic flow in the network.

There are some future research directions for this study. Firstly, this study only simulates one type of proactive speed adjustment scheme (i.e., the connected vehicle decreases speed to arrive the signalized intersection exactly at the end of the red traffic light). It is worthwhile to investigate other types of speed adjustment scheme as well. Secondly, it is considered that the traffic flow (both connected and non-connected vehicles) propagates on determined routes. However, as connected vehicles are more informed about the traffic situation in the downstream network, they may alternate routes dynamically during the trip.

3. AN OPTIMAL ESTIMATION APPROACH FOR THE CALIBRATION OF CONNECTED VEHICLES

In the test bed of connected vehicles, detailed trajectory data are collected for connected vehicles only. It brings challenges to study the car-following behavior of connected vehicles following non-connected vehicles. This chapter proposes an optimal estimation approach to calibrate connected vehicles' car-following behavior in a mixed traffic environment. Particularly, the state-space system dynamics is captured by the simplified car-following model with disturbances, where the trajectory of non-connected vehicles are considered as unknown states and the trajectory of connected vehicles are considered as measurements with errors. Objective of the reformulation is to obtain an optimal estimation of states and model parameters simultaneously. It is shown that the customized state-space model is identifiable with the mild assumption that the disturbance covariance of the state update process is diagonal. Then a modified Expectation-Maximization (EM) algorithm based on Kalman smoother is developed to solve the optimal estimation problem. The performance of the EM algorithm is validated through simulation data. The second part of the chapter applies the empirical data of connected vehicles from the Michigan test bed and analyzes the mobility impact of connected vehicles with different penetration rates and demand scenarios.

3.1 Introduction

Collectively known as V2X in the United States and Car2X in Europe, connected vehicle technologies have seen a rapid growth and received tremendous interests from academics, industries, and government agencies. Though connected vehicles are still yet launched to the public, many test beds have been established in the US, Europe,

and Asia. In the US, as of the date, there are five test beds affiliated to the US Department of Transportation (USDOT) supporting the public- and private-sector testing and certification activities of connected vehicles and connected infrastructure [57]. Typically, connected vehicles are tested in a selected real world network in the presence of regular vehicles (i.e., in a mixed traffic environment where connected and non-connected vehicles coexist). In the test bed of connected vehicles, it is routine that the detailed trajectory data are recorded for connected vehicles only. This empirical data greatly assists the analysis and evaluation of the characteristic of connected vehicles. However, this data set is seemingly insufficient to study the car-following behavior of connected vehicles following non-connected vehicles.

In general, the car-following behavior in a mixed traffic environment can be divided into three cases according to the relative position of vehicles as below:

- Non-connected vehicles following connected or non-connected vehicles.
- Connected vehicles following connected vehicles.
- Connected vehicles following non-connected vehicles.

For the first case, the car-following behavior of non-connected vehicles (i.e., regular vehicles) have been well studied in the literature. For the second case, both leading and following vehicles are connected vehicles whose trajectory data are assumed known. There is a large amount of literature on calibrating the car-following behavior based on trajectory data. A brief review is presented in Section II. Challenges occur in the third case, where the trajectories of leading vehicles (non-connected vehicles) are not available.

In this study, we propose an optimal estimation approach to account for the challenge in the third case. The main contributions of this chapter are:

- An optimal estimation approach is proposed to calibrate the car-following behavior of connected vehicles (whose trajectories are assumed known) following non-connected vehicles (whose trajectories are assumed unknown).

- The trajectory of non-connected vehicles are considered as unknown states. The trajectory of connected vehicles are considered as measurements with errors. The calibration problem is formulated as to obtain an optimal estimation for both states and model parameters based on measurements.

- State dynamics are captured by the simplified car-following model with disturbances. It is shown that the customized state-space model is identifiable under the mild assumption that the error covariance of the state update process is diagonal.

- A modified Expectation-Maximization (EM) algorithm based on Kalman smoother is proposed to solve the optimal estimation problem. The performance of the EM algorithm is validated through simulation data.

- A numerical case is conducted based on the empirical data of connected vehicles from the Michigan test bed to analyze the mobility benefit of connected vehicles with different penetration rates and demands.

The rest of the chapter is structured as follows. Related work is summarized in Section 3.2. Section 3.3 is devoted to the introduction of the simplified car-following model, reformulation of the calibration problem, the detailed steps of the EM algorithm, and the validation of the algorithm through simulation data. Section 3.4 describes the trajectories data of connected vehicles in the Michigan test bed, and conducts a numerical case to analyze the mobility benefits of connected vehicles under different market penetration rates and demand scenarios. Finally, Section 3.5 concludes the chapter and discusses the direction for future research.

3.2 Related work

Heterogeneous driver's anticipation or overreaction to unexpected events such as the sudden break or deceleration of the leading vehicle is the main cause of traffic oscillations[58, 59]. For example, an aggressive driver responds differently from a

conservative driver to the speed change of the leading vehicle. Connected vehicles behave differently from non-connected vehicles due to the communication feature. The communication feature warns vehicle about the potential danger in advance and enables the vehicle to quickly and robustly respond to the speed change of the leading vehicle. Thus, the traffic oscillation (or the stop-and-go waves) reduces in the connected vehicle environment [60].

In the literature, a popular research direction to model the traffic flow with connected vehicles is by integrating the traffic flow simulation and network communication simulation. Towards this end, one approach is to develop a trace-based mobility model and then insert the trace to the network communication simulation. The trace-based mobility model can be based on either real-world observations or traffic flow simulator. E.g., In [5], the trace-based mobility model is developed by using the GPS taxi data. In [6], the trace data is generated by running the traffic simulator VISSIM [7]. One major limitation of the trace-based mobility model is that the traffic simulation and network communication simulation are independent, i.e., there is no interaction between these two simulations. Addressing this issue, in [8], a coupled simulation platform is developed integrating the network simulator OMNET++ and traffic simulator SUMO [10], which allows dynamic interaction between both simulators. In [11], the impact of the penetration rate of connected vehicles on the stability of traffic flow and road capacity is studied. In the modeling framework, the inter-vehicle communication is modeled by a VANET simulator named JiST/SWANS [12], and the traffic flow is modeled by cellular automaton. It is found that the traffic efficiency is improved even for a 5% penetration rate of connected vehicles. However, the improvement is based on the connected vehicle's willingness to adjust acceleration and speed under certain circumstances. From a different perspective, a multi-agent framework is proposed in [61] including three layers, namely, the physical layer, the trust layer, and the communication layer. The cooperative driving behavior (e.g., car-following, lane changing) of connected vehicles is modeled by integrating the three layers.

Most of the above literature relies on making assumptions on the traffic flow dynamics of connected vehicles and is short of validating the assumption through empirical data from the real world. To overcome the limitation, a handful of researchers focus on calibrating car-following models for connected vehicles. Car-following models, which describe the process that vehicles follow one another in the traffic stream, have been studied for more than half a century since its inception in 1950s and are common in microscopic traffic simulators (e.g., VISSIM, PARAMICS, SUMO). In [23], car-following models are categorized into five categories: Gazis-Herman-Rothery models [21], safety distance or collision avoidance models [22], linear models [62], psychophysical or action point models, and fuzzy-logic based models. There is a vast literature for the calibration of car-following models by making use of detailed trajectory data [63, 64, 65, 66, 67, 68, 69, 70]. However, most of them require the trajectories of both leading and following vehicles to be known. They do not address the challenge in a mixed traffic environment where trajectories of non-connected vehicles are not available.

There is limited literature studying the car-following behavior of connected vehicles based on empirical data. In [71], four types of car-following models are calibrated based on the next-generation simulation program (NGSIM [72]) data. The models are reformulated as bidirectional car-following models to account for the backward information propagation in the connected vehicle environment. However, the NGSIM data are not collected from connected vehicles. In [73], a new car-following model is proposed assuming drivers can adjust acceleration rates according to the prevailing traffic information (especially the accident condition) from inter-vehicle communication. However, the model has not been verified or calibrated through empirical data, and the effect of different penetration rates is not revealed. In [74], different types of car-following models are calibrated based on the naturalistic driving data of 100 connected vehicles collected by the Virginia Tech Transportation Institute. Though the non-connected vehicles' information are not available in the naturalistic data, the car-following event can be identified through the radar object tracking data and the

forward-facing video data. However, due to the significant errors in the object tracking, the radar data are not reliable hence all car-following events are manually verified by using the recorded video data. Finally a total data set of 1,000 min of data from the initial 30,213 min of data were identified for the car-following calibration process. Nevertheless, it is concluded in [74] that the data reduction process is complex and costly. A sound method for studying the car-following behavior of connected vehicles remains to be explored.

3.3 An optimal estimation approach

It is a challenging task to calibrate the car-following behavior based on the following vehicle's trajectory only as: (1) parameters of the car-following model are unknown; (2) headways between the leading vehicle (non-connected vehicle) and following vehicle (connected vehicle) are unknown. To address these challenges, we consider the trajectory of non-connected vehicles as hidden states and the trajectory of connected vehicles as measurements of the state with errors. The simplified car-following model is applied to describe the state update dynamics. Thus the calibration problem is formulated as an optimal estimation problem where states and model parameters are to be estimated simultaneously.

3.3.1 The simplified car-following model

In this study, we focus on the simplified car-following model proposed by [24] due to its simplicity and effectiveness in simulation, as well as its flexibility to incorporate different types of driving behaviors. In [75], the simplified car-following model is verified by the trajectory of vehicles discharging at signalized intersections. In [76], the vehicle trajectory data shows that the formation and propagation of stop-and-go traffic oscillations are caused by different driving behaviors (e.g., the timid or the aggressive driving behavior). To simulate the traffic oscillation, the simplified car-

following model is extended to the behavioral car-following model which is validated by [77] in empirical observations.

The simplified car-following model provides an exact solution to the simplified version of the Lighthill-Whitham-Richards [78, 79] hydrodynamic model, whereby the fundamental diagram of traffic flow and density is assumed to be in a triangular form. As shown in Figure 3.1a, the fundamental diagram is described by the free flow speed, V, the shockwave speed, W, and the jam traffic density. On a single lane, considering that vehicle $(i+1)$ follows vehicle i, then we have:

$$g_{t+\tau_{i+1}}^{i+1} = \min\{g_t^i - d_j, g_t^{i+1} + V\tau_{i+1}\} \tag{3.1}$$

where g_t^i denotes the position of vehicle i at time t, τ_i denotes the response time of vehicle i, and d_j denotes the jam spacial headway.

The first term of (3.1) represents the congestion condition where two vehicles are separated by the jam spacing and the response delay, while the second term represents the free-flow traffic condition where vehicles travel in free flow speed. The spacing between the leading and the following vehicle are further expressed as (Figure 3.1b):

$$s_t^i = d_j + v_t^i \tau_i \tag{3.2}$$

where s_t^i represents the spacial headway between the leading vehicle i and the following vehicle $(i+1)$ at time t.

3.3.2 An optimal estimation formulation

As the trajectory of connected vehicles are known and that of non-connected vehicles are unknown, we consider the trajectory of connected vehicles as measurements and the trajectory of non-connected vehicles as hidden states. According to (3.2), the spatial headway is linear on the speed of the leading vehicle, i.e.,

$$s_t = d + \tau v_t \tag{3.3}$$

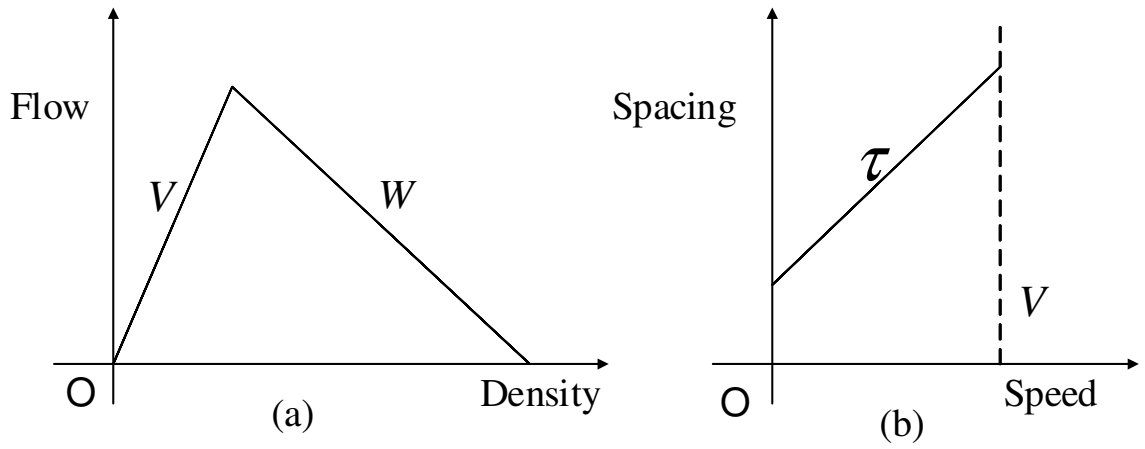

Fig. 3.1. (a) The flow-density fundamental diagram (b) The spacing-speed relationship

where the vehicle index i is omitted in the notation hereafter for the sake of brevity; d and τ are unknown model parameters.

In the literature, researchers have spent lots of efforts to calibrate the parameters for non-connected vehicles. However, little is known for the parameters of connected vehicles. The rest of this section is devoted to estimate and validate the most accurate parameters for connected vehicles.

Firstly, let g_t denote the position and v_t denote the speed of a non-connected vehicle, then we have:

$$g_{t+1} = g_t + v_t\delta + w_{g,t} \tag{3.4}$$

$$v_{t+1} = v_t + w_{v,t} \tag{3.5}$$

where $w_{g,t}$ and $w_{v,t}$ represents the disturbance of position and speed. Denote state variables in a vector form as $\mathbf{x}_t = \begin{bmatrix} g_t \\ v_t \end{bmatrix}$, then the dynamic model of states is written as:

$$\mathbf{x}_{t+1} = A\mathbf{x}_t + \mathbf{w}_t, \mathbf{w}_t \sim N(0, Q) \tag{3.6}$$

where $A = \begin{bmatrix} 1 & \delta \\ 0 & 1 \end{bmatrix}$, $\mathbf{w}_t = \begin{bmatrix} w_{g,t} \\ w_{v,t} \end{bmatrix}$, δ is the time step size. It is assumed that $\mathbf{w}_t$ follows a normal distribution with zero mean and covariance Q (unknown).

Similarly, we denote measurements as $\mathbf{y}_t = y_t$, where y_t represents the position of a connected vehicle. According to (3.3), we obtain the linear model of measurements as:

$$\mathbf{y}_t = C\mathbf{x}_t + d + \gamma_t, \gamma_t \sim N(0, R) \tag{3.7}$$

where $C = \begin{bmatrix} 1 \\ \tau \end{bmatrix}'$, γ_t represents the measurement noise. γ_t is assumed to follow a normal distribution with zero mean and variance R (unknown).

Now that we have formulated the calibration problem in the framework of linear state-space modeling (SSM). In the presentation, the latent process follows a vector autoregressive (VAR) model as shown in (3.6). The observed measurements are a linear mixture of the latent processes with white noise as shown in (3.7). In this estimation problem, both the state $\mathbf{x}_t$ and the part of the parameter matrix of the dynamic model (Q, τ, d, R) are unknown. The objective is to estimate states and model parameters simultaneously based on the measurement $\mathbf{y}$. Note that parameter matrix A and the first entry of C are known. However, if we directly apply (3.6) and (3.7) to estimate model parameters of the SSM, we may encounter the over-parameterization issue (i.e., it is possible to have an infinite number of parameterizations fulfilling (3.6) and (3.7)). This issue is also known as the lack of identifiability of SSM [80, 81]. To overcome this identifiability issue, we impose a mild assumption on the state update dynamics: there is no correlation between the position noise and the speed noise in the state update process. Then the covariance Q can be written as $Q = \begin{bmatrix} \sigma_1^2 & 0 \\ 0 & \sigma_2^2 \end{bmatrix}$, where σ_1^2 and σ_2^2 denote the variance of the position update error and the speed update error.

Notice that A is known, and parts of the parameter matrix Q and C are known. Based on these known parts, along with the mild assumption that $w_{g,t}$ and $w_{v,t}$ are uncorrelated, we show that the customized SSM is identifiable in Lemma 1.

Lemma 1. The customized SSM model given by (3.6) and (3.7) is identifiable if Q is diagonal .

Proof: Let $\Phi = \begin{bmatrix} a_1 & a_2 \\ a_3 & a_4 \end{bmatrix}$ be an arbitrary nonsingular matrix. Insert Φ into (3.6) and (3.7), then we have:

$$\Phi \mathbf{x}_{t+1} = \Phi A \Phi^{-1} \Phi \mathbf{x}_t + \Phi w_t, \Phi w_t \sim N\left(0, \Phi Q \Phi'\right) \tag{3.8}$$

$$\mathbf{y}_t = C \Phi^{-1} \Phi \mathbf{x}_t + d + \gamma_t, \gamma_t \sim N\left(0, R\right) \tag{3.9}$$

Note that A is transformed to $\Phi A \Phi^{-1}$. Since A is known, we have:

$$A = \Phi A \Phi^{-1} \Rightarrow A\Phi = \Phi A \tag{3.10}$$

Further, replace A with $A = \begin{bmatrix} 1 & \delta \\ 0 & 1 \end{bmatrix}$, we have:

$$\begin{bmatrix} 1 & \delta \\ 0 & 1 \end{bmatrix} \begin{bmatrix} a_1 & a_2 \\ a_3 & a_4 \end{bmatrix} = \begin{bmatrix} a_1 & a_2 \\ a_3 & a_4 \end{bmatrix} \begin{bmatrix} 1 & \delta \\ 0 & 1 \end{bmatrix} \Rightarrow a_3 = 0, a_1 = a_4 \tag{3.11}$$

Moreover, C is transformed to $C\Phi^{-1}$, we have:

$$\begin{aligned} C\Phi^{-1} &= \begin{bmatrix} 1 & \tau \end{bmatrix} \begin{bmatrix} a_1 & a_2 \\ a_3 & a_4 \end{bmatrix}^{-1} \\ &= \frac{1}{a_1 a_4 - a_2 a_3} \begin{bmatrix} 1 & \tau \end{bmatrix} \begin{bmatrix} a_4 & -a_2 \\ -a_3 & a_1 \end{bmatrix} \end{aligned} \tag{3.12}$$

Substituting $a_3 = 0$ and $a_1 = a_4$ into (3.12) leads to:

$$C\Phi^{-1} = \begin{bmatrix} \frac{1}{a_1} & \frac{-a_2 + a_1 \tau}{a_1} \end{bmatrix} \tag{3.13}$$

From the fact that $C(1) = 1$, we have: $a_1 = a_4 = 1$. Moreover, Since Q is transformed to $\Phi Q \Phi'$, we have:

$$\begin{aligned} \Phi Q \Phi' &= \begin{bmatrix} 1 & a_2 \\ 0 & 1 \end{bmatrix} \begin{bmatrix} \sigma_1^2 & 0 \\ 0 & \sigma_2^2 \end{bmatrix} \begin{bmatrix} 1 & a_2 \\ 0 & 1 \end{bmatrix}' \\ &= \begin{bmatrix} \sigma_1^2 + a_2^2 \sigma_2^2 & a_2^2 \sigma_2^2 \\ a_2^2 \sigma_2^2 & \sigma_2^2 \end{bmatrix} \end{aligned} \tag{3.14}$$

Since the first and the third entry of Q is known to be zero, we have:

$$a_2^2\sigma_2^2 = 0 \Rightarrow a_2 = 0 \tag{3.15}$$

In all, the arbitrary matrix Φ is restricted to be the identity matrix $\begin{bmatrix} 1 & 0 \\ 0 & 1 \end{bmatrix}$. $\square$

3.3.3 A modified EM algorithm

In the SSM model given by (3.6) and (3.7), both the latent state and model parameters are unknown. The Expectation-Maximization (EM) algorithm proposed by [82] is a potential solution for this problem. EM algorithm is a powerful tool to estimate the hidden model with missing data by maximizing the model log likelihood [83]. In [84, 85] the EM algorithm is extended in the linear state-space system to estimate latent state and missing parameters simultaneously. The EM algorithm alternates between two steps: E-step and M-step. The purpose of the E-step is to compute the expected log-likelihood based on the initiated or estimated values of model parameters, while the purpose of the M-step is to determine model parameters to maximize the expected log-likelihood function. This two-step process is iterated until the desired convergence requirement is fulfilled.

E-step of the EM algorithm

In the E-step of the EM algorithm, we apply the Kalman filter and smoother techniques [86, 87] to compute the expectation value of the state variable and other interim terms.

Firstly, denote $X_{t|n} = (X_t|Y_1 = \mathbf{y}_1, \cdots, Y_n = \mathbf{y}_n)$ as:

$$\begin{aligned} X_{t|n} = N\Big(&E\left(X_t|Y_1 = \mathbf{y}_1, \cdots, Y_n = \mathbf{y}_n\right), \\ &Var\left(X_t|Y_1 = \mathbf{y}_1, \cdots, Y_n = \mathbf{y}_n\right)\Big) \end{aligned} \tag{3.16}$$

which reads as $X_{t|n} = N\left(\hat{\mathbf{x}}_{t|n}, P_{t|n}\right)$.

The Kalman filter consists of two steps: the time update step and the measurement update step. In the time update step, we need to compute the priori distribution of $X_{t+1|t}$ from $X_{t|t}$:

$$\hat{\mathbf{x}}_{t+1|t} = A\hat{\mathbf{x}}_{t|t} \tag{3.17}$$

$$P_{t+1|t} = AP_{t|t}A' + Q \tag{3.18}$$

In the measurement update, we compute the posteriori distribution of $X_{t+1|t+1}$ as:

$$K_{t+1} = P_{t+1|t}C' \left(CP_{t+1|t}C' + R\right)^{-1} \tag{3.19}$$

$$\hat{\mathbf{x}}_{t+1|t+1} = \hat{\mathbf{x}}_{t+1|t} + K_{t+1}\left(\mathbf{y}_{t+1} - C\hat{\mathbf{x}}_{t+1|t} - d\right) \tag{3.20}$$

$$P_{t+1|t+1} = P_{t+1|t} - K_{t+1}CP_{t+1|t} \tag{3.21}$$

where K_{t+1} denotes the Kalman gain of the Kalman filter.

Note that Kalman filter only provides the forward update of the state variable, we also need to compute $X_{t|T_e}$ for $0 \leq t < T_e$, where T_e denotes the total number of time steps. The backward pass update is as below:

$$L_t = P_{t|t}A'P_{t+1|t}^{-1} \tag{3.22}$$

$$\hat{\mathbf{x}}_{t|T_e} = \hat{\mathbf{x}}_{t|t} + L_t\left(\mathbf{x}_{t+1|T_e} - \hat{\mathbf{x}}_{t+1|t}\right) \tag{3.23}$$

$$P_{t|T_e} = P_{t|t} + L_t\left(P_{t+1|T_e} - P_{t+1|t}\right)L_t' \tag{3.24}$$

The forward and backward pass process of Kalman smoother provides the needed input to compute the expected log-likelihood as below:

$$E\left(\mathbf{x}_t\right) = \hat{\mathbf{x}}_{t|T_e} \tag{3.25}$$

$$E\left(\mathbf{x}_t\mathbf{x}_t'\right) = P_{t|T_e} + \hat{\mathbf{x}}_{t|T_e}\hat{\mathbf{x}}_{t|T_e}' \tag{3.26}$$

$$E\left(\mathbf{x}_t\mathbf{x}_{t+1}'\right) = \hat{\mathbf{x}}_{t|t}\hat{\mathbf{x}}_{t+1|T_e}' + V_{t,t+1} \tag{3.27}$$

$$V_{t,t+1} = P_{t|t}L_{t+1}' + L_{t+1}\left(V_{t+1,t+2} - AP_{t|t}\right)L_{t+1}' \tag{3.28}$$

M-step of the EM algorithm

Firstly, the likelihood function of the model parameter based on $\mathbf{x}_t$ and $\mathbf{y}_t$ is given as:

$$\begin{aligned} L\left(Q,\tau,d,R|\mathbf{x},\mathbf{y}\right) &= p\left(\mathbf{x},\mathbf{y}|Q,\tau,d,R\right) \\ &= \prod_{t=2}^{T_e} p\left(\mathbf{x}_t|\mathbf{x}_{t-1}\right) p\left(\mathbf{y}_t|\mathbf{x}_t\right) \end{aligned} \tag{3.29}$$

Taking the log likelihood of (3.29) gives:

$$\ln L\left(Q,\tau,d,R|\mathbf{x},\mathbf{y}\right) = \ln \prod_{t=2}^{T_e} p\left(\mathbf{x}_t|\mathbf{x}_{t-1}\right) p\left(\mathbf{y}_t|\mathbf{x}_t\right) \tag{3.30}$$

The purpose of M-step is to maximize the expectation of the log likelihood. Thus, we have:

$$\begin{aligned} &E\left(\ln L|\mathbf{y}\right) = \\ &\sum_{t=1}^{T_e-1}\left(\frac{1}{2}\ln|Q^{-1}| - \frac{1}{2}\left(\mathbf{x}_t - A\mathbf{x}_t\right)' Q^{-1}\left(\mathbf{x}_t - A\mathbf{x}_t\right)\right) + \\ &\sum_{t=1}^{T_e}\left(\frac{1}{2}\ln|R^{-1}| - \frac{1}{2}\left(\mathbf{y}_t - C\mathbf{x}_t - d\right)^2 R^{-1}\right) + const \end{aligned} \tag{3.31}$$

where *const* denotes a constant term.

The log likelihood function can be further written as:

$$\begin{aligned} &E\left(\ln L|\mathbf{y}\right) = \sum_{t=1}^{T_e-1} \\ &\left(-\ln\sigma_1\sigma_2 - \frac{1}{2}\left(\frac{\left(\left(\mathbf{x}_{t+1} - A\mathbf{x}_t\right)_1\right)^2}{\sigma_1^2} + \frac{\left(\left(\mathbf{x}_{t+1} - A\mathbf{x}_t\right)_2\right)^2}{\sigma_2^2}\right)\right) \\ &+ \sum_{t=1}^{T_e}\left(-\frac{1}{2}\ln R - \frac{1}{2R}\left(\mathbf{y}_t - C\mathbf{x}_t - d\right)^2\right) + const \end{aligned} \tag{3.32}$$

where $\left(\mathbf{x}_{t+1} - A\mathbf{x}_t\right)_{1,2}$ refers to the first (or second) element of the vector $\left(\mathbf{x}_{t+1} - A\mathbf{x}_t\right)$.

To optimize the parameter for the deviation of position disturbance, i.e., σ_1, we have:

$$\frac{\partial E\left(\ln L|\mathbf{y}\right)}{\partial \sigma_1} = \sum_{t=1}^{T_e-1} -\frac{1}{\sigma_1} + \frac{\left(\left(\mathbf{x}_{t+1} - A\mathbf{x}_t\right)_1\right)^2}{\sigma_1^3} \tag{3.33}$$

$$\sigma_1^2 = \frac{1}{T_e - 1} \sum_{t=1}^{T_e-1} \left(\left(\mathbf{x}_{t+1} - A\mathbf{x}_t\right)_1\right)^2 \tag{3.34}$$

Similarly, to optimize the parameter for the deviation of speed disturbance, i.e., σ_2, we have:

$$\frac{\partial E\left(\ln L|\mathbf{y}\right)}{\partial \sigma_2} = \sum_{t=1}^{T_e-1} -\frac{1}{\sigma_2} + \frac{\left(\left(\mathbf{x}_{t+1} - A\mathbf{x}_t\right)_2\right)^2}{\sigma_2^3} \tag{3.35}$$

$$\sigma_2^2 = \frac{1}{T_e - 1} \sum_{t=1}^{T_e-1} \left(\left(\mathbf{x}_{t+1} - A\mathbf{x}_t\right)_2\right)^2 \tag{3.36}$$

To optimize the parameter for the critical headway, i.e., d, we have:

$$\frac{\partial E\left(\ln L|\mathbf{y}\right)}{\partial d} = R^{-1} \sum_{t=1}^{T_e} \left(\mathbf{y}_t - C\mathbf{x}_t - d\right) \tag{3.37}$$

$$d = \frac{1}{T_e} \sum_{t=1}^{T_e} \left(\mathbf{y}_t - C\mathbf{x}_t\right) \tag{3.38}$$

To optimize the parameter for the linear relationship between headway and speed, i.e., τ, we have:

$$\frac{\partial E\left(\ln L|\mathbf{y}\right)}{\partial \tau} = R^{-1} \sum_{t=1}^{T_e} \Big(\mathbf{y}_t - \left(\mathbf{x}_t\right)_1 - \left(\mathbf{x}_t\right)_2 \tau - d\Big) \left(\mathbf{x}_t\right)_2 \tag{3.39}$$

$$\tau = \left(\sum_{t=1}^{T_e} \Big(\mathbf{y}_t - \left(\mathbf{x}_t\right)_1 - d\Big) \left(\mathbf{x}_t\right)_2\right) \left(\sum_{t=1}^{T_e} \left(\left(\mathbf{x}_t\right)_2\right)^2\right)^{-1} \tag{3.40}$$

where $\left(\mathbf{x}_t\right)_{1,2}$ refers to the first (or second) element of the vector $\left(\mathbf{x}_t\right)$.

Applying (3.39) to (3.38), we have:

$$d = \frac{1}{T_e} \sum_{t=1}^{T_e} \Big(\mathbf{y}_t - \left(\mathbf{x}_t\right)_1 - \left(\mathbf{x}_t\right)_2 (\cdot)\Big) \tag{3.41}$$

where $(\cdot) = \left(\sum_{t=1}^{T_e} \Big(\mathbf{y}_t - \left(\mathbf{x}_t\right)_1 - d\Big) \left(\mathbf{x}_t\right)_2\right) \left(\sum_{t=1}^{T_e} \left(\left(\mathbf{x}_t\right)_2\right)^2\right)^{-1}$

To optimize the parameter for the variance of the measurement update disturbance, i.e., R, we have:

$$\frac{\partial E\left(\ln L|\mathbf{y}\right)}{\partial R^{-1}} = \frac{T_e}{2}R - \frac{1}{2}\sum_{t=1}^{T_e}\left(\mathbf{y}_t - C\mathbf{x}_t - d\right)^2 \tag{3.42}$$

$$R = \frac{1}{T_e}\sum_{t=1}^{T_e}\left(\mathbf{y}_t - C\mathbf{x}_t - d\right)^2 \tag{3.43}$$

Finally, the pseudo-code of the overall EM algorithm is presented in Algorithm 1.

Initialize: model parameters $\sigma_1, \sigma_2, d, \tau, R$, and $Check = 0$;
while $Check = 0$ **do**
  for *E-step(compute the expectation of the log likelihood)* **do**
    for $t = 1$ *to* T_e *//Forward pass* **do**
      Update $\hat{\mathbf{x}}_{t+1|t}, P_{t+1|t}$ according to (3.17) - (3.18);
      Update $K_{t+1}, \hat{\mathbf{x}}_{t+1|t+1}, P_{t+1|t+1}$ according to (3.19) - (3.21)
    end
    for $t = T_e - 1$ *to* 1 *//Backward pass* **do**
      Update $L_t, \hat{\mathbf{x}}_{t|T_e}, P_{t|T_e}$ according to (3.22) - (3.24)
    end
  end
  for *M-step (maximize the expectation of the log likelihood)* **do**
    Update σ_1 according to (3.34);
    Update σ_2 according to (3.36);
    Update d according to (3.41);
    Update τ according to (3.39);
    Update R according to (3.43);
  end
  If Convergence/MaxIteration is satisfied, $Check = 1$;
end

Algorithm 2: The pseudo-code of the overall EM algorithm

3.3.4 Simulation validation

It is preferable to test the performance of the EM algorithm through the empirical trajectory data. However, to the best of our knowledge, no test bed of connected vehicles has collected data for non-connected vehicles. Thus in this section we validate the performance of the EM algorithm by constructing simulation data. The validation procedure is as below. Firstly the traffic flow simulation data is constructed based on assumed model parameters for the mixed traffic environment. The trajectory of non-connected vehicles is considered as the real data in the comparison later. Then the trajectory of connected vehicles is extracted and fed into the EM algorithm. Once the convergence requirement fulfills, the EM algorithm outputs the estimated model parameters and trajectories of non-connected vehicles. Then we conduct a comparison analysis on the estimated trajectory and the real trajectory (from simulation) of non-connected vehicles.

In constructing the simulation data, in order to generate the traffic oscillation as realistic as possible, we consider three different types of driving behaviors for non-connected vehicles, i.e., aggressive, timid, and neutral driving behaviors [76, 77]. Figure 3.2 presents the demonstration of the trajectories for the three types of non-connected vehicles.

The car-following model is coded for these driving behaviors under a single lane scenario. Parameters of non-connected vehicles are applied from [76, 77]. Parameters of connected vehicles are assumed. In the simulation setting, the demand input is 600 vph, and the penetration rate of connected vehicles is 20%. Among the non-connected vehicles, the percentage of the neutral, timid, and aggressive driving behavior is assumed to be 40%, 40%, and 20%, respectively. Details of the parameter settings are presented in Table 3.1.

In the validation step, we consider three cases with varied model parameters of the SSM, as shown in Table 3.2. For each case, the trajectory of connected vehicle is extracted and considered as the only input to the EM algorithm which produces

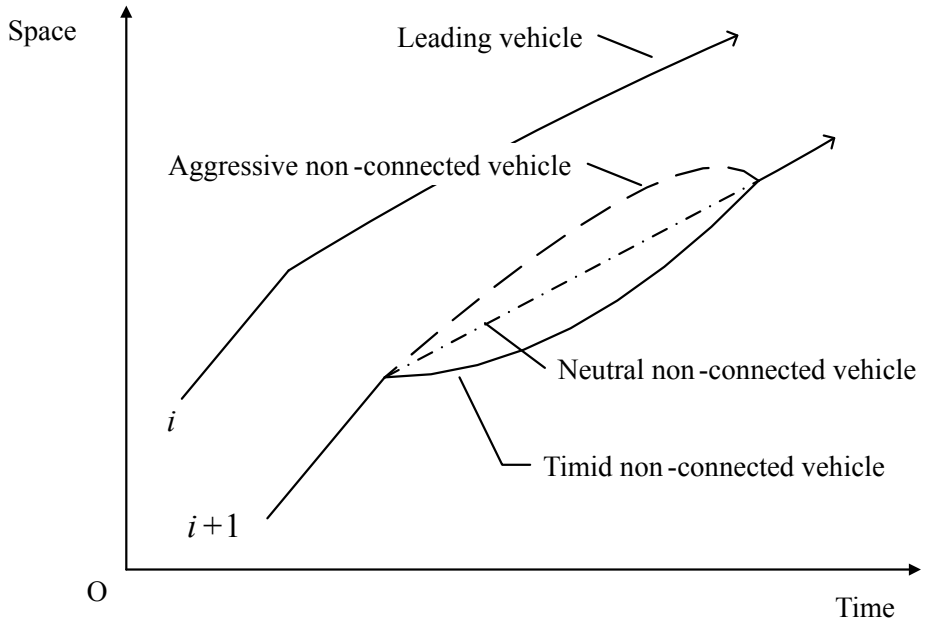

Fig. 3.2. Trajectory demonstration of different driving behaviors

Table 3.1.
Parameter settings of the simulation

Time	1800 s
Length	5000 mters
Free flow speed	50 mph
Shock wave speed ratio	0.5
Connected vehicle	Penetration:20%
Non-connected vehicle	Penetration:80%, $d^* = -20$ meters, $\tau^* = -2$
Neutral driving	Penetration:32%
Timid driving	Penetration:32%
Aggressive driving	Penetration:16%

the trajectory of non-connected vehicles and estimated model parameters. Table 3.2 presents the comparison of the estimated and true values of the model parameters. As expected, the estimated parameters and the true parameters do not always match

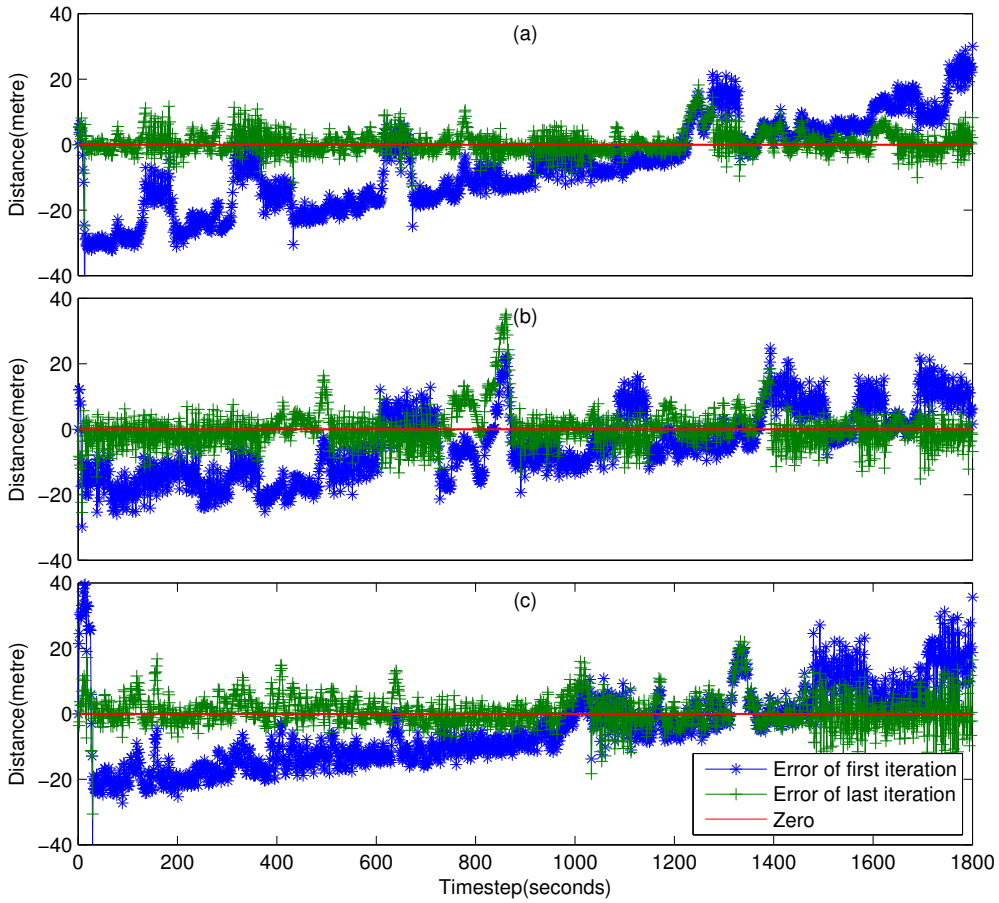

Fig. 3.3. Trajectory estimation error evolution: (a) Case 1, (b) Case 2, (c) Case 3

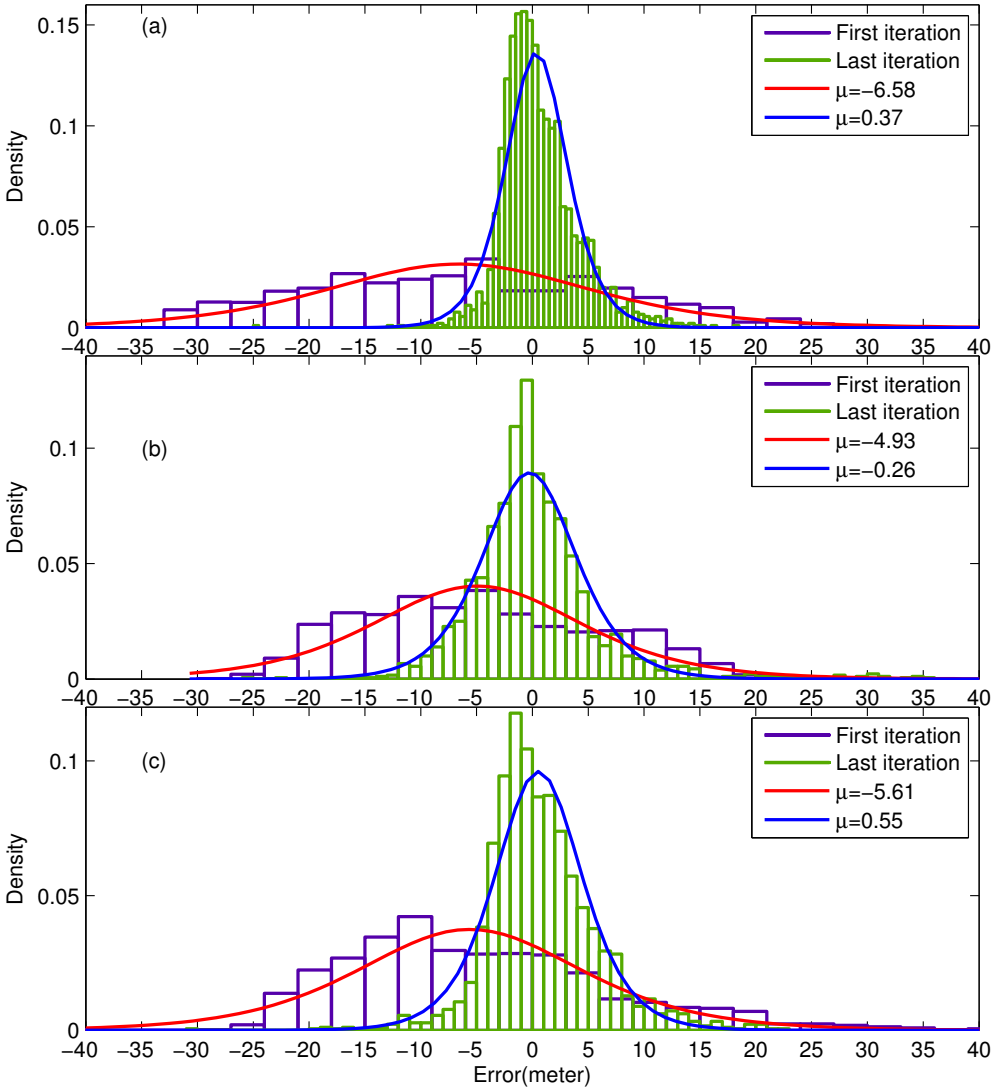

Fig. 3.4. Trajectory estimation error distribution: (a) Case 1, (b) Case 2, (c) Case 3

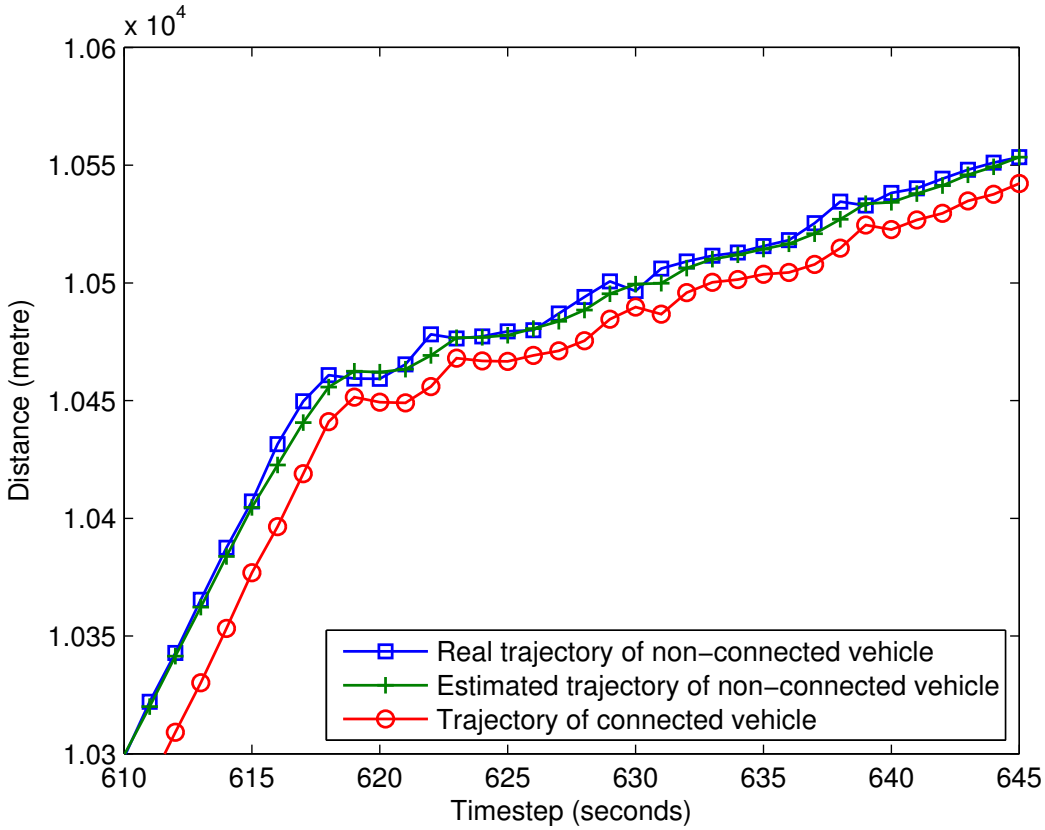

Fig. 3.5. Comparison of the estimated trajectory and the real trajectory

Table 3.2.
Comparison of the estimated and the true parameters

Parameters		d	σ_1	σ_2	R	τ
Case 1	True value	-10	1	1	1	-1
	Estimated value	-6.62	1	1	1.14	-1.23
Case 2	True value	-15	2	2	2	-1.36
	Estimated value	-18.03	2.68	1.95	2.38	-1.11
Case 3	True value	-18	3	3	3	-1.64
	Estimated value	-17.37	3.17	2.10	3.36	-1.13

due to the disturbance of the model dynamics and the challenge that both states and model parameters are unknown. Still, the difference between the estimated and true parameters are within a reasonable range. Figure 3.3 presents the evolution of the trajectory estimation error (difference between the estimated and real trajectories over time) for all the cases. For case 1 (2, 3), the mean and deviation of the error evolution are 0.64 (0.16, 0.80) meter and 3.52 (5.78, 5.02) meters, respectively. These results are encouraging. Case 2 is roughly the worst. Even in this case, the mean error is less than one meter. Moreover, the density distribution of the error evolution is presented in Figure 3.4 with the logistic distribution fitting curves. It confirms that the error course of the last iteration centers tightly around zero and significantly outperforms that of the first iteration across all three cases. Further, Figure 3.5 shows the estimated and real trajectories of a sampled (randomly selected) non-connected vehicle under case 1. Generally it is seen that the two trajectories match closely with each other. It confirms the performance of the modified EM algorithm in calibrating the car-following behavior of connected vehicles.

3.4 Numerical case study

3.4.1 Michigan test bed data analysis

The empirical data [88] in this section comes from the Michigan Test Bed of connected vehicles which is one of the Proof of Concept (POC) trials. The data were collected at test sites at Ann Arbor, Michigan, on August 25, 2008 between 16:00 and 23:20. The POC trial features fifty-two roadside equipment (RSE) stations within 45 square miles, as shown in Figure 3.6. There are 27 connected vehicles equipped with On-board Equipments (OBEs) and the Dedicated Short-Range Communications (DSRC) devices. The raw data are collected by the OBEs and the mounted sensors from the connected vehicles. Here we focus on the processed data of trajectories of connected vehicles obtained from the open-access Research Data Exchange (RDE) system [88].

Figure 3.7 presents the time-distance trajectories for a sample of connected vehicles. It is seen that the trajectories look sparse because they are only the connected vehicles' trajectories. In the mixed traffic environment, connected vehicles are mixed with non-connected vehicles. There may be non-connected vehicles traveling between connected vehicles. Still, from Figure 3.7, several observations can be made as follows. (1) The trajectories of connected vehicles also witness traffic oscillation, but the range of the oscillation is narrow. (2) The oscillation periods of connected vehicles are short. The traffic flow oscillation returns to equilibrium state quickly. (3) The spatial headway for connected vehicles is short.

Next, the trajectory data of connected vehicles are input into the modified EM algorithm, and the model parameters of connected vehicles are estimated. The estimated parameter values are as below: $Q = \begin{bmatrix} 1 & 0 \\ 0 & 1.69 \end{bmatrix}$, $C = \begin{bmatrix} 1 & -1.25 \end{bmatrix}$, $d = -8.92$, and $R = 0.42$. These estimated parameters will be applied to the numerical study in the following section.

Fig. 3.6. Location map of the road side equipment (RSE) stations [88]

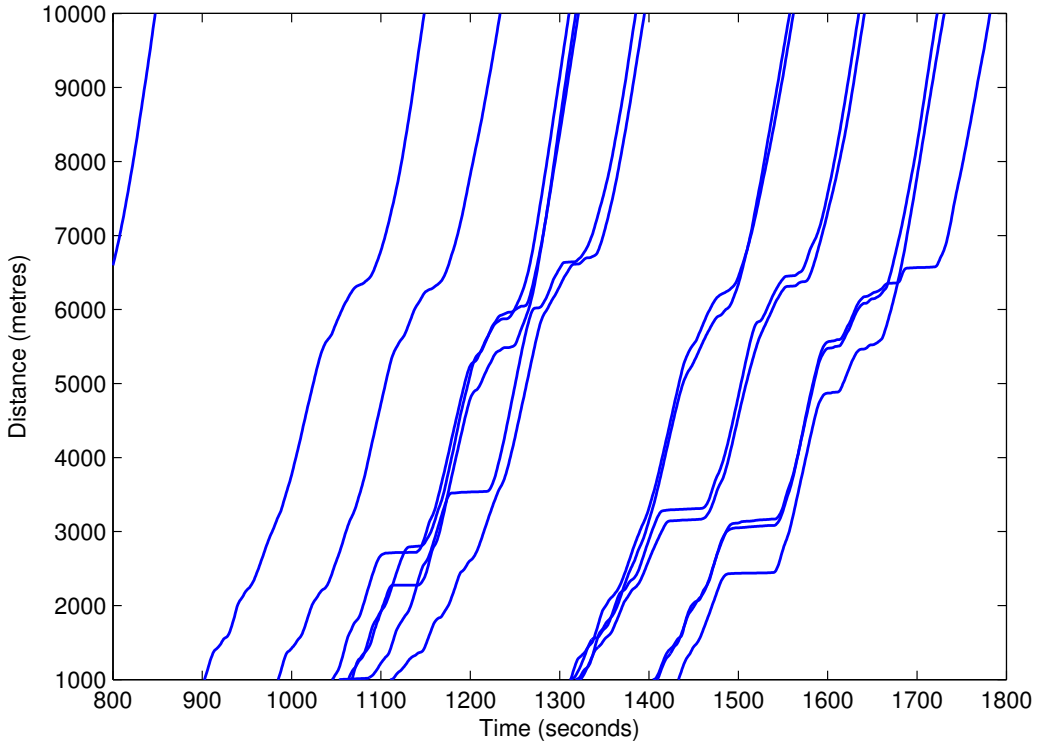

Fig. 3.7. Trajectories for a sample of connected vehicles in the Michigan test bed [88]

3.4.2 Experiment design

The purpose of this numerical case study is to test the mobility benefit of connected vehicles in the mixed traffic environment. Towards this end, we code the car-following model for a single lane scenario. Parameters of connected vehicles are estimated with the Michigan test bed data as presented in Section 3.4.1. Other parameters are the same as in Section 3.3.4 unless specified otherwise.

In the experiment design, we consider three demand scenarios including 600 vph, 900 vph, and 1200 vph to represent different levels of traffic loading. For penetration rates of connected vehicles, we consider five different scenarios include 0%, 20%, 40%, 60%, and 100%. For the non-connected vehicles, the neutral, timid, and aggressive driving behavior is assumed to account for 40%, 40%, and 20%, respectively.

For comparison analysis, we consider the total travel time and total traveled distance as the Measures Of Effectiveness (MOE). Total travel time refers to the summation of vehicles' travel time to reach the destination (set at 5000m), while the total traveled distance refers to the summed distance traveled by all the vehicles within the time period (set at 1800s).

3.4.3 Result analysis

The MOE results for different simulation scenarios are presented in Table 3.3. There are several observations from Table 3.3 as below:

- Across all three demand scenarios, the mobility benefit (in terms of both total travel time and distance) of connected vehicles is growing with the penetration rates of connected vehicles.

- The mobility benefit of connected vehicles also grows with the traffic demand. For example, with 100% connected vehicles, the total travel time reduces by 23.6% in the 1200 vph demand case, while the reduction drops to 14.6% in the 600 vph demand case.

Table 3.3.
Mobility benefit of connected vehicles under different penetration rates

Demand	MOE	CV penetration				
		0	20%	40%	60%	100%
600 vph	Travel time	0	-1.86%	-4.62%	-6.70%	-14.60%
	Distance	0	1.48%	4.01%	5.75%	13.05%
900 vph	Travel time	0	-1.48%	-5.28%	-8.05%	-17.03%
	Distance	0	2.06%	6.88%	10.48%	22.84%
1200 vph	Travel time	0	-3.64%	-6.93%	-10.46%	-23.58%
	Distance	0	5.08%	9.96%	15.63%	35.52%

- Though there is consistently positive mobility benefit for connected vehicles, the benefit is not significant under the low penetration case. For instance, in the case of 20% connected vehicles, the reduction in travel time never exceeds 4%.

- The benefit of connected vehicles is significant under the heavy traffic demand scenario. For instance, in the 1200 vph demand case, the reduction of travel time goes up to 23.6%, and the increase of traveled distance goes up to 35.5%.

3.5 Concluding remarks

This chapter is devoted to calibrating the car-following behavior of connected vehicles following non-connected vehicles based on the trajectory data of connected vehicles only. The calibration problem is formulated as an optimal estimation problem whereby the trajectory (unknown) of non-connected vehicles is considered as hidden states while the trajectory (known) of connected vehicles is considered as observations with errors. The state-space system dynamics is captured by the simplified

car-following model with unknown model parameters. As both states and model parameters are unknown, the formulated estimation problem causes the identifiability issue where there exists an infinite number of parameterizations. To solve this over-parameterization issue, the disturbance of the state update process is constrained to be uncorrelated. It is shown the customized system-space model is identifiable. Further, the Expectation-Maximization (EM) algorithm based on Kalman smoother is applied to obtain the optimal estimation of states and model parameters simultaneously. In the E-step, the Kalman smoother is employed to compute the expected log-likelihood based on the initiated (at the first iteration) or estimated (at other iterations) model parameters. In the M-step, model parameters are updated by maximizing the log likelihood of the state. As data of non-connected vehicles are rarely collected in the test bed of connected vehicles, we generate simulation data to validate the performance of the EM algorithm. In the validation, we compare the reconstructed trajectory with the real trajectory (from simulation) of non-connected vehicles. It is found that the two trajectories match closely. In the second part of the chapter, the empirical data of connected vehicles from the Michigan test bed is applied to estimate the car-following model of connected vehicles. A numerical case study is constructed to analyze the mobility benefit of connected vehicles with different penetration rates and demand scenarios. It is found that the mobility benefit of connected vehicles grows with the penetration rate and the traffic demand. The benefit of connected vehicles is especially significant under the heavy traffic demand scenario.

In the future, more and more connected vehicles may be equipped with ranging sensors such as millimeter wave radar, laser sensors, front cameras, etc. The characteristic of connected vehicles in a mixed traffic environment can be more thoroughly studied with the help of comprehensive data. However, the data reduction and fusion processes are complex and costly [74]. As a complement, this chapter provides an inexpensive solution to study the car-following behavior of connected vehicles following

non-connected vehicles based on the trajectory data of connected vehicles only. There are several limitations of this study that are worthwhile to address in the future.

- In the simulation validation section, though the error of the estimated trajectory is centered around zero, the deviation of the error evolution can go up to 5 meters. This reliability issue can be improved by collecting and incorporating the prior information about the non-connected vehicles (e.g., the headway data from the front-camera of connected vehicles).

- The most important feature of connected vehicles lies in the exchanging of short range and real time traffic information, based on which connected vehicles can alter routes or departure time. Incorporating both the cooperative driving behavior and the route choice behavior of connected vehicles will be an interesting topic.

- The empirical data from the Michigan test bed is of limited size. Given more test beds of connected vehicles are established in US, Europe, and Japan, it will be more convincing to develop and validate the car-following behavioral models for connected vehicles based on more empirical data.

Part II: Traffic Control

4. NETWORK WIDE TRAFFIC CONTROL: A COORDINATED MULTI-AGENT FRAMEWORK

This chapter develops a novel reinforcement learning algorithm for the challenging coordinated signal control problem. Traffic signals are modeled as intelligent agents interacting with the stochastic traffic environment. The model is built on the framework of coordinated reinforcement learning. The Junction Tree Algorithm (JTA) based reinforcement learning is proposed to obtain an exact inference of the best joint actions for all the coordinated intersections. The algorithm is implemented and tested with a network containing 18 signalized intersections in VISSIM. Results show that the JTA based algorithm outperforms independent learning (Q-learning), real-time adaptive learning, and fixed timing plans in terms of average delay, number of stops, and vehicular emissions at the network level.

4.1 Introduction

Vehicular traffic control on road networks is a complex decision making task in an inherently non-static environment. Heterogeneous agents (i.e., road users or vehicles, traffic controllers, pedestrians, system operators, and so on) interact with each other that shapes the dynamics of road traffic systems. Optimized traffic control systems directly contribute to travel time reduction, savings in fuel consumptions, and vehicular emissions reduction. Traffic signals are responsible for an estimated 5 to 10 percent of all traffic delays which is about 295 million vehicle-hours of delay on major roadways [89] alone. The 2012 National Traffic Signal Report Card [90] reports C grade for the current traffic signal operations and underscores the needs of optimizing traffic signals from system perspectives in a coordinated manner. Clearly there is a

need for developing efficient algorithms for coordinating traffic signals to improve the operations of traffic systems.

Recent advances in connected vehicle (CV) environment offer useful technologies in detection and acquisition of high fidelity data that can be used for more efficient traffic control strategies. CV environment facilitates communication platform where vehicles can talk to each other (Vehicle-to-Vehicle, V2V), to the infrastructure components (Vehicle-to-Infrastructure, V2I), and also infrastructure to infrastructure communication (I2I) is possible. CV has received significant attention in Europe where it is known as Car to Car (C2C) and Car to X (C2X) technology. The intelligent transportation systems (ITS) program of the U.S. Department of Transportation (DOT) emphasizes the CV research in the ITS Strategic Plan (2010-2014). Using the accessible information from the surrounding environment to develop an efficient and robust traffic control systems is of key interest to many researchers and practitioners in the traffic engineering area.

4.1.1 Related work

The signal control problem has been studies extensively in the literature. SCOOT [91], SCATS [92], PRODYN [93], OPAC [94], RHODES [95], UTOPIA [96], CRONOS [97], and TUC [98] are among the first adaptive signal control systems developed by traffic engineering community. SCOOT and SCATS are centralized systems based on real time information. OPAC and RHODES use dynamic optimization to obtain the signal settings. Further, existing literature include (not limited to) rolling horizon type of control [99], model predictive control [100], store-and-forward models for traffic control [101], mathematical programs with embedded traffic flow models [102, 103, 104, 105, 106] and so on. Most optimization models are computationally expensive and large scale implementation is often challenging. Additionally, most control schemes do not account for dynamic feedback from the traffic environment to

adjust the control scheme. In other words, control schemes do not use experience to optimize the decisions.

Identifying traffic control as a fundamental sequential decision making problem, researchers [107, 108, 109, 110, 111] applied the framework of Markov Decision Processes (MDP) and deployed approximate dynamic programming (ADP) or reinforcement learning techniques to solve the problem. RL based techniques are well suited for dynamic environment like the road traffic networks. A major advantage can be gained in terms of computational complexity because no optimization is necessary in real-time. In addition, the implementation of RL-based algorithms can be paired up with connected vehicle (CV) paradigm which is expected to play a significant role in the next generation intelligent transportation systems.

The coordinated signal control problem well fits into the coordinated multi agent system framework and researchers from diverse areas have studied the potential and applicability of RL algorithms to solve the traffic control problem. [112] proposed cooperative signal control scheme with a combination of evolutionary algorithm and reinforcement learning techniques. [113] introduced a hierarchical multi agent system to design a coordinated traffic light system. [114] proposed co-learning algorithms at network level to minimize the waiting time for the vehicles. The concept of co-learning was introduced that allows both cars and traffic lights to learn from the environment. [108] proposed a single stage coordination game for the synchronization of traffic signals. The concepts of evolutionary game theory are applied and the analyst has to define the payoff matrices. [111] recently developed a neighborhood coordinated RL based signal control that applies a joint decision framework. Other approaches include distributed constrained optimization with centralized cooperative [115], decentralized swarm based models [116], Tabu search [117], self organizing maps [118], mixed approach of RL and supervised learning [109].

Application of graphical models in the area of multi-agent coordination (especially to compute the best joint actions for multi-agents) is not common. Recently, max-plus algorithm [119, 120] has drawn the attention of a handful of researchers to solve traffic

control problem. Max-plus algorithm origins from the max-product or the max-sum algorithms [121] which is common in graphical models. [122] applied the algorithm as a coordinating strategy in the network-wide signal control problem. However, the max-plus algorithm has two key limitations.

First, it is only applicable to tree-structured networks. For general cyclic networks it cannot guarantee the convergence to an optimal solution, because the message passing in max-plus algorithm is directional. For cyclic graphs, the message passing can visit some node for multiple times. For some application it may converge, where as for others, it may not. Since cyclic structures are not uncommon in real world road networks, the quality of solution is compromised. Second, the same as the max-sum algorithm, the max-plus algorithm only provides a loopy brief propagation. Loopy brief propagation refers to the inexact messages received at a node. As there is loop in the graph, the algorithm may stop according to some criterion even if the convergence is not met. The message of a node is calculated using the most recently received incoming message. Hence the algorithm only provides an approximate inference of the exact message passing.

4.1.2 Contributions of the chapter

A potential alternative to max-plus is the junction tree based algorithm. In this study, we extended the junction tree algorithm (JTA) to obtain the best joint actions for the entire traffic network. Compared with the max-plus algorithm, JTA is an exact inference procedure capable of dealing with graphs having loops. However, JTA is originally developed to solve the general inference problem in graphical models. Accordingly, it is not readily applicable to the coordination problems in the context of traffic signal control.

To the best of our knowledge, JTA has not been applied to address the coordinated signal control problem. The advantages of proposing the JTA based RL algorithm to solve the coordinated signal control problem are as follows:

(a) it is computationally efficient.

(b) it is applicable to general cyclic or acyclic networks.

(c) it provides an exact inference of best joint selection.

(d) it has an intrinsic property that has potential to assist traffic control decision making, e.g. green wave corridor selection or link capacity improvement design.

Further, sustainable mobility has gained attention among the researchers [123, 124] and practitioners as an important element of sustainable development. Air quality and energy security in the context of urban transportation require effective policies and efficient traffic operations. Control algorithms must focus not only on the mobility aspect but also on the environmental impact of the implemented schemes. This research aims to assess the environmental benefits of the proposed control algorithm using the state-of-art emissions simulator MOVES2010.

To summarize, the research goals are:

(a) To propose multi-agent RL based signal control algorithm where agents coordinate their decisions for the benefit of the system

(b) To demonstrate the coordinated control algorithm as a potential application in the CV environment

(c) To assess the environmental impacts of the proposed controller using a dynamic emissions simulator (MOVES2010)

4.2 Introduction of Junction Tree Algorithm in signal coordination

The junction tree algorithm(JTA) originally comes from the area of machine learning in computer science. It is developed to solve the general inference problem in graphical models, which is to calculate the conditional probabilities of a node or a set

of nodes given the observed data. Hence JTA is not readily applicable to the coordination problems in the context of traffic signal control. To the best of our knowledge, junction tree algorithm has not been developed to address the coordinated graph problem as well.

However, the conditional probability inference problem in graphical models shares similarity with the coordination problem. One typical way of calculating the conditional probability is to apply the maximum a posteriori (MAP) method[125], which is to maximize the posteriori probability of the data, as shown below:

$$\max P(E|A) = \max \frac{P(A|E)P(E)}{P(A)} \ \max P(A,E) \tag{4.1}$$

Where A is the observed data, E is the prior parameter. Hence, $P(E|A)$ denotes the posterior probability.

Maximizing the posterior probability is the same as maximizing the joint probability, $P(A,E)$, as $P(A)$ is a constant. The joint probability $P(A,E)$ can be expressed in a general form by introducing the potential functions, which gives $P(A,E) = \prod_{i=1}^{N} \psi_i$. N denotes the number of nodes. By further taking the logarithm, we get that (4.1) is equal to:

$$MAP : \max \sum_{i=1}^{N} \ln \psi_i \tag{4.2}$$

On the other hand, the objective of the multi-agent reinforcement learning algorithm is to maximize the linear summation of the local Q values, which is written as:

$$\max Q = \max \sum_{i=1}^{N} Q_i \tag{4.3}$$

Comparing (4) and (5), we see that the best action selection problem in coordinated graph is analogous to maximizing the joint probability in probabilistic model. Both of the objectives optimize the performance of the entire network by decomposing the network into local sub-problems. Further more, both maintain the Markov properties. In probabilistic models, the probability of a node is dependent on its

adjacent node in a sequential manner. Similarly, in coordinated graph, the actions taken by one node are dependent on the actions taken by its adjacent node sequentially. Message-passing (also known as brief propagation) algorithms are promisingly plausible in the area of coordinated graph problems, as they make full use of the sequential dependencies between nodes. As an efficient message-passing algorithm, the Junction Tree Algorithm has great potential in solving the coordinated signal control problems. Solutions to the generalized vehicular traffic control mostly report the schedule of the signal phases(stage) in the timing plan and optimal duration of green time. A set of non-conflicting allowable movements is defined as phase or stage. As described earlier, coordinated signal control systems require to make the decisions from the system perspective. In other words, the agents (i.e., the controllers) work towards a general goal through coordination.

4.3 JTA based RL framework to solve the signal coordination problem

In this section, we thoroughly discuss the JTA based RL approach to solve the signal coordination problem. Firstly, we briefly explain the defined elements of RL in the context of traffic signal control, including the definition of state, action, and reward. Secondly, the best joint actions inference is obtained through the Junction Tree Algorithm. Finally, we present the step-by-step procedure of the solution algorithm to solve the problem.

4.3.1 Elements of the reinforcement learning framework

In the context of RL, the traffic network is the environment and the traffic controllers act as agents. An agent takes action by activating a particular phase at the decision interval and the state of the environment changes accordingly. The solution algorithm has to determine the optimal policy (mapping between the phase-activation and traffic states) that gives the maximum reward (e.g., average delay, number of stops, etc). The reward is obtained directly from the simulator of the environment

and one can observe the transition of the states. More details can be found in [126] and [127]. Three major components (state, action, and reward) of the RL framework are described as follows:

State definition

Before defining state, we need to define the residual queuing state for each lane group served by the signal phases at the intersection. Residual queuing state for lane i, is defined as:

$$w_p^t = \frac{q_i^t}{J} \times \frac{1}{l_i} \tag{4.4}$$

where w_p^t denotes the residual queuing state for phase p at step t, q_i^t denotes the queue length for lane i at time t, J denotes jam density, and l_i denotes length of lane. State in the context of signal control is a measure of the real time traffic environment, or the evolution of traffic flow. Note that the evolution of traffic flow is a continuous process, hence the state space is an infinite set. However, setting the state with high dimensions increases the computational complexity of the problem (curse of dimensionality). Here we define state at the phase level of an intersection and characterize the state of each phase into three discrete congestion levels: low, medium, and high. Specifically, the discretization of state for a phase is defined as:

$$\pi_p^t = \begin{cases} low & \text{if} \quad w_p^t \leq \theta_1 \\ medium & \text{else if} \quad w_p^t \leq \theta_2 \\ high & \text{else if} \quad w_p^t \leq \theta_3 \end{cases} \tag{4.5}$$

where π_p^t denotes the state of phase p at step t, and θ are configurable threshold parameters.

Action definition

An agent takes an action by switching on any of available phases in the signal timing plan. One should note that, there is no restriction on the sequence of the

phases. Flexible sequence in signal timing plan has been used by previous researchers and has been implemented in real world signalized intersections. Additionally,, the algorithm follows the minimum and maximum green constraints.

Reinforcement learning algorithms in general require a balance between exploitation and exploration in the strategies for selecting optimal action. To balance between exploitation and exploration, we apply the $\varepsilon-$ greedy method [126]. In this method, the agents behaves greedily by choosing the action that gives the maximum state-action value in most cases except at some cases it chooses a random action. The probability of this random behavior is ε and the probability of selecting the optimal action converges to greater than $1 - \varepsilon$.

Reward definition

Rewards can take many forms such as delays, stops, queue lengths. In this study, we define the length of all the queues for each phase as the reward for taking an action. Queue length is defined as the length of stopped vehicles at the intersection on red in real time.

4.3.2 Best joint action inference from JTA

Junction tree is a clique tree possessing the property that for every pair of cliques V and W, all cliques on the path between V and W contain $V \cap W$. The concept of clique refers to a subset of nodes contained in the graph where each pair of nodes are connected (in the context of signal control, it refers to a subset of signalized intersections). The general junction tree framework (the Hugin algorithm) contains the following five principal steps [125, 128].

a.Moralization

The moralization step applies to directed graphs. It converts a directed graph into an undirected graph by adding a link between any pair of variables with a common

child, and dropping the direction of the original links. The resulting graph is the moral graph.

b.Introduction of potential

Consider a directed chain as shown in Figure 1 (a), we get the joint probability as:

$$p(U) = p(A|B)p(B|C)p(C|D)p(D) \tag{4.6}$$

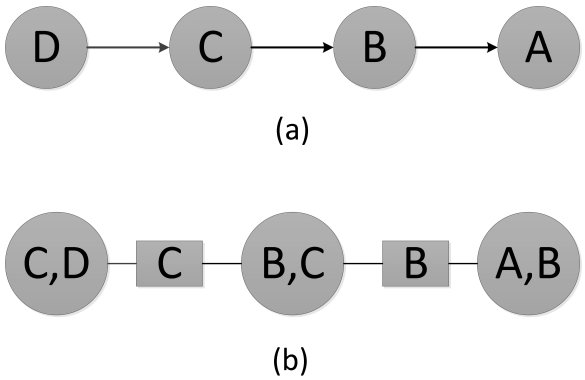

Fig. 4.1. (a)Directed chain network.(b)Cluster network

In the cluster graph network (Figure 1 b), we introduce a new term named potential to describe the characterization of the cluster. Let $\psi(A,B) = p(A|B), \psi(B,C) = p(B|C), \psi(C,D) = p(C|D)p(D), \psi(B) = 1, \psi(C) = 1$, (4.6) can be rewritten as:

$$p(U) = \frac{\psi(A,B)\psi(B,C)\psi(C,D)}{\psi(B)\psi(C)} \tag{4.7}$$

c.Triangulation

From the moralization step, we obtain a cluster tree, however it is not sufficient to show that we can form a junction tree out of the cluster graph. The triangulation operation guarantees that the resulted junction graph has a junction tree. To triangulate the graph, we ensure that every cycle or loop of length 4 or more has a chord. After the triangulation operation, cliques are different from the original junction graph. The potential of the new clique will be the product of the potentials of

original clique contained within the new clique.

d.Construction of junction tree

Note that not every clique tree obtained after the triangulation operation is a junction tree. A clique tree is a junction if and only if it is a maximal spanning tree. Hence we can construct a junction tree by finding the maximal spanning tree. To find the maximal spanning tree, the weight of the tree is equal to the sum of cardinalities of separators.

e.Propagation of messages

Initially, potentials for all the separator nodes are set at unity. One clique is selected as a root clique. Message passing from root node to leaves is called forward message passing, while message passing from leaves to root is called backward message passing.

A node v can send exactly one message to a downstream neighbor w through separator s when v has received messages from each of its upstream neighbors(the structure of the nodes is shown in Figure 2).

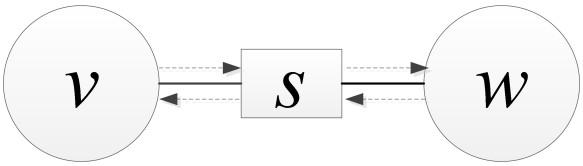

Fig. 4.2. Message passing demonstration

Endow cliques v and w with potential ψ_v,and ψ_w, and separator s with potential ϕ_s. In the forward message passing, we update the potential of s and w as:

$$\phi_s^{'} = arg_{v/s} \max \psi_v \tag{4.8}$$

$$\phi_w^{'} = \frac{\phi_s^{'}}{\phi_s} \psi_w \tag{4.9}$$

(4.8) maximize the potential ψ_v with respect to s and (4.9) re-scales the potential on w. After the forward message updating, the backward updating is processed in a similar way:

$$\phi_w^{''} = arg_{w/s} \max \psi_w^{'} \tag{4.10}$$

$$\phi_v^{''} = \frac{\phi_s^{''}}{\phi_s} \psi_v^{'} \tag{4.11}$$

Remark: The proposed JTA algorithm requires the realization of connected vehicle environment for an effective implementation. The I2V communications allows the controller to estimate the congestion level and accordingly the state for the JTA algorithm. Note that, video cameras, or loop detectors can also provide similar information. The key element in the context of coordinated control is the I2I communications. By means of I2I communications, the controllers share information and take the best joint decisions. The road side equipment (RSE) assists the coordination of the controllers. Since the coordination primarily requires I2I communication, the impact of the market share of equipped vehicles is expected to be minimal. The technology to enable I2I can be either dedicated short range communications (DSRC) or cellular networks. We acknowledge that the performance of the wireless technology (in terms of latency, robustness, and scale) will impact the coordinated control. However, this is beyond the scope of this chapter and will be a topic of our future research.

Initialize: $\psi_c = Q_c, \forall c \in Cliques$; $\psi_s = Q_s, \forall c \in Separators$; $Check = 0$;
while $Check = 0$ **do**
  Forward message updating;
  for *every agent* i **do**
    for *all neighbors of forward direction,* $j = \Gamma(i)$ **do**
      if $j \in Cliques$ **then**
        $\psi_j^{'} = \psi_j \frac{\psi_i^{'}}{\psi_i}$
      end
      if $j \in Separators$ **then**
        $\psi_j^{'} = \max_{I/j} \psi_i$
      end
    end
  end
  Backward message updating;
  for *every leaf* i **do**
    for *all neighbors of backward direction,* j **do**
      $\psi_j^{''} = \max_{I/j} \psi_i^{'}$;
      $A_j = arg \max_{I/j} \psi_i^{'}$
    end
  end
  If every node in $G(V, E)$ has been visited, $Check = 1$;
end

Algorithm 3: Junction Tree Algorithm to obtain best joint action

4.3.3 The whole procedure of the JTA based RL framework

With all elements set up for the reinforcement learning framework, we are now ready to present the whole picture of the framework. For the traffic dynamics in the network, there are two distinct properties: the similarity of traffic pattern (e.g., the traffic pattern at a particular link on each Monday during 11am-noon) and heterogeneity in the network congestion. To account for these attributes, this research deploys an average reward technique which is also known as advanced off-policy R-Learning [126]. We refer to this algorithm as R-Markov Average Reward Technique (R-MART). The step-by-step flowchart of the R-MART algorithm in the context of the signal coordination problem is presented in Figure 4.3.

Like most RL based schemes, the proposed algorithm has two phases: learning phase and implementation phase. The implementation phase takes place after the learning phase. The key difference in the techniques stated above is the process of updating the state-value function. During the learning phase the agents update the state-action value by interacting with the environment. Balancing the exploration and exploitation is important at this phase. Initially, the algorithm starts with $\varepsilon - greedy$ using higher ε value. Then the ε value gradually decreases towards the end of the learning phase. During the implementation period, the algorithm emphasizes on exploitation with very small value. Since the only change from the learning to implementation phase is the action selection strategy, only the learning phase algorithm is described in the flowchart.

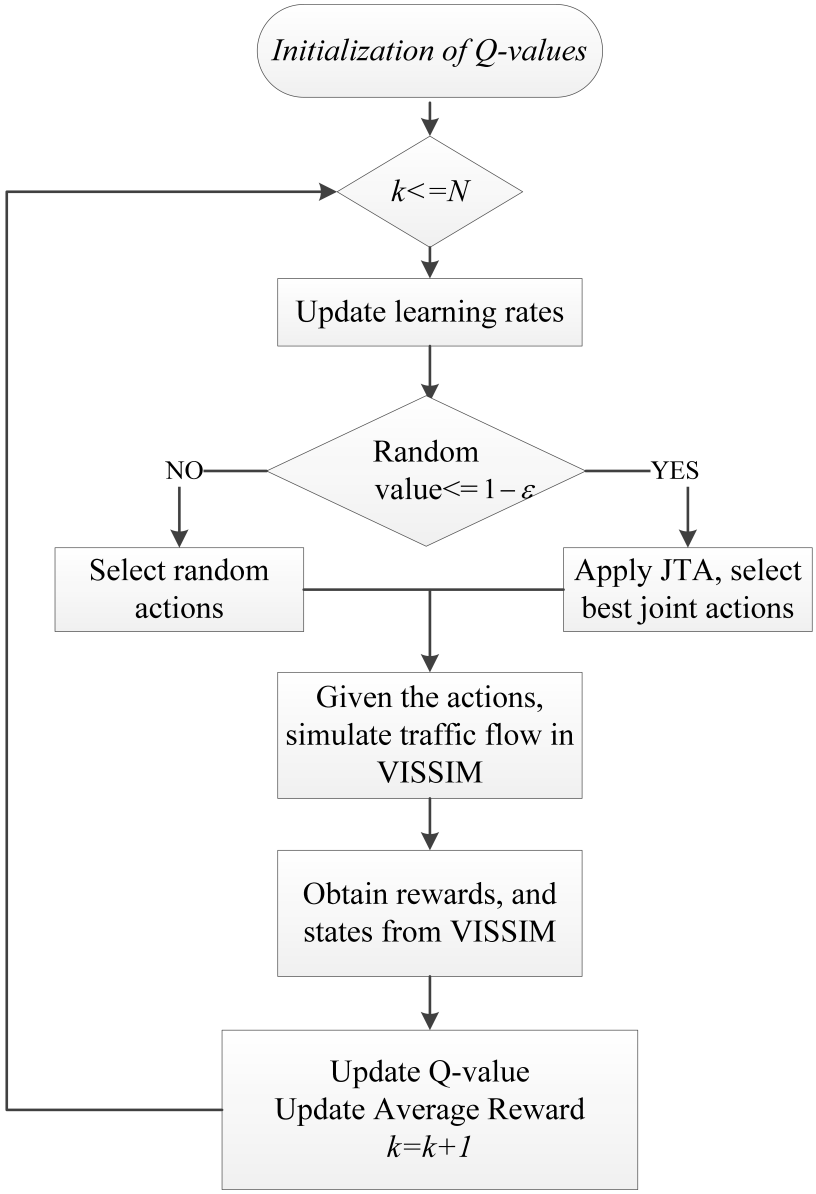

Fig. 4.3. Flow chart of the JTA based RL algorithm

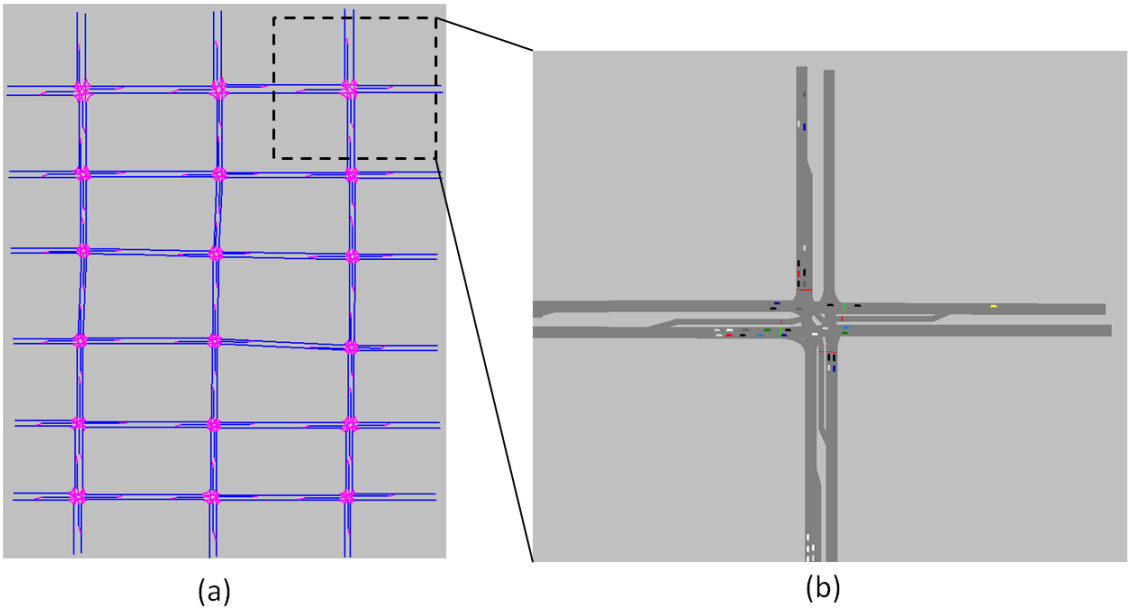

Fig. 4.4. (a)Center line representation of the network (b)Zooming in of one intersection

4.4 Test case study

This research uses traffic simulation tool VISSIM [129], which is a widely used traffic flow simulator by practitioners and researchers in traffic engineering area, to mimic the environment. The rewards and other performance metrics are obtained directly from VISSIM. Details about the modules in VISSIM (e.g., car-following, lane-changing, traffic light control, etc.) can be found in VISSIM manual [129]. The JTA based RL algorithm is coded in VB.net interacting with VISSIM through the Component Object Model (COM) interface. Note that JTA algorithm can be applied to any traffic flow model that simulates the environment.

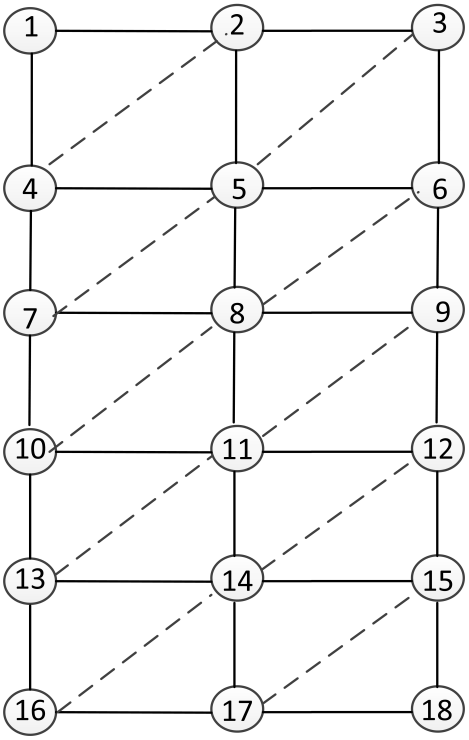

Fig. 4.5. Triangulation of the test network

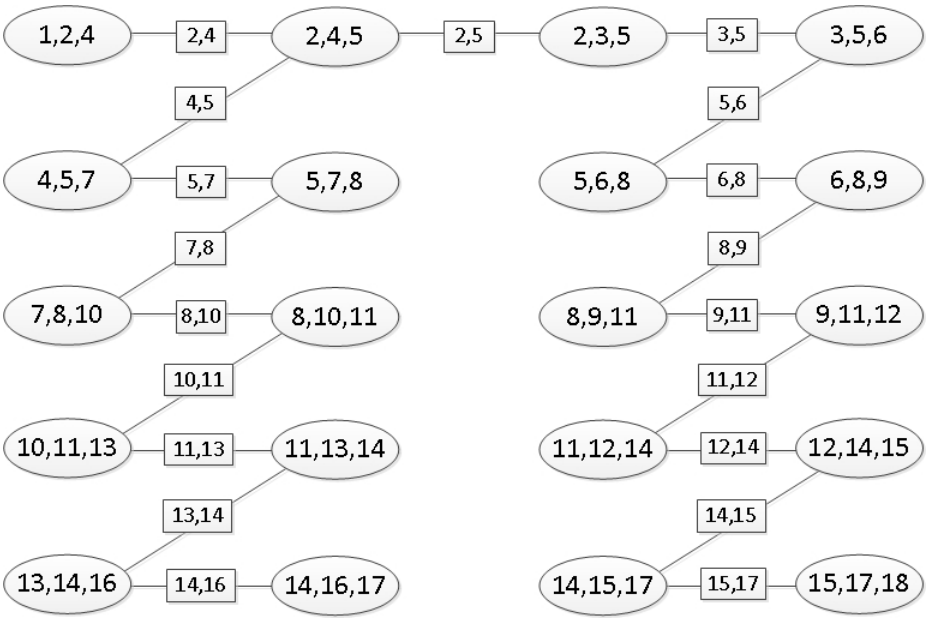

Fig. 4.6. Junction tree construction of the test network

4.4.1 Network description

The test network containing 18 intersections is shown in Figure 4.4 (a). The road segments in the network are of varied length ranging from 50 meters to 260 meters, and are of varied lane patterns (e.g., exclusive left lane, yielded right lane). The enlargement of one intersection is provided in Figure 4.4 (b). The preliminary step is to transform the given network into a junction tree structure network. The transformation process does not require much effort since the connectivity of a common traffic network is hardly dense (typically connectivity only establishes between physically adjacent intersections). To perform the transformation, we firstly triangulate the network by connecting the diagonal intersections within a grid (as shown in Figure 4.5), then apply a maximum spanning tree search algorithm on the triangulated network to obtain the final junction tree network (as shown in Figure 4.6).

In the test study, all 18 intersections in the test network are considered as coordinated intersections. We consider four phases:(a) E-W+W-E bound through and right turn, (b) N-S+S-N bound through and right turns, (c) Dual left from E-S+W-N bound, (d) dual left from S-W+N-E bound. The performance of JTA algorithm is tested at three levels of congestion: low, medium, and high. Traffic demand is input into the network through the 18 link origins in Figure 4.4. The congestion levels of low, medium, and high are reflected on the range of the demand input, which are 500 vph to 600 vph, 600 vph to 800 vph, and 900 vph to 1200 vph, respectively. We do not use the dynamic traffic assignment (DTA) feature of VISSIM (as DTA is not the focus of this study) but model the route choice behavior by setting the turning ratios of intersections as exogenously determined parameters.

4.4.2 Measures of effectiveness (MOEs) and experiment design

The evaluation metrics are: average delay per vehicle, average stopped delay at intersection per vehicle, and the average number of stops per vehicle. Note that, the number of stops is expressed as a fraction in the results. This is because the total

number of stops is averaged over the total number of vehicles passing the intersection during the simulation period. Moreover, the algorithms are also evaluated with respect to vehicular emissions including CO, GHG, NO_x, volatile organic compounds (VOC), PM_{10} and total fuel consumption. We use MOtor Vehicle Emission Simulator (MOVES2010b), developed by the U.S. EPA [130] to estimate the emissions.

To demonstrate the benefits of coordinated learning based algorithm, we compare the results from JTA algorithm with two specific classes of controllers: learning based controller without coordination, and real-time adaptive controller. Q-leaning based control schemes [107] without coordination are quite common in the literature. This research adapts Q-learning with an additional feature of neighborhood information sharing. The controller can share congestion information with its neighborhood controllers. Further, a variant of the Longest-Queue-First (LQF) algorithm [131] is chosen as a representative of real-time adaptive controller. To improve the efficiency of the LQF algorithm certain changes were made. The changes include provision for minimum and maximum green in the signal timing plan and adjustment for repetitive phases for the case when a particular approach is highly congested compared to all other approaches. Note that, there exist other learning based, and real-time adaptive controllers in the literature and practice. It is not feasible to compare with all other algorithms and accordingly, we choose these two as representative control schemes.

4.4.3 Statistical tests

It is important to conduct statistical tests to justify the findings from simulation based results. A sample containing 10 simulation runs (each with a different random seed) is collected from VISSIM. With unknown standard deviation we assume Student t distribution for the tests. The mean values of travel delay, stopped delay, and number of stops are reported at 95% confidence interval. The range of values in the population is determined as follows:

$$\bar{X} - t_{\alpha/2}(\frac{s}{\sqrt{n}}) < \mu < \bar{X} + t_{\alpha/2}(\frac{s}{\sqrt{n}}) \tag{4.12}$$

Where,

$\bar{X}$ = mean of the sample,

s = standard deviation of the sample,

μ = mean of the population,

n = sample size (10 in our case),

$t_{\alpha/2}$ = value from t distribution using degrees of freedom $(n-1)$.

Table 4.1 shows an example for JTA algorithm. The values represent the range in population. For instance, Table 4.1 reports the population mean range for stopped delay per vehicle at high demand as $5.17 < \mu < 5.75$. This implies that, with 95% confidence the population mean of stopped delay per vehicle at high demand lies between 5.17 and 5.75 seconds. Note that, similar tables can be produced for other algorithms. We report Table 1 as a sample.

4.4.4 Assessment of results at the system level

Independent (Q-learning) vs. coordinated (JTA) RL algorithms

Table 4.2 compares the system level metrics for JTA and Q-learning. Our test results show that both average delays and stopped delays per vehicle are lower for JTA when compared with Q-learning. We observe similar trends at all levels of congestion. Further, JTA yields fewer number of stops per vehicle at low and medium congestion levels. However, Q-learning has fewer stops per vehicle at high congestion level. At high congestion, JTA coordinates the actions of the controllers so that the queue lengths of the intersections can be minimized. To prevent queue spill-back in the downstream intersections, it is possible that JTA restricts vehicular flow at upstream intersections resulting in higher number of stops at high congestion.

Table 4.1.
Mean values of performance measures at 95% confidence interval for JTA algorithm (delay and stopped delay measures are expressed in seconds per vehicle)

Congestion level	Performance metric	Mean value	Population mean range
Low	Delay	6.24	$5.99 < \mu < 6.47$
	Stopped Delay	3.03	$2.85 < \mu < 3.21$
	No. of Stops	0.47	$0.46 < \mu < 0.48$
Medium	Delay	6.33	$6.04 < \mu < 6.62$
	Stopped Delay	2.88	$2.67 < \mu < 3.09$
	No. of Stops	0.48	$0.47 < \mu < 0.49$
High	Delay	11.22	$10.73 < \mu < 11.71$
	Stopped Delay	5.46	$5.17 < \mu < 5.75$
	No. of Stops	0.78	$0.73 < \mu < 0.82$

Further, we also report the results for the Max-plus [120] algorithm. Although the results show better performance for JTA compared with Max-plus, a rigorous conclusion cannot be made. Both Max-plus and JTA follow similar principles for coordination. The difference lies only in the convergence property for cyclic networks. To justify the better performance of JTA compared with Max-plus, we need to run numerous cases (both cyclic and acyclic networks) for significantly long durations. Note that, our goal is provide an alternative to Max-plus that can ensure convergence for cyclic networks.

The better performance of JTA at system level can be attributed to its ability to coordinate decision made by the agents (i.e., the signal controllers). Q-learning without any coordination allows the controller to take decisions that may be optimal to the local intersection only. On the contrary, JTA allows controllers to take decisions that aim to optimize the performance of the system as a whole.

The results from our experiment indicate that coordinated learning of signal controllers can lead to reduced delays at system level.

Table 4.2.
Independent vs. coordinated control: comparison between JTA and Q-learning

Congestion level	Algorithm	Delay (in seconds)	Stopped delay (in seconds)	Stops
Low	Q-learning	6.81	3.59	0.48
	Max-plus	6.55	3.31	0.48
	JTA	6.24	3.03	0.47
Medium	Q-learning	9.60	5.60	0.58
	Max-plus	6.36	2.89	0.48
	JTA	6.33	2.88	0.48
High	Q-learning	14.98	11.42	0.56
	Max-plus	11.83	5.90	0.79
	JTA	11.22	5.46	0.78

Learning based vs. real-time adaptive controllers

Table 4.3 compares the results from JTA with the real-time LQF controller. Also, we report the results of fixed timing plan (Webster's formula) which is commonly used in urban networks. At all levels of congestion in our experiment, JTA yields better system metrics when compared with LQF and fixed timing plans. Only exception is that average number of stops at low and high levels of congestion, where LQF performs better than JTA. This may result from the fact that JTA uses queue length as the reward and there is no explicit consideration of number of stops in the reward for the analyses reported here.

Learning based algorithms differ from adaptive real-time approaches in several ways. Major advantages of learning based algorithms include: a) memory from previ-

ous experiences offering more efficient improvements, b) direct interactions with the environment aiming at long term rewards, c) no involvement of optimization modules that significantly reduces the complexity for large scale implementation. The learning based controller may not initially perform well. When it is being trained sufficiently, the performance gets better with time (see Figure 4.7) .

Table 4.3.
Learning based vs. real-time adaptive controllers: comparison between JTA and LQF

Congestion level	Algorithm	Delay (in seconds)	Stopped delay (in seconds)	Stops
Low	LQF	7.07	3.99	0.44
	Fixed timing	15.79	11.93	0.58
	JTA	6.24	3.03	0.47
Medium	LQF	10.34	6.45	0.54
	Fixed timing	17.15	12.60	0.68
	JTA	6.33	2.88	0.48
High	LQF	14.93	9.55	0.71
	Fixed timing	25.67	17.56	1.32
	JTA	11.22	5.46	0.78

4.4.5 Assessment of results at the intersection level

Although system level metrics indicate better performance by the JTA, it is important to explore the performance measures at the intersection level. For the sake of brevity, this sections explain the results for four randomly chosen intersections in the network.

Average delay comparison

Figures 4.7 shows the average delays with time for the intersections 1, 4, 7, and 12 respectively. For all the intersections LQF performs worse than JTA and Q-learning. Intersection 7 has a marginal better performance for JTA compared with Q-learning. For the other intersections, average delay with time shows almost the same trend for JTA and Q-learning.

Further, one can observe the inconsistent patterns for the LQF algorithm. For intersection 4, 7 and 12, we observe a hike for the LQF algorithm. The graphs represent the high congestion level in Figure 7. Unlike JTA and Q-learning, decisions are made locally for LQF. Even for the Q-learning, it learns over time to take the optimal action at congested condition accounting for the state in adjacent intersections. LQF primarily seeks the queue information at all approaches and approaches with longer queues get priority. At high congestion, it is possible to have all approaches having long queues in which the algorithm rotates the phases as fast as possible. Still it is feasible to have some phases with higher delays. This may cause the peaks in delays.

Stopped delay comparison

Figure 8 shows the stopped delays with time for intersections 1, 4, 7, and 12 respectively. For all the intersections LQF performs worse than JTA and Q-learning. JTA performs better than Q-learning for intersection 1 and intersection 7. For intersection 12, the performance with time is almost the same. At the beginning of the simulation Q-learning performs significantly better than the other two algorithms.

Number of stops

Figure 9 shows the average number of stops with time for intersections 1, 4, 7, and 12 respectively. Intersection 7 does not have significant difference among the three algorithms in the performance in the long run. LQF performs worse than Q-learning

and JTA for the other two intersections. For intersection 12, the average number of stops is lower for Q-learning compared to JTA. However it starts to go up at the time lapses. This indicates the effect of coordinated learning vs. single agent learning as in Q-learning. The long term results are better for JTA.

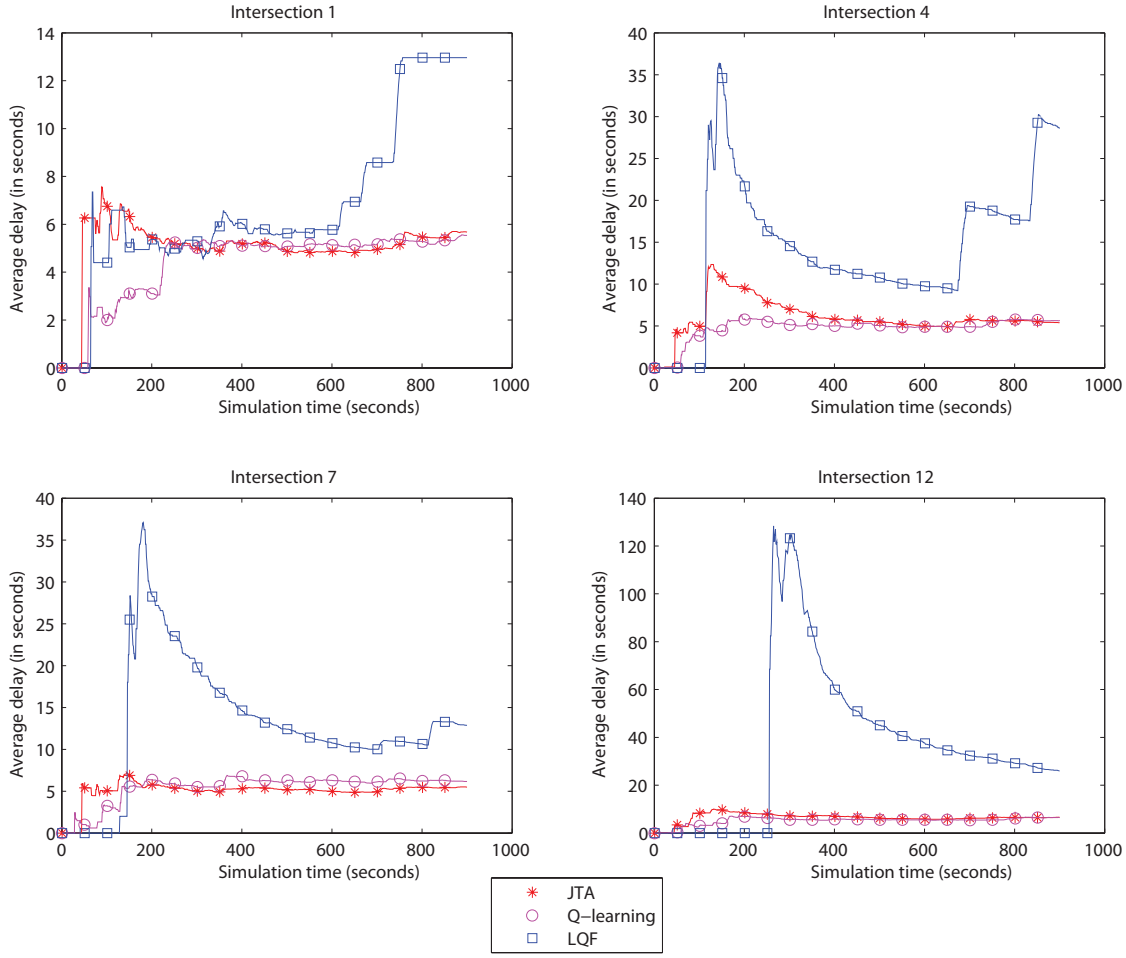

Fig. 4.7. Average delay comparison of different algorithms for intersection 1, 4, 7, and 12

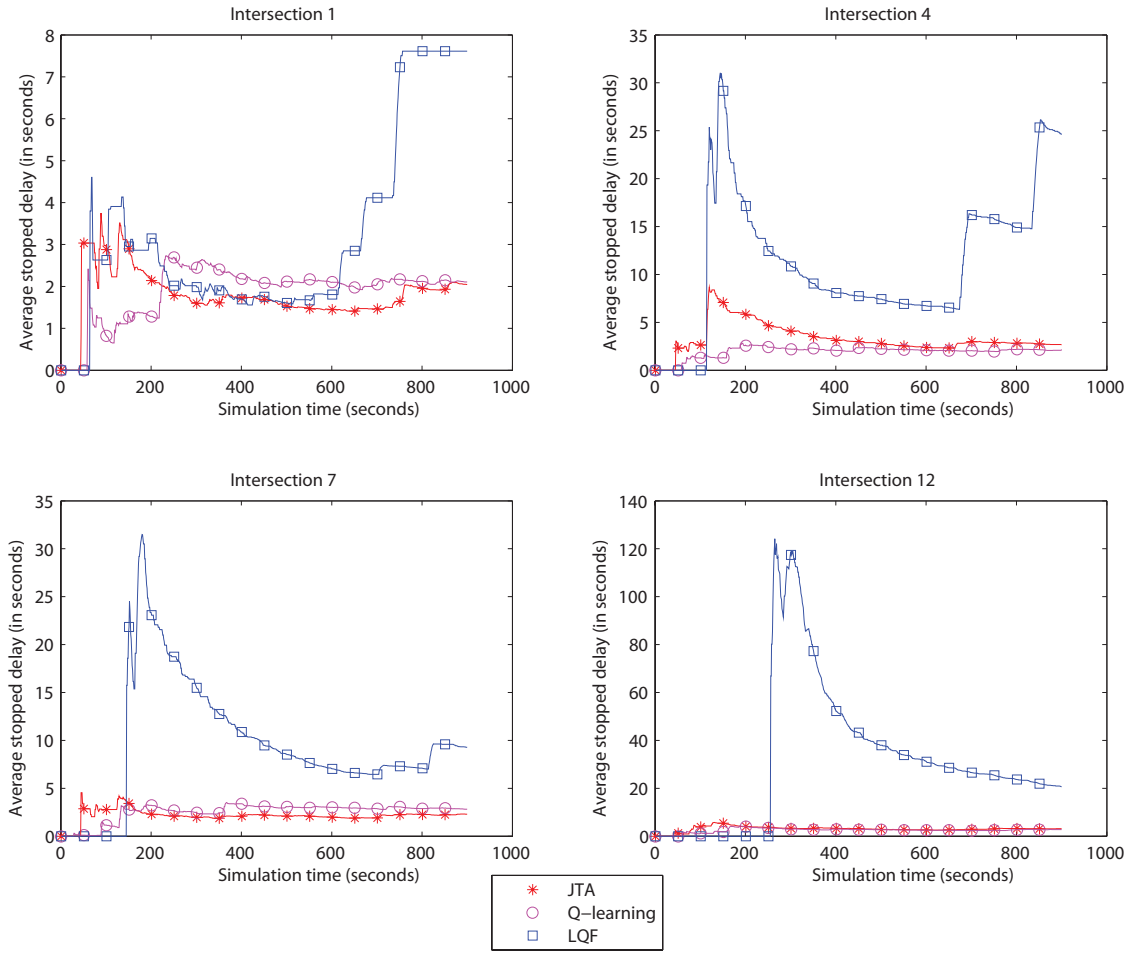

Fig. 4.8. Stopped delay comparison of different algorithms for intersection 1, 4, 7, and 12

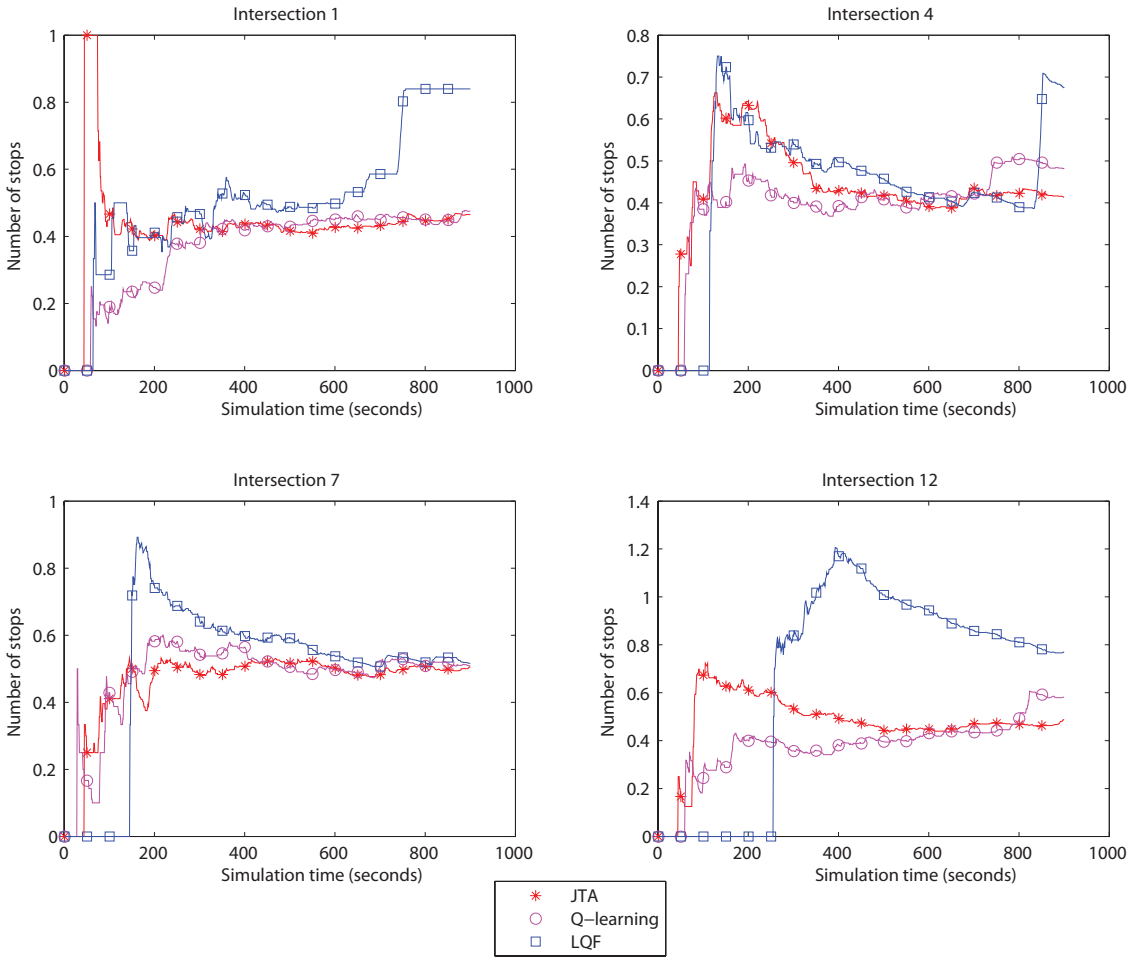

Fig. 4.9. Average number of stops comparison of different algorithms for intersection 1, 4, 7, and 12

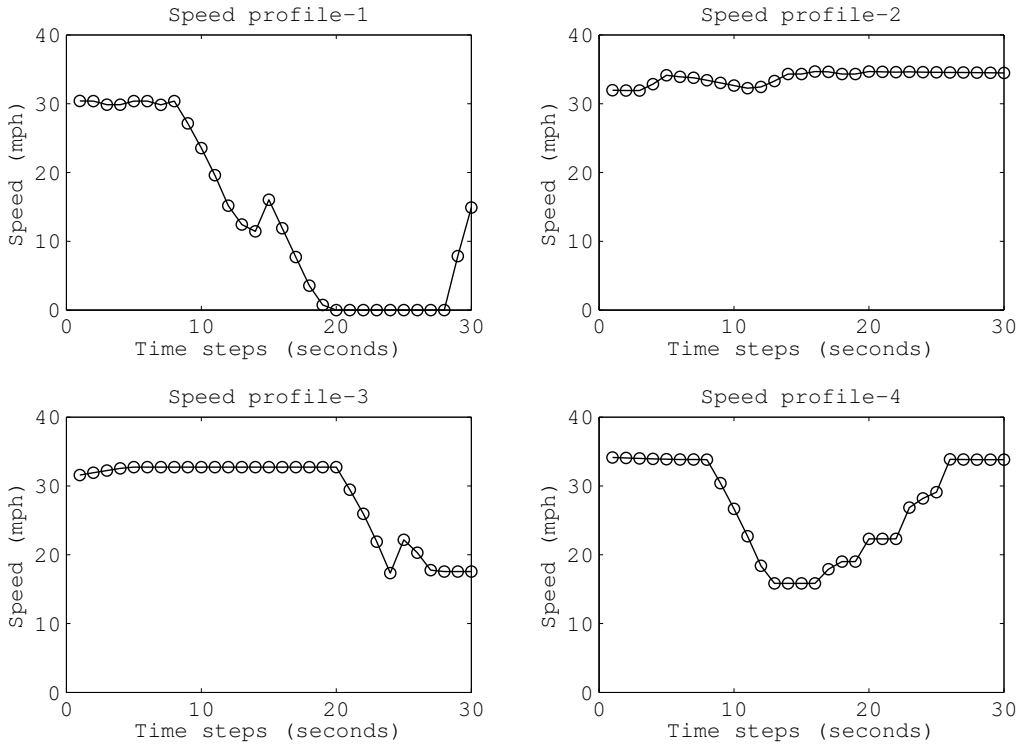

Fig. 4.10. Different activity patterns for vehicles on the same link

4.4.6 Assessment of environmental impact

The morning peak hour (8:00 am to 9:00 am) is simulated with higher level of congestion with default meteorological data (from MOVES) of Tippecanoe county, Indiana for the month of August in 2012. Passenger cars with gasoline fuel are considered in the analysis. Link driving schedules are used to estimate the emissions. Link driving schedules are constructed with the time-dependent speed profiles of vehicles on the links. The speed profiles on signalized intersections can take different forms based on the activities of the vehicles. Some vehicles stop at red and some do not based on the arrival pattern of vehicles at the signalized intersections. Figure 4.4.6 shows four representative link driving schedules of a particular link.

We estimated emissions for all the links in the network. All intersections in the test network are signalized and overlapping of links is obvious. Therefore, we report the emissions for all links instead of identifying each intersection separately. Table 4.4 shows the computed emissions for all links of the network. For each row the least emissions value is underlined to identify the algorithm producing least emissions. Although the values obtained are only for an hour, generally the analysis is done for the entire day or for the week. Therefore, the improvements will be much higher for a day or for the week.

Table 4.4.
Total emissions for all links in the network (computed from MOVES2010b)

Pollutant	JTA	Q-Learning	LQF	Fixed control
CO (g/hour)	<u>232776</u>	233852	265711	269186
GHG (kg/hour)	<u>106313</u>	107116	137045	139535
NO_x (g/hour)	<u>20384</u>	20446	21659	21871
VOC(g/hour)	<u>8522</u>	8571	10291	10452
PM_{10}	<u>1397</u>	1402	1545	1562

The speed profiles affects significantly the emissions from on-road vehicles. Acceleration profiles, idling activities, and variance in speed are three major factors that impact emissions. JTA coordinates actions of the controller to have less delays in the network and maximal throughput for the intersections. Accordingly, the speed profiles are improved in terms of less idling and less variation in speed. As a result, the network has less vehicular emissions

The following conclusions can be made:

(a) Learning based algorithms yield lower emissions than the fixed and adaptive controllers.

(b) To cut down GHG emissions JTA is more effective than the other algorithms

(c) For NO_x and VOC, the differences for average emissions among the algorithms are very small. However when accumulated for all links the savings become significant.

4.5 Concluding remarks

This research develops a coordinated RL-based signal control algorithm, namely the JTA, in a multi-agent framework. We apply the junction tree algorithm for learning based coordinated signal control that guarantee convergence for general traffic networks. The agents take control decisions accounting for the benefit of the system. The test results show significant advantages of coordinated learning over independent learning of agents. Additionally, the JTA can be implemented in large scale networks without a exponential state-space RL framework.

The proposed algorithm explicitly requires the facilitation of the Connected Vehicle (CV) environment and can be seen as an important application in CV based ITS. By means of the multi-agent based reinforcement learning algorithm, the agents (controllers) coordinate their actions to achieve the system level goals. The results from a test network containing 18 intersections show better performance of the JTA algorithm over adaptive (LQF) and single-agent RL based control (Q-learning). The key contributions are as follows:

First, the primary contribution of this research is the development of a coordinated RL based algorithm with convergent property for both cyclic and acyclic traffic networks. Additionally, the results show that the JTA algorithm perform at least as good as the max-plus algorithm [120]. Note that, max-plus cannot always guarantee convergence for cyclic networks.

Second, JTA has never been implemented in context vehicular traffic control to the best of the authors' knowledge. We demonstrated an application of graphical models in context of traffic signal controls that initiates a new path in the traffic control research.

Third, the vehicular emissions are estimated using the state-of-art tool MOVES to explore the environmental benefits of the algorithm. Instead of average speed based technique we account for different vehicular activities on link (Figure 4.4.6). Our test results indicate that, JTA not only improves mobility but also cuts down GHG emissions from the network significantly. Therefore, the JTA algorithm justifies itself as a suitable candidate that ensures sustainable mobility in traffic networks.

Along the stream of this study, several elements of future research can be identified. (1)The results reported here are from a hypothetical network. The primary focus of this research is the development of coordinated algorithm with learning feature and convergent property for general networks and demonstration of the proof-of-concept. Results from real world implementation would make our conclusions stronger. (2)The CV environment can be modeled with more details using wireless communications simulation tools. This would help to assess the resilience and stability of the control schemes with variation in communication strengths. Moreover, the proposed algorithm does not explicitly consider environmental objectives in the reward functions. Learning algorithms with fuel consumption or emissions objective can get to the next dimension of sustainable mobility. (3)Additionally, it would be interesting to assess the variance of performance metrics at intersection level. Although the system is improved, some intersections may always experience poor operations. Modified schemes can be developed that optimize the system ensuring desired level of performance at local intersections.

5. AUTONOMOUS INTERSECTION CONTROL: A LINEAR PROGRAMMING FORMULATION

This chapter develops a novel linear programming formulation for autonomous intersection control (LPAIC) accounting for traffic dynamics within a connected vehicle environment. Firstly, a lane based bi-level optimization model is introduced to propagate traffic flows in the network, accounting for dynamic departure time, dynamic route choice, and autonomous intersection control in the context of system optimum network model. Then the bi-level optimization model is transformed to the linear programming formulation by relaxing the nonlinear constraints with a set of linear inequalities. One special feature of the LPAIC formulation is that the entries of the constraint matrix has only values in -1, 0, 1. Moreover, it is proved that the constraint matrix is totally unimodular, the optimal solution exists and contains only integer values. Further, it shows that traffic flows from different lanes pass through the conflict points of the intersection safely and there are no holding flows in the solution. Three numerical case studies are conducted to demonstrate the properties and effectiveness of the LPAIC formulation to solve autonomous intersection control.

5.1 Introduction

Connected vehicle (CV) technology grows rapidly since its inception owing to the development of wireless communication technology, especially the Dedicated Short Range Communications (DSRC) technology. DSRC has great potential in the area of intelligent transportation systems (ITS), as it facilitates the inter-vehicle communication (IVC). The CV technology is the first step towards the next generation transportation system featuring self-driving vehicles, auto highways, auto parking lots, and auto intersection managements. On the one hand, the CV technology

greatly improves the transportation system. According to the U.S. Department of Transportation's (DOT) Research and Innovative Technology Administration (RITA, 2014), the CV technology will potentially reduce 81 % of all-vehicle target crashes, 83 % of all light-vehicle target crashes, and 72 % of all heavy-truck target crashes annually. It will also improve the congestion problem in US which consumes up to 4.2 billion hours and 2.8 billion gallons of fuel annually. Due to this benefit, the U.S. DOT National Highway Traffic Safety Administration [1] plans to mandate IVC technology on every single vehicle by 2016. On the other hand, the CV technology brings new challenges to the area of traffic control. A key motivation of this study is to address the intersection control problem under the CV environment.

5.1.1 Related work

[132] examined the impact of Cooperative Adaptive Cruise Control under the CV environment and found that both the traffic flow stability and efficiency are improved. However, the study is limited to the cooperation of only connected vehicles. [133, 134, 135] proposed the multi-agent framework for autonomous intersection management (AIM) where vehicles cooperate not only with other vehicles but also with infrastructure (e.g., the intersection controller). In AIM, autonomous vehicles and intersection controller are modeled as intelligent agents. Before reaching the intersection, vehicle agents send requests to signals ahead of the intersection. In consequence, the intersection agent reserves conflict-free trajectories for vehicles to safely pass through the intersection. It is shown that AIM tremendously improves traffic throughout in isolated intersections. [136] further examined the performance of AIM in the case of multi-intersections and significant improvements were also observed as compared to conventional signal control. Following this research stream but from a different perspective, [137] developed the Cooperative Vehicle Intersection Control (CVIC) system. In the framework, autonomous intersection control is formulated as an optimization problem with the objective to minimize the total length of

overlapped trajectories. To solve the optimization problem, the active-set algorithm and interior point algorithm are proposed. However, these two algorithms may not necessarily output collision-free solutions due to the complexity of the optimization problem (both the objective function and constraints are nonlinear and non-convex). Accordingly, a Genetic Algorithm based solution is included in the final solution set of the problem. Still the final solution set may contain solutions that cause vehicle trajectory collision. To guarantee the safety of vehicle movements, an accident-free scheme is incorporated in the control strategies of the intersection controller. Later [138] extended the CVIC framework to the case of multi-intersections and investigated the safety and environmental benefits of autonomous intersection control. Notice that the traffic flow models in the above literature are all second-order traffic flow models. For example, in [133, 134], the acceleration schedule for the driver agent needs to be determined in the modelling component called First-Come-First-Service policy. In [137, 138], the microscopic traffic simulator VISSIM is integrated to model traffic flows in the network. Though second-order traffic flow model provides detailed output at the individual vehicle level, it may compromise more computational effort, as well as increase the difficulty of resolving the problem. On the contrary, the first order traffic flow models are more computationally efficient and more favorable for analytical analysis. The cell transmission model (CTM) developed by [139, 140] is one of the widely used first order traffic flow models. It provides a convergent approximation to a simplified version of the LWR hydrodynamic model [78, 79], whereby the fundamental diagram of traffic flow and density is assumed to be a piecewise linear function. The model is capable of capturing the traffic propagation phenomena such as spill back, kinematic wave, and physical queue. CTM has been used for various dynamic problems in the last decade. To name a few, [141, 142] incorporated CTM into the user equilibrium dynamic traffic assignment problem using the variational inequality approach. [143] efficiently solved the dynamic user optimal problem embedding CTM. [144, 145] formulated the cell-based dynamic user equilibrium problem using complementarity theory. One limitation of CTM lies in its uniform cell based

discretization structure. [146] addressed the issue by presenting the link transmission model (LTM). [147] proposed a link based dynamic network loading model which is equivalent to CTM. Other link based first order dynamic network loading models include the merge and diverge model [148], multiclass model [149], continuous time model [150]. For a more comprehensive review, please refer to [151, 152]. Note that CTM is originally developed in the nonlinear form for traffic simulation. [153] transformed the nonlinear and bi-level structure CTM into a linear programming problem, whereby the nonlinear constraints and the bi-level structure are relaxed with a set of linear inequalities. One problem due to the linear relaxation is known as the holding back problem [154]. [155] verified that Hos algorithm [156] can be utilized to eliminate the unnecessary holding flows in the network. [157] proved that the original cell based system optimal DTA problem is equivalent to the earliest arrival flow (EAF) problem. [158] utilized the concept of fair propagation and proposed a novel formulation that completely eliminates the holding-back phenomenon for networks with multiple OD pairs. Most recently, [159] resolved the holding-back problem by introducing penalty labels to the objective function of the linearized CTM formulation. The penalty label provides sufficient incentive for the formulation to completely remove the holding flows. Besides network analysis, CTM has also been widely applied in the area of traffic control management. Among the wealth of literature, [160, 161] modeled the signal control problem as a mixed integer linear programming problem embedding the CTM model. However the mixed integer programming problem is a NP hard problem. It is difficult to find or prove the existence of global optimal solutions. [162] addressed the uncertainty from demand by proposing the robust system optimal signal control model. Still, it is a difficult task to find an optimal solution of the problem. As acknowledged by the authors, the quality of solutions from the commercial solver changes with the increase of the number of scenarios.

5.1.2 Contributions of the chapter

One limitation from the above literature on autonomous intersection control lies in the complexity of the formulated problem. Generally the complexity of the problem is inherent due to the special requirement of autonomous intersection control: the vehicle trajectories must not intercept at the conflict points of the intersection, otherwise collision occurs. Satisfying the requirement usually causes the problem to be nonlinear, non-convex, and intractable. Consequently, the problem belongs to the class of NP-hard optimization problems and requires considerable computational efforts to find exact optimal solutions. Another limitation from the literature is that the study of autonomous intersection control (e.g., [133, 134, 137, 138] and the study of dynamic traffic assignment (e.g., [141, 142, 144, 145]) are always viewed separately although clear linkages exist between dynamic network assignment and autonomous control algorithms. This chapter fills the research gap by proposing a linear programming formulation accounting for both autonomous intersection control and a system optimum based dynamic traffic. Firstly, stemming from [146, 147] we propose a new lane based traffic flow model. To account for conflict-free vehicle movements in autonomous intersection, we introduce the complementarity constraint to the model, resulting in a nonlinear and bi-level formulation. The traffic flow propagation in the model is proved to be consistent with the previous study [146]. Then the bi-level optimization formulation is transformed to the linear programming version (LPAIC) by relaxing the nonlinear constraints with a set of linear equations. One special feature of the LPAIC formulation is that the entries of the constraint matrix only consists of -1, 0, 1. Moreover, it is found that the LPAIC formulation has several nice properties:

- The matrix of the constraint domain is proved to be totally unimodular, implying the polytope of the formulation is integral.
- There exists optimal solution to the LPAIC formulation, and the optimal solutions are integers.

- The intersection safety is guaranteed, i.e., traffic flows from different phases do not have conflict points concurrently.

- There are no holding-back flows in the solution.

- The formulation captures dynamic departure time and dynamic route choice behavior in the context of system optimum.

To demonstrate the properties and performance of the LPAIC formulation, we have constructed three numerical case studies including an X shape network, an isolated intersection, and a grid network.

Moreover, it is important to note that currently the concept of autonomous intersection is still in its infancy, however, the realization in the real world may not be in the distant future. As predicted from various publications (Broggi, 2012), traffic lights will be eliminated and 75% of vehicles will be autonomous vehicles by the year 2040. The LPAIC formulation in this chapter provides preliminary and important insights on the implementation of autonomous intersection in the real world. The key points are as below:

- The output of the LPAIC formulation includes the time-dependent traffic flow that travels through the intersection. The traffic flow is at the individual vehicle level. In the real world, it can be realized by the cooperation between intersection controller and connected vehicles (or autonomous vehicles) through the V2I communication.

- In the real world application, let the intersection be installed with the distributed controller that is able to access the privacy-protected information (e.g., speed, position, destination) of approaching connected vehicles through the V2I communication. The controller then applies the LPAIC formulation to obtain traffic flow solutions. The traffic flow solution is time-specific. It can be viewed as the time schedule (it is similar to the reservation system proposed by (Dresner and Stone, 2008)) of individual vehicles passing through the intersection.

Then the controller communicates the time schedule back to the approaching connected vehicles which will adjust the speed and obey the schedule. Finally connected vehicles pass through the intersection safely and efficiently without the need for traffic lights.

- Distinct from the previous studies (e.g., Dresner and Stone, 2008; Lee and Park, 2012) which require special treatments on exceptional cases such as solution failures due to the complexity of the optimization problem, the LPAIC formulation bypasses such issue due to its linear nature. Given the extensive research in the area of LP, it is efficient to solve the LPAIC formulation and obtain the exact solution.

The rest of the chapter is structured as follows. Section 5.2 is devoted to the introduction of a lane based traffic flow model from [146, 147]. Section 5.3 transforms the model into the linear programming formulation by relaxing the nonlinear constraints with linear equations. It is proved that the optimal solution of the linear programing problem exists and is consisting of integers. Section 5.4 conducts three numerical studies to demonstrate the properties and performance of the formulation including the ordinary lane, an isolated intersection, and a grid network. Finally, Section 5.5 summarizes the findings of the chapter and discusses the directions for future research.

Sets:		
C	:	Set of all lanes
$C_{R,S}$	:	Set of origin, or destination lanes
$C-O,D,M$	:	Set of ordinary, or diverging, or merging lanes
E	:	Set of all connectors
$E_{O,D,M}$	:	Set of ordinary, or diverging, or merging lane connectors
E_F	:	Set of conflict lane connectors
$\Gamma^{-1}(i)$	:	Set of predecessors of lane i
$\Gamma(i)$	:	Set of successors of lane i
U	:	Set of all OD pairs
R	:	Set of all paths
R^w	:	Set of paths for OD pair w
Parameters:		
S	:	Saturation flow rate
T	:	Size of time step
T_f	:	Time horizon for traffic flow modeling
T_d	:	Time horizon for departure time choice.
N_i^t	:	Jam density of lane i at time t
Q_i^t	:	Inflow or outflow capacity of lane i at time t
W_i	:	Shockwave speed of lane i
V_i	:	Free flow speed of lane i
h_i^r	:	Penalty label of path r at lane i
D^w	:	Total demand of original lane i
Variables:		
$x_i^{r,t}$	:	Lane occupancy of lane i at time t on path r
$y_{i,j}^{r,t}$	:	Flow from lane i to j at time t on path r
x_i^t	:	Aggregate lane occupancy of lane i at time t
$y_{i,j}^t$	:	Aggregate flow from lane i to j at time t

5.2 A lane based traffic flow model for autonomous intersection control

5.2.1 Assumptions of the formulation

Assumption 5.2.1 All vehicles and intersections in the consideration are installed with wireless communication devices to facilitate the Vehicle to vehicle (V2V) communication and vehicle to infrastructure (V2I) communication in the network.

Assumption 5.2.2 The communication network is fully connected during the time period, and there are negligible transmission delays, packet loss, interference, etc, in the communication process of V2V and V2I.

Assumption 5.2.3 Vehicles pass through the intersection according to the traffic flow propagation from the LPAIC formulation. This is achieved by vehicles cooperating with one another and with the intersection controller through the wireless communication under the CV environment.

Assumption 5.2.4 The vehicle movements or the traffic flow propagation is based on system optimum routing in the dynamic traffic network. In this study, the objective is to minimize the total travel time.

Assumption 5.2.5 The other major assumptions are similar to that in the cell transmission model (CTM). For instance, the traffic flow is homogeneous, there is no lane changing, the fundamental diagram is assumed as a piece-wise linear function, etc.

5.2.2 Lane based traffic flow modeling

Stemming from [146, 147], this chapter develops a new lane based traffic flow model featuring dynamic departure time, dynamic route choice, and autonomous intersection control. Similar to [146, 147], the lane based traffic flow model is a discrete time model where the time space is discretized into time steps. However, one special requirement is imposed on the resolution of time step in this study: the

time step size is determined in the way that the outflow capacity is one unit per time step. For instance, if the saturation flow rate is 1800 veh/hour (or 0.5 veh/second), then the size of time step is determined as 2 seconds such that the outflow capacity is one ($0.5 \times 2 = 1$) vehicle per time step. Moreover, the traffic flow propagation in the network is lane based. The number of vehicles within the lane is defined as the occupancy of the lane, denoted as $x_i^t, i \in C$. The number of vehicle moving from one lane to another is defined as the traffic flow of the lane connector, denoted as $y_{i,j}^t, (i,j) \in E$. The traffic flow propagation is realized by updating temporal values of $x_i^t, i \in C$ and $y_{i,j}^t, (i,j) \in E$ in the network.

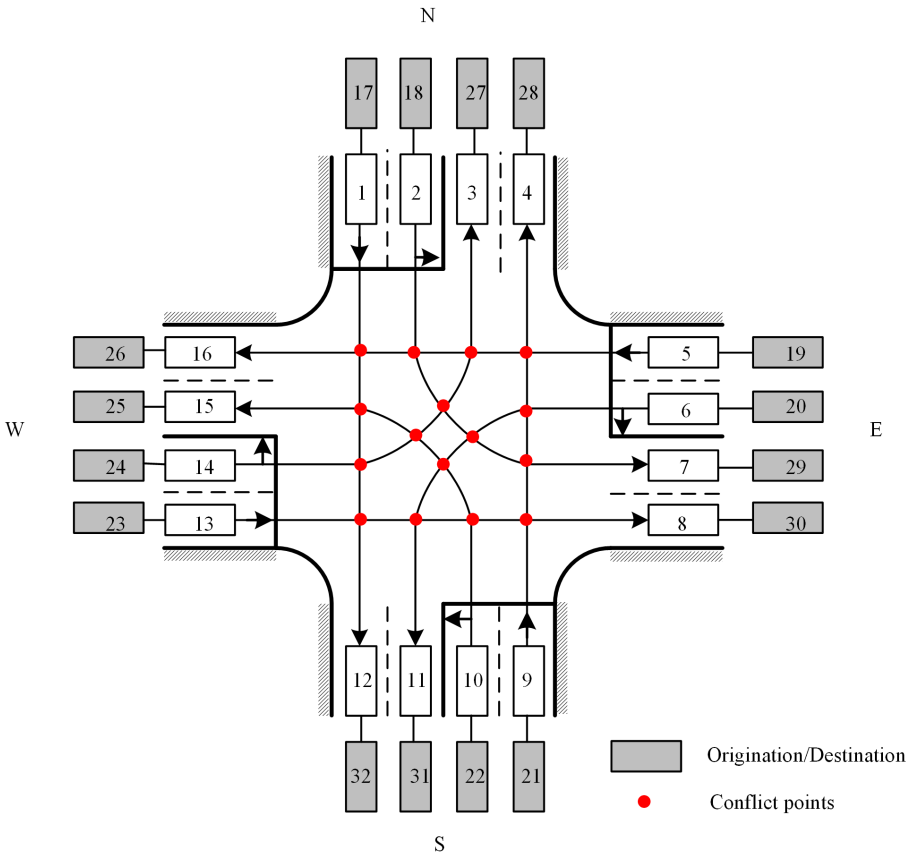

Fig. 5.1. Demonstration of conflict points in a typical 4-lane 4-leg intersection

Further, we specify conflict lane connectors which represent the paired lanes that have conflict points in the intersection. Conflict points indicate the potential collision

areas of the intersection where traffic flows from different phases use the same road. To ensure safety, it must guarantee that vehicles do not go through the conflict points at the same time. For demonstration purposes, Figure 5.1 shows the example of a typical 4-leg and 4-lane intersection. The red points represent conflict points. As shown in the figure, there are 20 conflict points for approaching vehicles from east (E), west (W), south (S), and north (N) bound. For example, lane connector (1, 12) corresponds to the through movement from North bound, and lane connector (13, 8) corresponds to the through movement from the West bound. Traffic flows cannot propagate on these two conflict lane connectors concurrently, otherwise collisions occur. In other words, we must have $y^t_{1,12} > 0, y^t_{13,8} = 0$, or $y^t_{1,12} = 0, y^t_{13,8} > 0$, or $y^t_{1,12} = y^t_{13,8} = 0$ for any t. Mathematically, such relationship can be written in the complementarity form as $0 \leq y^t_{1,12} \perp y^t_{13,8} \geq 0, \forall t$. Generalizing this example, let E_F denote the set of paired conflict lane connectors, then the complementarity constraint for conflict-free traffic flows is written as:

$$0 \leq y^t_{i,j} \perp y^t_{k,l} \geq 0, \forall (i,j,k) \in E_F, \forall t \tag{5.1}$$

For the updating of lane occupancies, we apply the flow conservation constraints. Specifically, we adopt the same logic as in CTM [139, 140] and [147]:

Demand satisfaction constraint:

$$\sum_{t=1}^{T_d} \sum_{r \in R^w} \sum_{i \in C_R} \sum_{j \in \Gamma(i)} y^{r,t}_{i,j} = D^w, \forall w \in U \tag{5.2}$$

Aggregation of lane occupancy and outflow constraints:

$$x^t_i = \sum_{\forall r} x^{r,t}_i, \forall i \in C \tag{5.3}$$

$$y^t_{i,j} = \sum_{\forall r} y^{r,t}_{i,j}, \forall (i,j) \in E \tag{5.4}$$

Lane occupancy constraints:

$$x^{r,t}_i = x^{r,t-1}_i - \sum_{j \in \Gamma(i)} y^{r,t-1}_{i,j} \forall i \in C_R \tag{5.5}$$

Sink lanes:

$$x_i^{r,t} = x_i^{r,t-1} + \sum_{k \in \Gamma^{-1}(i)} y_{k,i}^{r,t-1} \forall i \in C_S \tag{5.6}$$

Ordinary lanes:

$$x_i^{r,t} = x_i^{r,t-1} + y_{k,i}^{r,t-1} - y_{i,j}^{r,t-1} \forall i \in C_O, k \in \Gamma^{-1}(i), j \in \Gamma(i) \tag{5.7}$$

Merging lanes:

$$x_i^{r,t} = x_i^{r,t-1} + \sum_{k \in \Gamma^{-1}(i)} y_{k,i}^{r,t-1} - y_{i,j}^{r,t-1} \forall i \in C_M, j \in \Gamma(i) \tag{5.8}$$

Diverging lanes:

$$x_i^{r,t} = x_i^{r,t-1} + y_{k,i}^{r,t-1} - \sum_{j \in \Gamma(i)} y_{i,j}^{r,t-1} \forall i \in C_D, k \in \Gamma^{-1}(i) \tag{5.9}$$

For the updating of traffic flows connecting different lanes, we derive the traffic flow updating procedure for ordinary lane connectors and show that it is consistent with the previous study (Yperman, 2007), then develop similar equations for diverging and merging lane connectors.

Ordinary lane connectors, $\forall (i,j),(j,l) \in E_O$:

$$y_{i,j}^{r,t} = \min \left\{ x_i^{r,t+1-L_i/V_i} - \sum_{k=t+1-L_i/V_i}^{t-1} y_{i,j}^{r,k}, Q_i^t, Q_j^t, N_j - x_j^t - \left(\sum_{k=t+1-L_i/W_i}^{t-1} y_{j,l}^k \right) \right\} \tag{5.10}$$

Proposition 5.2.1 The traffic flow updating procedure in (10) is consistent with the flow updating procedure in LTM (Yperman, 2007).

Proof (a) In chap 4, equation 4.31 (Yperman, 2007), the sending flow in the link model is formulated as:

$$S_i(t) = \min\left(\left(N\left(x_i^0, t + \Delta t - \frac{L_i}{v_{f,i}}\right) - N\left(x_i^L, t\right)\right), q_{M,i}\Delta T\right) \tag{5.11}$$

Where $S_i(t)$ represents sending flow of link i at time t, x_i^0andx_i^L represent the entry and exit location of link i, L_i represents the length of link i, $v_{f,i}$ represents the free flow speed of link i, $q_{M,i}$ represents the link capacity of link i, and $N(\cdot)$ represents the accumulative vehicle numbers. Notice that in the context of this study, the accumulative number of vehicles is considered as the aggregation of traffic flows, which gives:

$$N\left(x_i^0, t + \Delta t - \frac{L_i}{v_{f,i}}\right) = \sum_{k=1}^{t-L_i/V_i} y_{l,i}^{r,k}, l \in \Gamma^{-1}(i) \tag{5.12}$$

$$N\left(x_i^L, t\right) = \sum_{k=1}^{t-1} y_{i,j}^{r,k} \tag{5.13}$$

Moreover, according to the definitions in this chapter, $q_{M,i}\Delta T = Q_i$. Thus, substitute (12) and (13) into (11), we have:

$$S_i(t) = \min\left(\sum_{k=1}^{t-L_i/V_i} y_{l,i}^{r,k} - \sum_{k=1}^{t-1} y_{i,j}^{r,k}, Q_i\right), l \in \Gamma^{-1}(i), j \in \Gamma(i) \tag{5.14}$$

Note from (5.7), we have:

$$x_i^{r,t+1-L_i/V_i} = \sum_{k=1}^{t-L_i/V_i} y_{l,i}^{r,k} - \sum_{k=1}^{t-L_i/V_i} y_{i,j}^{r,k}, l \in \Gamma^{-1}(i), j \in \Gamma(i) \tag{5.15}$$

Substitute (5.15) into (5.14), we get:

$$S_i(t) = \min\left(x_i^{r,t+1-L_i/V_i} - \sum_{k=t+1-L_i/V_i}^{t-1} y_{i,j}^{r,k}, Q_i^t\right), l \in \Gamma^{-1}(i), j \in \Gamma(i) \tag{5.16}$$

(b) Similarly, when it turns to receiving flow in the link model, the constraint (chap 4, equation 4.35, (Yperman, 2007)) on the receiving flow is formulated as:

$$R_j(t) = \min\left(\left(N\left(x_j^L, t + \Delta t + \frac{L_j}{w_j}\right) + k_{jam}L_j - N\left(x_j^0, t\right)\right), q_{M,j}\Delta T\right) \tag{5.17}$$

Where $R_j(t)$ represents sending flow of link j at time t, k_{jam} represents the jammed density of the link and w_j (of negative value) represents the shock wave speed of link j. Following the same procedure as (5.12) - (5.16), we obtain:

$$R_j(t) = \min\left(N_j - x_j^t - \left(\sum_{k=t+1-L_i/W_i}^{t-1} y_{j,l}^k\right), Q_j\right) \tag{5.18}$$

Combining (5.16) and (5.18), we have (5.10). This ends the proof. ■

As the proposed traffic flow model is consistent with LTM, it is capable of capturing the traffic propagation phenomena such as spill back, kinematic wave, and physical queue. However, note that (10) only applies to ordinary lanes. For diverging and merging lanes, the popular approach is to exogenously determine a set of time-dependent turning proportions for these links (Daganzo, 1995, 1994). Here we apply the approach from (Zhu and Ukkusuri, 2013; Ziliaskopoulos, 2000), which is more flexible in the sense that the turning proportions either for diverging lane connecters or merging lane connectors are determined to optimize the total system cost.

Diverging lane connectors, $\forall (i,j) \in E_D$:

$$\max \sum_{j\in\Gamma(i)} y_{i,j}^{r,t} \tag{5.19}$$

$$\begin{aligned}
&\sum_{j\in\Gamma(i)} y_{i,j}^{r,t} \le x_i^{r,t+1-L_i/V_i} - \sum_{k=t+1-L_i/V_i}^{t-1} y_{i,j}^{r,k},\\
&\sum_{j\in\Gamma(i)} y_{i,j}^{r,t} \le Q_i^t,\\
&y_{i,j}^{r,t} \le Q_j^t, j \in \Gamma(i)\\
&y_{i,j}^{r,t} \le N_j - x_j^t - \left(\sum_{k=t+1-L_i/W_i}^{t-1} y_{j,l}^k\right)
\end{aligned} \tag{5.20}$$

Merging lane connectors, $\forall (i,j) \in E_M$:

$$\max \sum_{i\in\Gamma^{-1}(j)} y_{i,j}^{r,t} \tag{5.21}$$

$$
\begin{aligned}
& y_{i,j}^{r,t} \leq x_i^{r,t+1-L_i/V_i} - \sum_{k=t+1-L_i/V_i}^{t-1} y_{i,j}^{r,k}, \\
& \sum_{i \in \Gamma^{-1}(j)} y_{i,j}^{r,t} \leq Q_j^t, \\
& y_{i,j}^{r,t} \leq Q_i^t, i \in \Gamma^{-1}(j) \\
& \sum_{i \in \Gamma^{-1}(j)} y_{i,j}^{r,t} \leq N_j - x_j^t - \left(\sum_{k=t+1-L_i/W_i}^{t-1} y_{j,l}^{k} \right)
\end{aligned}
\tag{5.22}
$$

Remark 5.2.6 Due to the complex constraints of Equation (1), (10), (19), and (21), it is hard to obtain an exact optimal solution to the problem. One popular approach is to reformulate the problem as an optimization problem with complementarity constraints. Then the problem becomes a mathematical program with equilibrium constraints (MPEC). Note that MPEC problems are usually intractable and difficult to solve.

5.2.3 The nonlinear optimization formulation

Similar to [153, 159], the objective of the problem is to minimize the total travel time. Thus the whole formulation is presented as:

Nonlinear optimization formulation for autonomous intersection control (NAIC):

$$
\min z(\mathbf{x}) = \sum_{\forall t} \sum_{\forall i \in C \setminus C_S} x_i^t \tag{5.23}
$$

Subject to: (5.1) - (5.10), (5.19) - (5.22).

5.3 Linear programming formulation of the lane based traffic flow model

5.3.1 Linear programming formulation for autonomous intersection control

The nonlinear nature of complementarity constraints (Equation (5.1)), minimum constraints (Equation (5.10)), as well as the bi-level optimization structure (Equation (5.19) and (5.21)), increase the difficulty of analytical analysis for the problem.

Following the previous work by [153, 159], we transform the nonlinear optimization problem into a linear programming problem, whereby the nonlinear constraints are relaxed with a set of linear inequalities. It is worthy to note in advance that the complementarity constraints (i.e., Equation (5.1)) would be implicitly addressed in the formulation, as revealed later in Proposition 5.3.2 in Section 5.3.2.

Linear programming formulation for autonomous intersection control (LPAIC):

$$\min z(\mathbf{x}) = \sum_{\forall t} \sum_{\forall i \in C \setminus C_S} h_i x_i^t \tag{5.24}$$

Subject to:

Lane occupancy constraints: (5.2) - (5.9)

Lane connector constraints:

Ordinary lane connectors, $\forall\,(i,j) \in E_O$:

$$\begin{aligned} y_{i,j}^{r,t} &\le x_i^{r,t+1-L_i/V_i} - \sum_{k=t+1-L_i/V_i}^{t-1} y_{i,j}^{r,k}, \\ y_{i,j}^{r,t} &\le Q_i^t, \\ y_{i,j}^{r,t} &\le Q_j^t, \\ y_{i,j}^{r,t} &\le N_j - x_j^t - \left(\sum_{k=t+1-L_i/W_i}^{t-1} y_{j,l}^{k} \right) \end{aligned} \tag{5.25}$$

Diverging lane connectors, $\forall\,(i,j) \in E_D$: (5.20) Merging lane connectors, $\forall\,(i,j) \in E_M$: (5.22) Conflict lane connectors, $\forall\,(i,j,k,l) \in E_F$:

$$y_{i,j}^t + y_{k,l}^t \le 1 \tag{5.26}$$

Non-negativity constraints:

$$x_i^t \ge 0, y_{i,j}^t \ge 0, \forall i \in C, (i,j) \in E \tag{5.27}$$

Remark 5.3.1 The objective function in (5.24) is different from the NAIC formulation in (5.23). In (5.24) we have introduced the penalty label h_i. The purpose of

introducing this penalty label is to remove the holding flows from the traffic flow propagation (Zhu and Ukkusuri, 2013). The determination principle of the penalty label is that h_i must be strictly positive and strictly greater than that of the downstream lane:

$$0 < h_j < h_i, \forall i \in C; j \in \Gamma(i) \tag{5.28}$$

In addition, the difference between h_i and h_j needs to be made small enough that the solution also applies to the case of not introducing penalty labels (Zhu and Ukkusuri, 2013).

5.3.2 Properties of the LPAIC formulation

For the sake of brevity, we denote the domain of the LPAIC formulation as:

$$\begin{aligned} &\mathbf{AX} \leq \mathbf{b}; \\ &\mathbf{X} \geq \mathbf{0} \end{aligned} \tag{5.29}$$

Where $\mathbf{X} = [\mathbf{x}, \mathbf{y}], \mathbf{x}, \mathbf{y}$ represents the set of all variables, $x_i^t, y_{i,j}^t, \forall i \in C, (i,j) \in E$. Moreover, $\mathbf{AX} \leq \mathbf{b}, \mathbf{X} \geq \mathbf{0}$ represents all the linear relationships of the constraints of the LPAIC formulation.

In this study, the meaning of occupancies (i.e., x_i^t) and flows (i.e., $y_{i,j}^t$) is corresponding to the number of vehicles. Hence we are interested in integer values for all the valuables. Following this logic, when presetting the values of parameters, e.g., Q_i, N_i ,etc, it is required to assign integer values.

Proposition 5.3.1 The constraint matrix of the LPAIC formulation, i.e., $\mathbf{A}$, is totally unimodular.

Proof Firstly, the entries in $\mathbf{A}$ are all within -1, 0, +1. Next, consider a general variable, $y_{i,j}^{r,t}, (i,j) \in E_O$. It appears in seven rows of $\mathbf{A}$ corresponding to Equation (5.4), (5.7), and (5.25), namely, one in (5.4), two in (5.7), and four in (5.25). If we divide these rows into two subsets. Subset 1 contains (5.4), (5.7), and half of (5.25).

Subset 2 contains the other half of (5.25). Hence the summation of the coefficients of $y_{i,j}^{r,t}$ in Subset 1 and Subset 2 are 3 and 2, respectively. Thus the difference is 1. Similar logics can be applied to other variables. In all, according to the Ghouila-Houris Characterization (Theorem 19.3, [163]), **A** is totally unimodular. ■

Theorem 5.3.2 There exists an optimal solution for the LPAIC formulation, denoted as $\mathbf{X}*$. Moreover, $\mathbf{X}*$ are integers, i.e., $\mathbf{X}* \in Z^n$.

Proof (1) As coefficients of the objective function are all positive and **X** is feasible and bounded, the objective function is bounded from below. Following Theorem 4.2.3 [164], there exists an optimal solution for the LPAIC formulation. (2) From proposition 5.3.1, we have **A** is totally unimodular. Moreover, **b** is an integer vector. Directly following Lemma 8.2.4 [164], we get that $\mathbf{X}*$ are integers, i.e., $\mathbf{X}* \in Z^n$. ■

Proposition 5.3.2 Let $\mathbf{X}* = \arg LPAIC(\mathbf{X})$, then $y_{i,j}^t y_{k,l}^t = 0, \forall (i,j,k,l) \in E_F, \forall t$.

Proof From constraint (5.26), we have $y_{i,j}^t + y_{k,l}^t \leq 1$. From Theorem 5.3.2, $y_{i,j}^t, y_{k,l}^t$ are integer. Accordingly, $y_{i,j}^t y_{k,l}^t = 0, \forall (i,j,k,l) \in E_F, \forall t$. ■

Proposition 5.3.2 implies that the LPAIC formulation strictly satisfies the complementarity constraints (i.e., Equation (5.1)) in the NAIC formulation. In other words, optimal solution of the LPAIC formulation ensures that traffic flows pass through the conflict points of the intersection safely.

Proposition 5.3.3 Consider the following linear programming formulation:

$$\begin{aligned} &\min z(\mathbf{x}) = \sum_{\forall t} \sum_{\forall i \in C \setminus C_S} x_i^t \\ &s.t. \\ &\mathbf{AX} \leq \mathbf{b}; \\ &\mathbf{X} \geq \mathbf{0} \end{aligned} \tag{5.30}$$

There exists the set of $h_i, i \in C$, such that $\mathbf{X}* = \arg LPAIC(\mathbf{X})$ also serves as the optimal solution of (5.30).

Proof Consider $h_i, i \in C$ as a set of parameters that can vary. Then the LPAIC formulation becomes a parametric linear program of (5.30). According to Lemma 6.2 [165], there exists a nontrivial and positive range for $h_i, i \in C$ such that the optimality of (5.30) maintains. ■

Proposition 5.3.4 Let $(\mathbf{x}*, \mathbf{y}*) = LPAIC(\mathbf{x}, \mathbf{y})$, then

$$y_{i,j}^t = \min\left\{x_i^t, Q_i^t, Q_j^t, \delta\left(N_j^t - x_j^t\right)\right\}, (i,j) \in E_O \tag{5.31}$$

$$y_{i,j}^t = \min\left\{x_i^t, Q_i^t\right\}, \text{and} \sum_{i \in \Gamma^{-1}(j)} y_{i,j}^t = \min\left\{Q_j^t, \delta\left(N_j^t - x_j^t\right)\right\}, (i,j) \in E_M \tag{5.32}$$

$$\sum_{j \in \Gamma(i)} y_{i,j}^t = \min\left\{x_i^t, Q_i^t\right\}, \text{and} y_{i,j}^t = \min\left\{Q_j^t, \delta\left(N_j^t - x_j^t\right)\right\}, (i,j) \in E_D \tag{5.33}$$

Proof Please refer to a similar proof in (Zhu and Ukkusuri, 2013). ■

Interpretation: There is no holding-back flows in the optimal solution of the LPAIC formulation.

Theorem 5.3.3 Let $(\mathbf{x}*, \mathbf{y}*) = LPAIC(\mathbf{x}, \mathbf{y})$, then $(\mathbf{x}*, \mathbf{y}*) = NAIC(\mathbf{x}, \mathbf{y})$. Interpretation: the optimal solution of the LPAIC formulation also serves as the solution of the NAIC formulation.

Proof This immediately follows from Proposition 5.3.2, 5.3.3, and 5.3.4. ■

Remark 5.3.4 For implementation of autonomous intersection in the real world, traffic flows should follow the solution from the LPAIC formulation. This is achievable through the inter-vehicle communication system. Firstly, intersections need to be installed with distributed controllers and vehicles need to be equipped with wireless communication devices. Controllers are able to communicate with vehicles through

the DSRC based communication. When vehicles approach the intersection, the controller will access the privacy-protected information (e.g., speed, position, destination, etc) of the vehicle and apply the LPAIC formulation to obtain the solution. The solution is time-specific at the individual vehicle level. For instance, $y_{i,j}^t$ indicates the traffic flow from lane i to lane j at time t . It can be viewed as the time schedule that the vehicle moves from one end to the other end of the intersection. Notice that the LPAIC formulation is an LP problem. It can be solved efficiently in no time. Then the controller broadcasts the time schedule of vehicle movements back to the approaching vehicles. After receiving the time schedule, vehicles will need to corporately adjust speed in order to pass through the intersection safely and efficiently.

5.4 Numerical case studies

5.4.1 X shape network demonstration

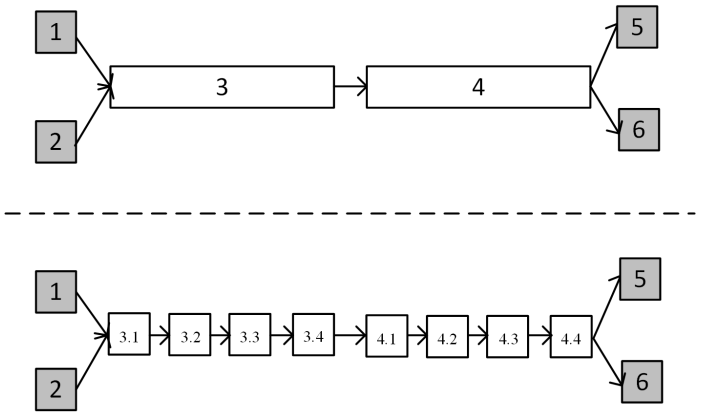

Fig. 5.2. The X shape network (upper level is lane-based; lower level is cell-based)

The representation of the X shape network is shown in Figure 5.2. It is consisting of diverging and merging lanes. The purpose of constructing this simple case is to demonstrate the accuracy of the LPAIC formulation in traffic flow propagation. This

is done by showing the consistency of the traffic flow outputs between the LPAIC formulation, LTM, and CTM, since the latter two are well-accepted traffic flow simulation models. In Figure 5.2, the upper level represents the lane-based network, and the lower level represents the cell-based network. These two representations represent the same network. For example, cell 1 is the same as lane 1, and the combination of cell 3.1-3.4 (4.1-4.4) in the lower level forms lane 3 (4) in the upper level. The dark lanes (cells) represent the originations or destinations, and the light lanes (cells) represents ordinary lanes (cells). The detailed setting for the network is as below. The saturation rate is 1800 veh/hour. The time step is 2-second. Hence outflow capacity is one vehicle/time step (as required in the LPAIC formulation). The ratio between the shock wave speed and the free flow speed is fixed at one. The holding capacity is 6 for cell 1 to cell 6, and lane 1. Proportionally, the holding capacity is 24 for lane 3 and lane 4. Since cells (lanes) 5 and 6 are destinations, the capacity is set to infinity. The departure time horizon is 20 time steps, and the whole time horizon is 30 time steps. The demand input is generated randomly according to the Bernoulli process as shown in Appendix Table 5.6. Table 5.6 also presents the occupancy outputs of the network from the LPAIC formulation and LTM. They are exactly the same. Appendix Table 5.7 presents the occupancy output from CTM. The dark area of Table 5.7 indicates the occupancy of the accumulated cells in parallel with the lane based representation in the LPAIC formulation. It is seen that the results in Table 5.7 are exactly the same as those in Table 5.6. Therefore it is concluded that the LPAIC formulation propagates traffic flow consistently as LTM and CTM in this demonstrative example. This finding is in accordance with the statement in Proposition 5.2.1.

5.4.2 Isolated intersection

In order to show the mobility benefit of applying autonomous intersection control, we have constructed this isolated intersection case (Figure 5.1). For the performance measure of mobility, we apply the total travel time as the indicator since it consti-

tutes the objective of the LPAIC formulation. The comparison is conducted between the autonomous intersection control (i.e., the LPAIC formulation) and the actuated longest queue first (LQF) signal control [131]. As shown in Figure 5.1, we consider the typical 4-lane 4-leg isolated intersection. The settings of the intersection are consistent with the network in Section 5.4.1 unless specified elsewhere. The holding capacity is 24 for all the lanes except the destination lanes (the capacity is set to infinity). The departure time horizon is 60 time steps, and the whole time horizon is 120 time steps. The demand input is the same for both LPAIC and LQF, and is generated randomly according to the biased Bernoulli process. In the experiment design, we have constructed five scenarios according to different volume/capacity (V/C) ratios ranging from 0.4 to 0.8. The V/C ratio corresponds to the probability of success for the Bernoulli trial in generating the demand input. For the sake of space, we do not present the solution outputs (they are confirmed to be integers) of the LPAIC formulation but present the results of total travel time between LQF and LPAIC as shown in Table 5.1. Overall, it is seen that autonomous intersection control outperforms actuated signal control across all the V/C ratio cases. Especially, the improvement is as high as up to 18.8% in the 0.4 V/C ratio case. One interesting finding is that the difference between LQF and LPAIC is decreasing when the V/C ratio increases. In other words, the advantage of autonomous intersection control over actuated signal control is becoming less when the traffic congestion is worsening. Intuitively, vehicles are forced to go through the stop-and-go process when the intersection is heavily congested regardless of any control strategy. Accordingly, autonomous intersection control may not gain significantly more benefits over actuated control. Such finding is also observed from the previous work [133]. It is worthwhile to perform a sensitivity analysis on the performance of autonomous intersection control, however, it is out of the scope of this chapter. We leave this topic to future research.

Table 5.1.
Total travel time (in units of time steps) comparison with different V/C ratio

V/C	LQF	LPAIC	Difference
0.4	3039	2468	-18.79%
0.5	6643	5466	-17.72%
0.6	8010	6664	-16.80%
0.7	10863	9508	-12.47%
0.8	10957	9991	-8.82%

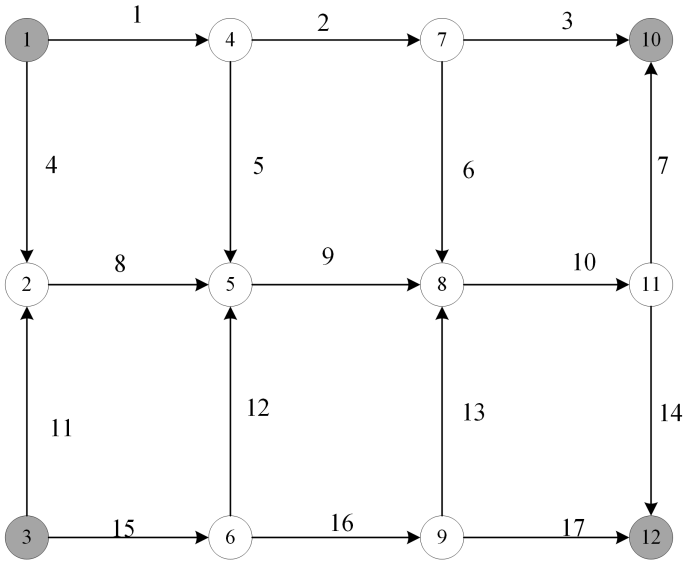

Fig. 5.3. The 12-node grid network

5.4.3 Grid network

The third example is a grid network consisting of 12 nodes, 17 single-lane links and 4 OD pairs, as shown in Figure 5.3. The setting of the network is consistent with Section 4.2 unless specified elsewhere. Node 1 and 3 are origin nodes, and node 10 and 12 are destination nodes. The route choice setting for different OD pairs are listed in Table 5.2. The purpose of constructing the grid network example is to demonstrate the LPAIC formulation's capability of accounting for dynamic departure time and route choice behavior. To serve this purpose, we design two scenarios as following. 1) Vary the demand. 2) Accident on one network link.

Varied demands scenario

In this scenario, we vary the demand input of the network. Demand case 1 is the base case with demand input for OD pair (1,10), (3,10), (1,12), and (3,12) as 15, 6, 4, and 10, respectively. Then the demand of case 2 is twice of that of case 1. Similarly, demand cases 3 and 4 are 3 and 4 times of that of case 1. Across all demand cases,

Table 5.2.
Route choices setting for the grid network

OD	Route number	Nodes in the Route	OD	Route number	Nodes in the Route
(1,10)	1	1-4-7-10	(1,12)	1	1-4-5-8-11-12
	2	1-2-5-8-11-10		2	1-4-7-8-11-12
	3	1-4-5-8-11-10		3	1-2-5-8-11-12
	4	1-4-7-8-11-10			
(3,10)	1	3-2-5-8-11-10	(3,12)	1	3-6-9-12
	2	3-6-5-8-11-10		2	3-2-5-8-11-12
	3	3-6-9-8-11-10		3	3-6-5-8-11-12
				4	3-6-9-8-11-12

Table 5.3.
Route choices for various demand cases

OD pair	Route #	Demand Cases			
		1	2	3	4
(1,10)	1	14	25	37	49
	2	1	5	8	11
	3	0	0	0	0
	4	0	0	0	0
(1,12)	1	0	0	0	0
	2	0	0	0	0
	3	6	12	18	24
(3,10)	1	0	2	4	7
	2	4	6	8	9
	3	0	0	0	0
(3,12)	1	10	20	30	40
	2	0	0	0	0
	3	0	0	0	0
	4	0	0	0	0

the departure time horizon is 60 time steps, and the whole time horizon is 120 time steps. For the sake of brevity, here we only present the traffic assignment solution (i.e., route choices) for all the 4 demand cases in Table 5.3. From Table 5.3, we see that almost all the vehicles pick the shortest route in demand case 1 since the demand load is lowest. When the demand increases, the traffic flow spreads from the original shortest route (the one under demand case 1) to other routes (see, e.g., OD pair (1,10), (3,10)), as the original shortest route may not be the shortest due to the increasing demand. However, for OD pair (1,12) and (3,12), vehicles still take the original shortest routes. It implies that the shortest route remains the same.

Accident case

In this case, we assume that an accident happens on lane 8. Due to the accident, the flow capacity from lane 8 to lane 9 is constrained to be zero from time step 5 to 10. The departure time horizon is 30 time steps, and the whole time horizon is 40 time steps. The total demand inputs for (1,10), (3,10), (1,12), and (3,12) are 10, 11, 9, and 8, respectively. The results of the departure rates for the two scenarios are shown in Table 5.4 and Table 5.5, respectively. As seen from the comparison of Table 5.4 and Table 5.5, in the non-accident scenario, all 9 units of traffic traveling from node 1 to node 12 take route 3. However, when there is an accident at lane 8 and the flow capacity from link 8 to 9 is affected, 2 units of traffic will take route 1 instead of route 3. For the case of OD pair (3,10), we also see that the route choice behavior is different in the two scenarios. Moreover, for the OD pair (3,12), though all 8 units of traffic would pick route 1 for both non-accident and accident cases, the departure rates are different, as highlighted in dark in Table 5.5. The encouraging results from both the varied demand case and the accident case demonstrate the benefit of applying the proposed formulation in dynamic traffic assignment related areas such as network design, traffic control management, and evacuation.

5.5 Concluding remarks and discussions

The recent growth in wireless-enabled traffic network offers useful technologies that are valuable for more efficient traffic control strategies. Overcoming the traditional stop-and-go traffic flow pattern, autonomous intersection control is greatly beneficial for the transportation system. However, one should also acknowledge the difficulty of finding the conflict-free control strategies. One limitation from most, if not all, of the literature on autonomous intersection control lies in the complexity of the formulated problem. This chapter contributes significantly to the area of autonomous intersection control by proposing a linear programming formulation accounting for both autonomous intersection control and dynamic traffic assignment.

Table 5.4.
Departure rates under the non-accident scenario

OD pair	Route #	Time																Sum
		1	2	3	4	5	6	7	8	9	10	11	12	13	14	15	16	
(1,10)	1	1	1	1	1	1	1	1	1	1	1	0	0	0	0	0	0	10
	2	0	0	0	0	0	0	0	0	0	0	0	0	0	0	0	0	0
	3	0	0	0	0	0	0	0	0	0	0	0	0	0	0	0	0	0
	4	0	0	0	0	0	0	0	0	0	0	0	0	0	0	0	0	0
(1,12)	1	0	0	0	0	0	0	0	0	0	0	0	0	0	0	0	0	0
	2	0	0	0	0	0	0	0	0	0	0	0	0	0	0	0	0	0
	3	1	0	1	1	1	0	1	1	0	0	1	1	1	0	0	0	9
(3,10)	1	0	1	0	0	0	1	0	0	1	1	0	0	0	0	0	0	4
	2	0	0	0	0	0	0	0	0	1	1	1	1	1	1	1	0	7
	3	0	0	0	0	0	0	0	0	0	0	0	0	0	0	0	0	0
(3,12)	1	1	1	1	1	1	1	1	1	0	0	0	0	0	0	0	0	8
	2	0	0	0	0	0	0	0	0	0	0	0	0	0	0	0	0	0
	3	0	0	0	0	0	0	0	0	0	0	0	0	0	0	0	0	0
	4	0	0	0	0	0	0	0	0	0	0	0	0	0	0	0	0	0

Table 5.5.
Departure rates under the accident scenario

OD pair	Route #	Time																Sum
		1	2	3	4	5	6	7	8	9	10	11	12	13	14	15	16	
(1,10)	1	0	1	1	1	1	0	1	1	1	1	1	1	0	0	0	0	10
	2	0	0	0	0	0	0	0	0	0	0	0	0	0	0	0	0	0
	3	0	0	0	0	0	0	0	0	0	0	0	0	0	0	0	0	0
	4	0	0	0	0	0	0	0	0	0	0	0	0	0	0	0	0	0
(1,12)	1	1	0	0	0	1	0	0	0	0	0	0	0	0	0	0	0	2
	2	0	0	0	0	0	0	0	0	0	0	0	0	0	0	0	0	0
	3	1	1	0	0	1	1	1	1	1	0	0	0	0	0	0	0	7
(3,10)	1	0	0	1	1	0	0	0	0	0	0	0	0	0	0	0	0	2
	2	0	1	1	1	1	0	1	0	0	0	0	0	1	1	1	1	9
	3	0	0	0	0	0	0	0	0	0	0	0	0	0	0	0	0	0
(3,12)	1	1	0	0	0	1	0	1	1	1	1	1	1	0	0	0	0	8
	2	0	0	0	0	0	0	0	0	0	0	0	0	0	0	0	0	0
	3	0	0	0	0	0	0	0	0	0	0	0	0	0	0	0	0	0
	4	0	0	0	0	0	0	0	0	0	0	0	0	0	0	0	0	0

Firstly, based on the previous work from (Yperman, 2007; Zhu and Ukkusuri, 2014) we propose a new lane based traffic flow model that is capable of capturing most of the traffic realisms, e.g., traffic shock-waves, spill back effects due to heavy congestion. The formulation is in a nonlinear form and has a bi-level structure to account for conflict-free vehicle movements in the network. Then the bi-level optimization formulation is transformed to the linear programming problem by relaxing the nonlinear constraints with a set of linear equations. One special feature of the LPAIC formulation is that the entries of the constraint matrix are consisting of values in {-1,0,1}. This feature brings the LPAIC formulation several nice properties. E.g., the matrix of the constraint domain is totally unimodular; the optimal solutions are integers; the intersection safety is secured, i.e., traffic flows from different phases do not go through the conflict points concurrently, etc. In the second part of the chapter, we have provided three numerical case studies. The first case is an X shape network consisting of diverging and merging lanes. It is confirmed that the traffic flow propagation from the LPAIC formulation is identical with that from the LTM model and the CTM model. The second case is a 4-lane 4-leg isolated intersection. In terms of travel time reduction, the autonomous intersection control outperforms actuated signal control over different V/C ratio scenarios. It is also found that the difference between autonomous intersection control and actuated signal control is decreasing when the V/C ratio increases. The third test case is a grid network with multiples OD pairs. We have designed the non-accident and accident scenarios. It shows that the route choice and departure time behavior are different under these scenarios. This chapter is a starting point of applying linear programming in the area of autonomous intersection control. One interesting extension is to apply the LPAIC formulation in traditional signal control. One challenge in this extension is how to capture the minimum and maximum green time in signal control. Note that the LPAIC formulation is readily applicable to traditional signal control if there is no requirement on the range of green time. The second valuable topic is to investigate the sensitivity analysis to demonstrate the benefits of autonomous intersection control.

It is found that the gains from autonomous intersection control are decreasing when the V/C ratio increases. The third future research direction is to utilize the LPAIC formulation to address the dynamic traffic assignment (DTA) problem. The LPAIC formulation in this chapter is limited to the area of system optimum. How to adjust the formulation to account for user equilibrium (UE) behavior is an important extension that deserves future study. Last but not the least, it is worthwhile to address the lane changing issue. Lane changing behavior is realistic and necessary in traffic flow modeling. However, we are unable to capture it in the proposed formulation due to the complexity and nonlinear nature of the lane changing constraint. The LPAIC formulation will be more complete and powerful if there is a way to transform the nonlinear constraint of lane changing to a linear form.

5.6 Appendix:

Table 5.6.
Occupancy output of the LPAIC formulation and LTM (both are the same)

Time	Demand1	Demand2	Lane3	Lane4
0	0	0	0	0
1	0	1	0	0
2	0	0	0	0
3	1	0	1	0
4	0	1	1	0
5	0	0	2	0
6	0	1	3	0
7	0	1	2	1
8	1	0	3	1
9	0	0	3	2
10	0	0	3	3
11	1	0	3	2
12	1	0	2	3
13	0	1	2	3
14	0	0	2	3
15	1	0	3	3
16	0	0	3	2
17	0	0	3	2
18	1	0	2	2
19	0	0	1	3
20	0	1	2	3
21	0	0	1	3
22	0	0	2	2
23	0	0	2	1
24	0	0	1	2
25	0	0	1	1
26	0	0	0	2
27	0	0	0	2
28	0	0	0	1
29	0	0	0	1
30	0	0	0	0

Table 5.7.
Occupancy output of CTM

Time	Demand1	Demand2	C3.1	C3.2	C3.3	C3.4	Sum	C4.1	C4.2	C4.3	C4.4	Sum
0	0	0	0	0	0	0	0	0	0	0	0	0
1	0	1	0	0	0	0	0	0	0	0	0	0
2	0	0	0	0	0	0	0	0	0	0	0	0
3	1	0	1	0	0	0	1	0	0	0	0	0
4	0	1	0	1	0	0	1	0	0	0	0	0
5	0	0	1	0	1	0	2	0	0	0	0	0
6	0	1	1	1	0	1	3	0	0	0	0	0
7	0	1	0	1	1	0	2	1	0	0	0	1
8	1	0	1	0	1	1	3	0	1	0	0	1
9	0	0	1	1	0	1	3	1	0	1	0	2
10	0	0	1	1	1	0	3	1	1	0	1	3
11	1	0	0	1	1	1	3	0	1	1	0	2
12	1	0	0	0	1	1	2	1	0	1	1	3
13	0	1	1	0	0	1	2	1	1	0	1	3
14	0	0	1	1	0	0	2	1	1	1	0	3
15	1	0	1	1	1	0	3	0	1	1	1	3
16	0	0	0	1	1	1	3	0	0	1	1	2
17	0	0	1	0	1	1	3	1	0	0	1	2
18	1	0	0	1	0	1	2	1	1	0	0	2
19	0	0	0	0	1	0	1	1	1	1	0	3
20	0	1	1	0	0	1	2	0	1	1	1	3
21	0	0	0	1	0	0	1	1	0	1	1	3
22	0	0	1	0	1	0	2	0	1	0	1	2
23	0	0	0	1	0	1	2	0	0	1	0	1
24	0	0	0	0	1	0	1	1	0	0	1	2
25	0	0	0	0	0	1	1	0	1	0	0	1
26	0	0	0	0	0	0	0	1	0	1	0	2
27	0	0	0	0	0	0	0	0	1	0	1	2
28	0	0	0	0	0	0	0	0	0	1	0	1
29	0	0	0	0	0	0	0	0	0	0	1	1
30	0	0	0	0	0	0	0	0	0	0	0	0

Part III: Traffic Impact Analysis

6. EFFICIENT AND FAIR SYSTEM STATES IN DYNAMIC TRANSPORTATION NETWORKS

This chapter sets out to model an efficient and fair transportation system accounting for both departure time choice and route choice of a general multi OD network within a dynamic traffic assignment environment. Firstly, a bi-level optimization formulation is introduced based on the link-based traffic flow model. The upper level of the formulation minimizes the total system travel time, whereas the lower level captures traffic flow propagation and the user equilibrium constraint. Then the bi-level formulation is relaxed to a linear programming formulation that produces a lower bound of an efficient and fair system state. An efficient iterative algorithm is proposed to obtain the exact solution. It is shown that the number of iterations is bounded, and the output traffic flow solution is efficient and fair. Finally, two numerical cases (including a single OD network and a multi-OD network) are conducted to demonstrate the performance of the algorithm. The results consistently show that the travel time of different departure rates of the same OD pair are identical and the algorithm converges within two iterations across all test scenarios.

6.1 Introduction

Advances in intelligent transportation systems (ITS) promise to enable advanced traveler information systems (ATIS) and the related travel guidance (e.g., route choice, departure time choice) systems for individual travelers. Particularly, with the recent development of information and communication technology, the personalized guidance customized to the need of individual drivers is rapidly becoming a reality. However, individual users may not comply with the guidance if the guidance is not efficient and fair.

Personalized traffic guidance system aims to provide travelers with real-time traffic information and reliable guidance information on route selection and departure time choice. Usually, the traffic information in any guidance system can be classified into two categories: the descriptive information (that faithful represents the system state) and the prescriptive information (that provides useful guidance to the individual users). (1) Descriptive information typically refers to the traffic state data collected through traffic sensors including loop detectors, camera video processing, the Global Positioning System (GPS), and so on. Especially, GPS is widely used in automotive navigation. Almost all the smart phones are equipped with GPS-based positioning functionalities. Meanwhile, the recent development of ITS emphasizes the application of Dedicated Short Range Communications (DSRC) in vehicle-to-vehicle and vehicle-to-infrastructure wireless communications, which may significantly reinforce the traffic information propagation in the network. (2) Prescriptive information is typically transitioned from descriptive information through a modeling and computing process. Most current versions of GPS navigation devices provide prescriptive guidance based on static data. More recently real-time information based guidance has been provided by few private firms in the United States (e.g., Google Map, Inrix, Telenav, and Dash). However, the real-time guidance is based on the reactive information of current network state or limited predictive models that do not account for user behavior. It is likely that the continued growth and acceptance of navigation devices will hinge upon the capability of such devices to accurately predict future system states and consistently provide reliable guidance to travelers.

As an increasing number of travelers start using navigation devices, the limitation of static or limited-predictive models could undermine the true benefits realizable through these devices. There is a pressing need for navigation devices to provide reliable (both efficient and fair) guidance to travelers. The personalized travel guidance systems are envisaged as a tool that will assist travelers make efficient travel decisions by providing network state information both pre-trip and en-route. This paradigm of personalized guidance raises many fundamental research questions in terms of fairness

and efficiency, well beyond the traditional traffic flow modeling and estimation. A key fundamental research question in dynamic transportation networks is: can we characterize and compute system states which are close to system optimal (i.e., efficient) but does not make any individual user worse off (i.e., fair)? To answer this question, we need to solve a combined system optimum and user equilibrium problem.

6.1.1 Related work

Note that the study of this chapter is in the context of dynamic traffic assignment (DTA). DTA plays an important role in transportation network modeling since it provides a clear representation of time varying conditions in traffic networks. Based on the behavioral assumption of individual user's travel decision making, DTA problems can be classified into two categories: the dynamic system optimal problem and the dynamic user equilibrium problem. (1) For the dynamic system optimal (DSO) problem, [166, 167] modeled the traffic flow propagation with a nonlinear exit-flow function that is also non-convex. [168] reformulated the M-N model [166, 167] as a convex non-linear program by relaxing the non-convex exit-flow function with a set of inequity constraints. Then [169] proposed a marginal cost approach to solve the non-linear optimization problem of DSO. But the analysis is based on a point queue model. Later different approaches [170, 171, 172, 173] based on the physical queue model have been developed to compute the path marginal cost. (2) For the dynamic user equilibrium (DUE) problem, [174] formulated the problem as an equivalent continuous time optimal control problem. [175] firstly proposed a variational inequality formulation considering both simultaneous route choice and departure time decisions. [41, 42] incorporated the cell-based model into the user equilibrium dynamic traffic assignment problem using the variational inequality approach. [176] efficiently solved the dynamic user optimal problem embedding cell transmission model. [43, 44] formulated the cell-based dynamic user equilibrium problem using complementarity theory.

However, most of the above models are nonlinear and intractable. Solving a nonlinear DSO or DUE problems usually requires a specialized algorithm. From a different direction, to avoid the nonlinearity of the problem, a handful of researchers investigated in developing DTA models based on linear programming. For the DSO problem, [177] transformed the nonlinear cell-based SODTA formulation into a linear programming problem, whereby the nonlinear constraints and the bi-level structure are relaxed with a set of linear inequalities. One problem due to the linear relaxation is known as the holding back problem [178]. [179] proposed a variant of the M-N model [166, 167] using a piecewise linear exit-flow function, and verified that Ho's algorithm [180] can be applied to eliminate the unnecessary holding flows in the network. Most recently, [181] resolved the holding-back problem by introducing penalty labels to the objective function of the linearized formulation. For the DUE problem, [182] firstly formulated the cell-based DUE problem in a linear programming formulation. In the formulation, a Mt vector is associated with the arrival flows in the objective function to provide incentives to the traffic flow to arrive the destination as soon as possible. One limitation of the formulation lies in the difficulty of obtaining a proper Mt vector for a large network.

There is limited literature addressing the combined problem of system optimum and user equilibrium. Solving the combined problem is a challenging task even in the case of static traffic assignment. [183, 184] formulated the problem as minimizing the maximum latency of flows in networks with congestion. It is showed that in static traffic assignment, even in a single OD network with a linear link cost function, the combined system optimum and user equilibrium problem is NP hard. [185] firstly proposed a constrained system-optimum model that guarantees user fairness, and developed a constrained shortest path algorithm to solve the optimization problem. However, the model and the algorithm are limited to the case of static traffic assignment. A sound method of studying the combined problem of system optimum and user equilibrium in the context of dynamic traffic assignment remains to be explored.

6.1.2 Contributions of the chapter

This chapter sets out to model a transportation system that is both efficient (from the system's perspective) and fair (from an individual user's perspective) within a dynamic traffic assignment environment. The modeling framework is capable of accounting for dynamic departure time and route choice at the network level. Contributions of the chapter are summarized as below.

- We propose a bi-level optimization formulation based on the link transmission model [37, 186]. At the upper level, the objective is to optimize the total system travel time of the traffic flow at the network level (efficient). At the lower level, the objective is to propagate traffic flows in the network and equilibrate the travel cost of individual users (fair).

- The bi-level optimization formulation is relaxed to a linear programming formulation where the nonlinear constraints are replaced by a set of linear inequality constraints. The linear programming (LP) relaxation produces a lower bound of an efficient and fair system state.

- Based on the lower bound of the LP relaxation, an efficient iterative algorithm is proposed to obtain the exact solution of an efficient and fair system state. Every iteration, the algorithm produces a new and tighter lower bound on the efficient and fair system state. It is proved that the number of iterations of the algorithm is bounded and the travel time cost of different departure rates under the same OD pair are the same.

- Two numerical case studies including a single OD network [177] and a multi-OD [187] network are conducted to demonstrate the performance of the algorithm. The results consistently confirm that the traffic flow solution is efficient and fair. Moreover, it takes no more than two iterations for all the test scenarios.

The rest of the chapter is structured as below. Section 6.2 is devoted to the formulation of an efficient and fair transportation network. The bi-level optimization

formulation is firstly introduced, and then is relaxed to a linear programming formulation. Section 6.3 introduces an efficient algorithm to obtain the solution of an efficient and fair system state. Section 6.4 conducts numerical studies on two test networks to demonstrate the performance of the algorithm including a single OD network and a multi-OD network. Finally, Section 6.5 concludes the chapter and discusses future research directions of this study.

Notations:

Sets

$\mathbf{Z}$	:	Set of all links
$\mathbf{Z}_{G,S,O,D,M}$	:	Set of origin, destination, ordinary, diverging, or merging links
$\mathbf{E}$	:	Set of all connectors
$\mathbf{E}_{O,D,M}$	:	Set of ordinary, diverging, or merging link connectors, respectively
$\Gamma^{-1}(i)$	:	Set of predecessors of link i
$\Gamma(i)$	:	Set of successors of link i
$\mathbf{U}$	:	Set of all OD pairs
$\mathbf{P}^{o,d}$	:	Set of all paths of OD (o,d)

Parameters

δ	:	Size of the time step
T	:	Entire time horizon
T_d	:	Time horizon of departure time choice, $T_d \leq T$
N_i	:	Jam density of link i
Q	:	Maximum out flow of an OD pair at any departure time
S_i^t	:	Inflow or outflow capacity of link i at time t
W_i	:	Shock wave speed of link i
V_i	:	Free flow speed of link i
$D^{o,d}$	:	Total demand of OD pair (o,d) during the departure period
L_i	:	Length of link i
ε	:	Tolerance of fairness

Variables

$x_i^{o,d,p}(\bar{t},t)$	:	Occupancy (number of vehicles) of link i at time t on path p departed at time $\bar{t}$ of OD (o,d)
$y_{i,j}^{o,d,p}(\bar{t},t)$	:	Flow from link i to j at time t on path p departed at $\bar{t}$ of (o,d)
$x_i(t)$	:	Aggregate occupancy of link i at time t
$y_{i,j}(t)$	:	Aggregate flow from link i to j at time t
$r^{o,d}(p,\bar{t})$	:	Departure rate at departure time $\bar{t}$ of path p of OD (o,d), $\bar{t} \in [1, T_d]$. Note that $r^{o,d,p}(\bar{t}) = \sum_{\forall t} y_{o,j}^{o,d,p}(\bar{t},t), o \in \mathbf{Z}_G, j \in \Gamma(o)$
$c^{o,d}(p,\bar{t})$	:	Travel cost of departure rate $r^{o,d,p}(\bar{t})$ at departure time $\bar{t}$ of path p of OD (o,d), $\bar{t} \in [1, T_d]$
$l^{o,d}(p,\bar{t})$	:	Average travel time of departure rate at departure time $\bar{t}$ of path p of OD (o,d), $\bar{t} \in [1, T_d]$
$l_{avg}^{o,d}(k)$	:	Average travel time of all departure rates of OD (o,d) at k iteration

6.2 Formulation of an efficient and fair transportation network

6.2.1 Assumptions

Assumption 6.2.1 The departure rate of all paths at any departure time under the same OD pair is non-negative and no greater than Q, i.e.,

$$0 \leq \sum_{\forall p \in \mathbf{P}^{o,d}} r^{o,d}(p, \bar{t}) \leq Q, \forall (o,d) \in \mathbf{U}, \bar{t} \in [0, T_d] \tag{6.1}$$

and the total demand $D^{o,d}$ is a positive integer multiple of Q, i.e., $\dfrac{D^{o,d}}{Q} \in \mathbb{Z}_+$.

Assumption 6.2.2 The outflow capacity of any link at any time is a nonnegative integer multiple of Q, i.e., $\forall i \in \mathbf{Z}, \forall t \in [0, T], \dfrac{S_i^t}{Q} \in \{0, \mathbb{Z}_+\}$.

Remark 6.2.3 The outflow capacity of a link is allowed to be zero in order to capture the traffic realism of capacity drops in the real world. For example, if the end of the link is a signalized intersection, the capacity becomes zero when the traffic light is red. For another example, the outflow capacity of a link may become zero for a while when an accident occurs.

6.2.2 Bi-level optimization formulation

In this study, we apply the link based traffic flow model [37, 186] to propagate traffic flows in the network. However, it is worth to note that the methodology of this chapter is also readily applicable to other types of traffic flow model, as long as the traffic flow model can be formulated in a linear form (e.g., [27, 177, 181]). The link based traffic flow model is a discrete time model where the time space is discretized into time steps. Traffic flow propagation in the network is link based. The number of vehicles within the link is defined as the occupancy of the link, denoted as $x_i(t), i \in \mathbf{Z}$. The number of vehicle moving from one link to another is defined as the traffic flow of the link connector, denoted as $y_{i,j}(t), (i,j) \in \mathbf{E}$. The traffic flow propagation is realized by updating temporal values of $x_i(t), i \in \mathbf{Z}$ and $y_{i,j}(t), (i,j) \in \mathbf{E}$ in the network.

The bi-level optimization formulation of an efficient and fair network (BOEFN):

$$\min \mathbf{z}_1 = \sum_{t=1}^{T} \sum_{i \in \mathbf{Z} \setminus \{\mathbf{Z}_G, \mathbf{Z}_S\}} x_i(t) \tag{6.2}$$

Subject to:

Demand satisfaction constraint:

$$\sum_{\bar{t}=1}^{T_d} \sum_{p \in \mathbf{P}^{o,d}} r^{o,d}(p, \bar{t}) = D^{o,d} \tag{6.3}$$

Aggregation of link occupancy and outflow constraints:

$$x_i(t) = \sum_{(o,d) \in \mathbf{U}} \sum_{p \in \mathbf{P}^{o,d}} \sum_{\bar{t}=1}^{T_d} x_i^{o,d,p}(\bar{t}, t), \forall i \in \mathbf{Z} \tag{6.4}$$

$$y_{i,j}(t) = \sum_{(o,d) \in \mathbf{U}} \sum_{p \in \mathbf{P}^{o,d}} \sum_{\bar{t}=1}^{T_d} y_{i,j}^{o,d,p}(\bar{t}, t), \forall (i,j) \in \mathbf{E} \tag{6.5}$$

Link occupancy constraints:

Source links, $\forall i \in \mathbf{Z}_G, p \in \mathbf{P}^{o,d}, \bar{t} \in [0, T_d]$:

$$x_i^{o,d,p}(\bar{t}, t) = x_i^{o,d,p}(\bar{t}, t-1) - \sum_{j \in \Gamma(i)} y_{i,j}^{o,d,p}(\bar{t}, t-1) \tag{6.6}$$

Sink links, $\forall i \in \mathbf{Z}_S, p \in \mathbf{P}^{o,d}, \bar{t} \in [0, T_d]$:

$$x_i^{o,d,p}(\bar{t}, t) = x_i^{o,d,p}(\bar{t}, t-1) + \sum_{k \in \Gamma^{-1}(i)} y_{k,i}^{o,d,p}(\bar{t}, t-1) \tag{6.7}$$

Ordinary links, $\forall i \in \mathbf{Z}_O, p \in \mathbf{P}^{o,d}, \bar{t} \in [0, T_d]$:

$$x_i^{o,d,p}(\bar{t}, t) = x_i^{o,d,p}(\bar{t}, t-1) + y_{k,i}^{o,d,p}(\bar{t}, t-1) - y_{i,j}^{o,d,p}(\bar{t}, t-1), k \in \Gamma^{-1}(i), j \in \Gamma(i) \tag{6.8}$$

Merging links, $\forall i \in \mathbf{Z}_M, p \in \mathbf{P}^{o,d}, \bar{t} \in [0, T_d]$:

$$x_i^{o,d,p}(\bar{t}, t) = x_i^{o,d,p}(\bar{t}, t-1) + \sum_{k \in \Gamma^{-1}(i)} y_{k,i}^{o,d,p}(\bar{t}, t-1) - y_{i,j}^{o,d,p}(\bar{t}, t-1), j \in \Gamma(i) \tag{6.9}$$

Diverging links, $\forall i \in \mathbf{Z}_D, p \in \mathbf{P}^{o,d}, \bar{t} \in [0, T_d]$:

$$x_i^{o,d,p}(\bar{t}, t) = x_i^{o,d,p}(\bar{t}, t-1) + y_{k,i}^{o,d,p}(\bar{t}, t-1) - \sum_{j \in \Gamma(i)} y_{i,j}^{o,d,p}(\bar{t}, t-1), k \in \Gamma^{-1}(i) \tag{6.10}$$

Link connector constraints:

Ordinary link connectors, $\forall (i,j) \in \mathbf{E}_O, p \in \mathbf{P}^{o,d}, \bar{t} \in [0, T_d]$

$$\max y_{i,j}^{o,d,p}(\bar{t}, t) \tag{6.11}$$

$$\begin{cases} y_{i,j}^{o,d,p}(\bar{t}, t) & \leq x_i^{o,d,p}(\bar{t}, t+1-\frac{L_i}{V_i}) - \sum_{k=t+1-\frac{L_i}{V_i}}^{t-1} y_{i,j}^{o,d,p}(\bar{t}, k) \\ y_{i,j}(t) & \leq S_i^t \\ y_{i,j}(t) & \leq S_j^t \\ y_{i,j}(t) & \leq N_j - x_j(t) - \sum_{k=t+1-\frac{L_i}{W_i}}^{t-1} y_{j,l}(k) \end{cases} \tag{6.12}$$

Diverging link connectors, $\forall i \in \mathbf{Z}_D, p \in \mathbf{P}^{o,d}$

$$\max y_{i,j}^{o,d,p}(\bar{t}, t) \tag{6.13}$$

$$\begin{cases} \sum_{j \in \Gamma(i)} y_{i,j}^{o,d,p}(\bar{t}, t) & \leq x_i^{o,d,p}(\bar{t}, t+1-\frac{L_i}{V_i}) - \sum_{k=t+1-\frac{L_i}{V_i}}^{t-1} y_{i,j}^{o,d,p}(\bar{t}, k) \\ \sum_{j \in \Gamma(i)} y_{i,j}(t) & \leq S_i^t \\ y_{i,j}(t) & \leq S_j^t, j \in \Gamma(i) \\ y_{i,j}(t) & \leq N_j - x_j(t) - \sum_{k=t+1-\frac{L_i}{W_i}}^{t-1} y_{j,l}(k), j \in \Gamma(i) \end{cases} \tag{6.14}$$

Merging link connectors, $\forall j \in \mathbf{Z}_M, p \in \mathbf{P}^{o,d}$

$$\max y_{i,j}^{o,d,p}(\bar{t}, t) \tag{6.15}$$

$$\begin{cases} y_{i,j}^{o,d,p}(\bar{t}, t) & \leq x_i^{o,d,p}(\bar{t}, t+1-\frac{L_i}{V_i}) - \sum_{k=t+1-\frac{L_i}{V_i}}^{t-1} y_{i,j}^{o,d,p}(\bar{t}, k), i \in \Gamma^{-1}(j) \\ \sum_{i \in \Gamma^{-1}(j)} y_{i,j}(t) & \leq S_j^t \\ y_{i,j}(t) & \leq S_i^t, i \in \Gamma^{-1}(j) \\ \sum_{i \in \Gamma^{-1}(j)} y_{i,j}(t) & \leq N_j - x_j(t) - \sum_{k=t+1-\frac{L_i}{W_i}}^{t-1} y_{j,l}(k), l \in \Gamma(j) \end{cases} \tag{6.16}$$

User equilibrium constraints:

To compute the path travel time, if $r^{o,d}(p, \bar{t}) > 0, p \in \mathbf{P}^{o,d}, o \in \mathbf{Z}_G, d \in \mathbf{Z}_S, \bar{t} \in [1, T_d]$, then:

$$l^{o,d}(p, \bar{t}) = \frac{\sum_{t=1}^{T} \sum_{i \in \Gamma^{-1}(d)} t \cdot y_{i,d}^{o,d,p}(\bar{t}, t) - \sum_{t=1}^{T_d} \sum_{j \in \Gamma(o)} t \cdot y_{o,j}^{o,d,p}(\bar{t}, t)}{r^{o,d}(p, \bar{t})} \tag{6.17}$$

User equilibrium condition, $\forall p \in \mathbf{P}^{o,d}, \bar{t} \in [1, T_d]$:

$$0 \leq r^{o,d}(p, \bar{t}) \perp l^{o,d}(p, \bar{t}) - l_* \geq 0 \tag{6.18}$$

Nonnegative constraints: $y_{i,j}^{o,d,p}(\bar{t}, t) \geq 0, i \in \mathbf{Z}, j \in \Gamma(i), (o, d) \in \mathbf{U}, p \in \mathbf{P}^{o,d}, \bar{t} \in [0, T_d], t \in [0, T]$.

□

Remark 6.2.4 The traffic flow updating procedure of link connectors, i.e., (6.12) - (6.16) is consistent with the flow update procedure of the LTM model [186].
Proof. A similar proof can be found at [37]. □

Remark 6.2.5 Constraint (6.18) is a complementarity constraint. It is mathematically equal to: $r^{o,d}(p, \bar{t}) \geq 0, l^{o,d}(p, \bar{t}) - l_* \geq 0$, and $r^{o,d}(p, \bar{t})(l^{o,d}(p, \bar{t}) - l_*) = 0$. It essentially indicates that if $r^{o,d}(p, \bar{t}) > 0$, $l^{o,d}(p, \bar{t}) = l_*$; if $l^{o,d}(p, \bar{t}) > l_*$, $r^{o,d}(p, \bar{t}) = 0$.

Remark 6.2.6 Equation (6.17) computes the average travel time of the departure rate of path p departed at time $\bar{t}$. It is computed by dividing the difference between the accumulative arrival travel time and the accumulative departure travel time over the departure rate. In (6.17), $\sum_{t=1}^{T_d} \sum_{j \in \Gamma(o)} t \cdot y_{o,j}^{o,d,p}(\bar{t}, t)$ represents the accumulative time of the traffic departs at origin o, and $\sum_{t=1}^{T} \sum_{i \in \Gamma^{-1}(s)} t \cdot y_{i,s}^{o,d,p}(\bar{t}, t)$ represents the accumulative time this traffic arrives at destination d. Similar approach to compute path travel time can also been seen in [42, 44]. Figure 6.1 presents an example to demonstrate the idea. In this example, supposing 2 units of traffic flow depart at time 1 from O to D. One unit arrives at time 7, and the other unit arrives at time 9. Thus the average travel time is $(7 + 9 - 2)/2 = 7$.

6.2.3 Linear programming relaxation

Similar to the relaxation scheme in [37, 177], we relax the nonlinear constraints of the bi-level optimization program with a set of linear inequities. The linear relaxation

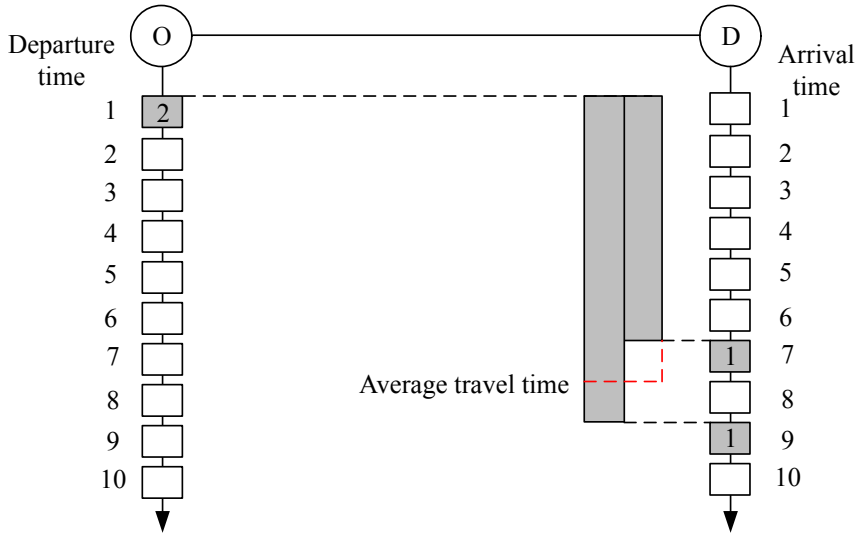

Fig. 6.1. A demonstrative example of average path travel time calculation

formulation is presented as below. It is worth to note that the linear relaxation does not produce the solution of an efficient and fair network, but provides a lower bound of the solution. We will present the algorithm of computing the efficient and fair system state later in Section 6.3.1.

The linear programming relaxation of an efficient and fair network:

$$\min \mathbf{z}_2 = \sum_{\forall(o,d)} \sum_{\forall p} \sum_{\forall \bar{t}} c^{o,d}(p, \bar{t}) \tag{6.19}$$

Subject to:

Demand satisfaction constraint: (6.3)

Aggregation of link occupancy and outflow: (6.4), (6.5)

Link occupancy constraints: (6.6), (6.7), (6.8), (6.9), (6.10)

Link connector constraints: (6.12), (6.14), (6.16)

Constraints from Assumption 1: (6.1)

User equilibrium constraints, $\forall p \in \mathbf{P}^{o,d}, t \in [1, T_d]$:

$$c^{o,d}(p,\bar{t}) = \sum_{t=1}^{T} \sum_{i \in \Gamma^{-1}(d)} t \cdot y_{i,d}^{o,d,p}(\bar{t},t) - \sum_{t=1}^{T_d} \sum_{j \in \Gamma(o)} t \cdot y_{o,j}^{o,d,p}(\bar{t},t) \tag{6.20}$$

$$\sum_{\forall p \in \mathbf{P}^{o,d}} \frac{c^{o,d}(p,\bar{t})}{Q} D^{o,d} \leq \sum_{\forall p \in \mathbf{P}^{o,d}} \sum_{t=1}^{T_d} c^{o,d}(p,\bar{t}) \tag{6.21}$$

Nonnegative constraints: $y_{i,j}^{o,d,p}(\bar{t},t) \geq 0, i \in \mathbf{Z}, j \in \Gamma(i), (o,d) \in \mathbf{U}, p \in \mathbf{P}^{o,d}, \bar{t} \in [0,T_d], t \in [0,T]$.

□

Lemma 6.2.7 The accumulative departure rate of all paths $p \in \mathbf{P}^{o,d}$ at any departure time $\bar{t}$ is either 0 or Q, i.e., $\sum_{\forall p \in \mathbf{P}^{o,d}} r^{o,d}(p,\bar{t}) \in \{0,Q\}, \bar{t} \in [0,T_d]$.

Proof. From Assumption 1, $0 \leq \sum_{\forall p \in \mathbf{P}^{o,d}} r^{o,d}(p,\bar{t}) \leq Q$. From Assumption 2, the bottleneck of the network is either zero or greater than Q, and the objective is to minimize the total system travel time. Thus, $\sum_{\forall p \in \mathbf{P}^{o,d}} r^{o,d}(p,\bar{t}) \in \{0,Q\}$. □

Lemma 6.2.8 Let $c_*^{o,d}(p,\bar{t})$ denote the solution of the LP relaxation. If $\sum_{\forall p \in \mathbf{P}^{o,d}} c_*^{o,d}(p,\bar{t}) > 0$, then $\sum_{\forall p \in \mathbf{P}^{o,d}} c_*^{o,d}(p,\bar{t}) = c_*, \forall \bar{t} \in [0,T_d]$.

Proof. Let $\bar{c}_*^{o,d}(p,\bar{t})$ denote the $c_*^{o,d}(p,\bar{t})$ that is positive. Then, from (6.21), we have:

$$\sum_{\forall p \in \mathbf{P}^{o,d}} \frac{\bar{c}_*^{o,d}(p,\bar{t})}{Q} \leq \sum_{\forall p} \sum_{\forall \bar{t}} \frac{\bar{c}_*^{o,d}(p,\bar{t})}{D^{o,d}} \tag{6.22}$$

Moreover, define $\gamma^{o,d}(\bar{t}) \geq 0$, such that (6.22) can be rewritten as:

$$\sum_{\forall p \in \mathbf{P}^{o,d}} \frac{\bar{c}_*^{o,d}(p,\bar{t})}{Q} = \sum_{\forall p} \sum_{\forall \bar{t}} \frac{\bar{c}_*^{o,d}(p,\bar{t})}{D^{o,d}} - \gamma^{o,d}(\bar{t}) \tag{6.23}$$

where $0 \leq \gamma^{o,d}(\bar{t}) \leq \sum_{\forall p \in \mathbf{P}^{o,d}} \frac{c_*^{o,d}(p,\bar{t})}{Q}, \bar{t} \in [0,T_d]$.

Sum up both sides of (6.23) over $\bar{t}$, we have:

$$\sum_{\forall p}\sum_{\forall \bar{t}} \frac{\bar{c}_*^{o,d}(p,\bar{t})}{Q} = \frac{D^{o,d}}{Q}\sum_{\forall p}\sum_{\forall \bar{t}} \frac{\bar{c}_*^{o,d}(p,\bar{t})}{D^{o,d}} - \sum_{\forall \bar{t}} \gamma^{o,d}(\bar{t}) \tag{6.24}$$

$$\Rightarrow \sum_{\forall p}\sum_{\forall \bar{t}} \frac{\bar{c}_*^{o,d}(p,\bar{t})}{Q} = \sum_{\forall p}\sum_{\forall \bar{t}} \frac{\bar{c}_*^{o,d}(p,\bar{t})}{Q} - \sum_{\forall \bar{t}} \gamma^{o,d}(\bar{t}) \tag{6.25}$$

$$\Rightarrow \sum_{\forall \bar{t}} \gamma^{o,d}(\bar{t}) = 0 \tag{6.26}$$

Since $\gamma^{o,d}(\bar{t}) \geq 0$, we get $\gamma^{o,d}(\bar{t}) = 0$. Thus:

$$\sum_{\forall p \in \mathbf{P}^{o,d}} \bar{c}_*^{o,d}(p,\bar{t}) = \frac{Q}{D^{o,d}}\sum_{\forall p}\sum_{\forall \bar{t}} \bar{c}^{o,d}(p,\bar{t}) \tag{6.27}$$

□

Remark 6.2.9 The proof of Lemma 2 is triggered by a simple example as below. Suppose there are three positive variables a, b, and c, with the constraint: $0 < a, b, c \leq d$, where $d = \frac{a+b+c}{3}$. The interest here is to prove that $a = b = c = d$. Firstly, let $a = d-\gamma_1, b = d-\gamma_2$, and $c = d-\gamma_3$, where $\gamma_{1,2,3} \geq 0$. Then $a+b+c = 3d-\sum_{i=1,2,3}\gamma_i$, which can be simplified to: $\sum_{i=1,2,3}\gamma_i = 0$. Thus $\gamma_{1,2,3} = 0$, and we have $a = b = c = d$. The proof of Lemma 2 is simply a generalized version of the proof of this example.

6.3 On computing an efficient and fair system state

6.3.1 An algorithm to obtain an efficient and fair system state

Firstly, we present an important extra constraint as below:

$$c^{o,d}(p,\bar{t}) \geq r^{o,d}(p,\bar{t})LB^{o,d}(k) \tag{6.28}$$

where $LB^{o,d}(k)$ is an exogenous constant, denoting the lower bound of the travel time at equilibrium for OD (o,d) at the k iteration.

Then we add this constraint to the LP relaxation. For the sake of brevity, we denote the domain of the LP relaxation plus constraint (6.28) as: $\mathbf{AY} \leq \mathbf{b}, \mathbf{Y} \geq \mathbf{0}$, where $\mathbf{Y}$ represents the set of variables of the LP relaxation, and $\mathbf{AY} \leq \mathbf{b}, \mathbf{Y} \geq \mathbf{0}$

represents all the linear constraints of the LP relaxation plus constraint (6.28). Thus, the updated LP formulation (denoted as LP2) can be written as:

$$\min \mathbf{z}_2 = \sum_{\forall(o,d)} \sum_{\forall p} \sum_{\forall \bar{t}} c^{o,d}(p,\bar{t}) \tag{6.29}$$

$$S.t.: \qquad \mathbf{AY} \leq \mathbf{b}, \mathbf{Y} \geq \mathbf{0} \tag{6.30}$$

Next, it is vital to obtain an estimate of $LB^{o,d}(k)$. At the initial stage, let $k = 0, LB^{o,d}(k) = 0$. Then the LP2 formulation reduces to the LP relaxation. After solving the LP relaxation, we compute the average travel time of OD pair (o,d) as $l^{o,d}_{avg}(k) = \frac{\sum_{\forall p} \sum_{\forall \bar{t}} c^{o,d}(p,\bar{t})}{D^{o,d}}$. Then update $LB^{o,d}(k+1) = \lceil l^{o,d}_{avg}(k) \rceil$, where $\lceil l^{o,d}_{avg}(k) \rceil$ denotes the nearest integer greater than or equal to $l^{o,d}_{avg}(k)$. Summary of the algorithm is presented in Algorithm 1.

Initialize: $k = 0, LB^{o,d}(k) = 0, check = 1$ **while** $check > 0$ **do**
  $k = k + 1$; Solve LP2 to obtain $l^{o,d}_{avg}(k) = \frac{\sum_{\forall p} \sum_{\forall \bar{t}} c^{o,d}(p,\bar{t})}{D^{o,d}}$;;
  If$LB^{o,d}(k) < \lceil l^{o,d}_{avg}(k) \rceil$ Update: $LB^{o,d}(k+1) = \lceil l^{o,d}_{avg}(k) \rceil$;;
  $check = 0$;;
end

Algorithm 4: Towards an efficient and fair system state

Proposition 6.3.1 At each iteration k, $LB^{o,d}(k)$ is an lower bound of the travel time for OD (o,d) under the condition of an efficient and fair system state.

Proof. We prove this proposition by the principle of mathematical induction.

In the initial stage, $k = 1$, and the LP2 formulation reduces to the LP relaxation. It is obvious that the LP relaxation is a lower bound of the efficient and fair system state.

Assuming that $LB^{o,d}(k), k \geq 1$ is an lower bound of an efficient and fair system state. In the $(k+1)$ iteration, the LP relaxation is solved with the lower bound of $LB^{o,d}(k)$ and outputs a new lower bound $l^{o,d}_{avg}(k+1)$. $LB^{o,d}(k+1)$ takes the value

of the nearest inter great than or equals to $l_{avg}^{o,d}(k+1)$, because the time space is discretized to time steps and the travel time is an integer multiple of the time steps. Thus, $LB^{o,d}(k+1)$ is also a lower bound. □

Proposition 6.3.2 The number of iterations of Algorithm 1 is upper bounded by $\max\{l_*^{o,d}(p,\bar{t}) : \forall(o,d) \in \mathbf{U}, p \in \mathbf{P}^{o,d}, \bar{t} \in [0,T_d]\}$, where $l_*^{o,d}(p,\bar{t})$ denotes the solution of an efficient and fair system state.

Proof. Firstly, it is easy to see that $\exists(o,d) \in \mathbf{U}$, such that $LB^{o,d}(k+1) \geq LB^{o,d}(k)+1$. Otherwise, $LB^{o,d}(k) = \lceil l_{avg}^{o,d}(k) \rceil$, the iteration stops.

Thus, in the worst scenario, when $LB^{o,d}(k)$ reaches $\max\{l_*^{o,d}(p,\bar{t}) : \forall(o,d) \in \mathbf{U}, p \in \mathbf{P}^{o,d}, \bar{t} \in [0,T_d]\}$, the algorithm ends. □

Remark 6.3.1 Note that after the first iteration, $LB^{o,d}(1) = \lceil l_{avg}^{o,d}(1) \rceil$. Thus the remaining number of iterations equals to $\max\{l_*^{o,d}(p,\bar{t}), \forall(o,d) \in \mathbf{U}, p \in \mathbf{P}^{o,d}, \bar{t} \in [0,T_d]\} - \lceil l_{avg}^{o,d}(1) \rceil$. It is worthwhile to note that $\lceil l_{avg}^{o,d}(1) \rceil$ provides a tight lower bound on the solution, because of which this algorithm converges very fast in practice. Of all the tests in the numerical case studies of Section 6.4, the number of iterations is less than or equal to two.

Lemma 6.3.2 Algorithm 1 stops at $l_{avg}^{o,d}(k) = \lceil l_{avg}^{o,d}(k) \rceil$.

Proof. As shown in line 5, Algorithm 1 ends when $LB^{o,d}(k) = \lceil l_{avg}^{o,d}(k) \rceil$. Firstly, from (6.28), we have:

$$c^{o,d}(p,\bar{t}) \geq r^{o,d}(p,\bar{t}) \lceil \frac{\sum_{\forall p} \sum_{\forall \bar{t}} c^{o,d}(p,\bar{t})}{D^{o,d}} \rceil \tag{6.31}$$

$$\Rightarrow \sum_{\forall p \in \mathbf{P}^{o,d}} c^{o,d}(p,\bar{t}) \geq \sum_{\forall p \in \mathbf{P}^{o,d}} r^{o,d}(p,\bar{t}) \lceil \frac{\sum_{\forall p} \sum_{\forall \bar{t}} c^{o,d}(p,\bar{t})}{D^{o,d}} \rceil \tag{6.32}$$

$$\Rightarrow \sum_{\forall p \in \mathbf{P}^{o,d}} c^{o,d}(p,\bar{t}) \geq Q \lceil \frac{\sum_{\forall p} \sum_{\forall \bar{t}} c^{o,d}(p,\bar{t})}{D^{o,d}} \rceil \quad \text{(From Lemma 1)} \tag{6.33}$$

From (6.27) of Lemma 2, we have:

$$\frac{Q}{D^{o,d}} \sum_{\forall p} \sum_{\forall \bar{t}} c^{o,d}(p,\bar{t}) \geq Q\lceil \frac{\sum_{\forall p} \sum_{\forall \bar{t}} c^{o,d}(p,\bar{t})}{D^{o,d}} \rceil \tag{6.34}$$

$$\Rightarrow \quad \frac{Q}{D^{o,d}} \sum_{\forall p} \sum_{\forall \bar{t}} c^{o,d}(p,\bar{t}) = Q\lceil \frac{\sum_{\forall p} \sum_{\forall \bar{t}} c^{o,d}(p,\bar{t})}{D^{o,d}} \rceil \tag{6.35}$$

$$\Rightarrow \quad l^{o,d}_{avg}(k) = \lceil l^{o,d}_{avg}(k) \rceil \tag{6.36}$$

□

Theorem 6.3.3 Any sequence of the departure rate pattern generated by Algorithm 1 converges to the solution of an efficient and fair system state.

Proof.

(1) *Fair.*

From Lemma 6.3.2, when Algorithm 1 ends, $LB^{o,d}(k) = l^{o,d}_{avg}(k)$. From (6.28), we have:

$$\frac{c^{o,d}(p,\bar{t})}{r^{o,d}(p,\bar{t})} \geq l^{o,d}_{avg}(k) \tag{6.37}$$

Now, introduce a new set of variable, $\mu^{o,d}(p,\bar{t}) \geq 0$, such that:

$$\frac{c^{o,d}(p,\bar{t})}{r^{o,d}(p,\bar{t})} \geq l^{o,d}_{avg}(k) + \mu^{o,d}(p,\bar{t}) \tag{6.38}$$

$$\Rightarrow \quad c^{o,d}(p,\bar{t}) \geq r^{o,d}(p,\bar{t}) l^{o,d}_{avg}(k) + r^{o,d}(p,\bar{t}) \mu^{o,d}(p,\bar{t}) \tag{6.39}$$

$$\Rightarrow \quad \sum_{\forall p \in \mathbf{P}^{o,d}} c^{o,d}(p,\bar{t}) \geq \sum_{\forall p \in \mathbf{P}^{o,d}} r^{o,d}(\cdot) l^{o,d}_{avg}(k) + \sum_{\forall p \in \mathbf{P}^{o,d}} r^{o,d}(\cdot) \mu^{o,d}(\cdot) \tag{6.40}$$

$$\Rightarrow \quad \sum_{\forall p \in \mathbf{P}^{o,d}} c^{o,d}(p,\bar{t}) \geq Q l^{o,d}_{avg}(k) + Q \mu^{o,d}(p,\bar{t}) \tag{6.41}$$

$$\Rightarrow \quad \frac{Q}{D^{o,d}} \sum_{\forall p} \sum_{\forall \bar{t}} c^{o,d}(p,\bar{t}) \geq \frac{Q}{D^{o,d}} \sum_{\forall p} \sum_{\forall \bar{t}} c^{o,d}(p,\bar{t}) + Q \mu^{o,d}(p,\bar{t}) \tag{6.42}$$

$$\Rightarrow \quad \mu^{o,d}(p,\bar{t}) = 0 \tag{6.43}$$

Further, from (6.38), we have:

$$\frac{c^{o,d}(p,\bar{t})}{r^{o,d}(p,\bar{t})} = l^{o,d}_{avg}(k) \tag{6.44}$$

Note that $l^{o,d}(p,\bar{t}) = \dfrac{c^{o,d}(p,\bar{t})}{r^{o,d}(p,\bar{t})}$. Thus, $l^{o,d}(p,\bar{t}) = l^{o,d}_{avg}(k), \forall p \in \mathbf{P}^{o,d}, \bar{t} \in [0, T_d]$.

(2) *Efficient.*

From Proposition 1, at every iteration, Algorithm 1 produces the lower bound of an efficient and fair system state. Thus the output of Algorithm 1 is the most efficient system state under the condition that the solution is fair. □

6.3.2 ε-*tolerant* fairness

The solution of Algorithm 1 requires that all the departure rates of the same OD experience the equal and minimum travel time. Here we propose the notion of tolerance-based fairness adapted from the behavioral notion of bounded-rationality [188]. The tolerance-based fairness only requires the travel time of all departure rates of the same OD to be within an acceptable tolerance level (i.e., ε) from the minimum travel time [189]. The tolerance ε is an exogenous parameter capturing the network user's behavior of tolerating unfairness. To model the ε-*tolerant* fairness, we firstly obtain the solution of an efficient and fair system state, then solve the LP2 formulation with the modified constraint (6.21) and (6.28) as below:

$$\sum_{\forall p \in \mathbf{P}^{o,d}} c^{o,d}(p,\bar{t}) \leq \frac{Q}{D^{o,d}} \sum_{\forall p \in \mathbf{P}^{o,d}} \sum_{t=1}^{T_d} c^{o,d}(p,\bar{t}) + \varepsilon Q \tag{6.45}$$

$$c^{o,d}(p,\bar{t}) \leq r^{o,d}(p,\bar{t}) \left(LB_*^{o,d} + \varepsilon\right) \tag{6.46}$$

where $LB_*^{o,d}$ denotes the solution of Algorithm 1.

6.4 Numerical studies

In this section, we construct two types of test networks: a single OD network [177] and a multi-OD network [187] to demonstrate the performance of the proposed framework in modeling an efficient and fair transportation system for a general network. For the purpose of comparison, we compare the results under the condition of efficient and fair system state with the results under the condition of system optimal (SO). To obtain the solution under the SO condition, we directly solve the LP relaxation formulation without the user equilibrium constraint (6.21).

6.4.1 Test network 1: [177]'s network

The network representation of [177]'s network is shown in Figure 6.2. The settings of this test case are as follows. The size of time interval is 2 s, and the saturation rate is 1800 veh/h. Thus the outflow capacity is 1 vehicle per time step. The jam density for link 1 and 10 is of a large value 100, while for other links, the holding capacity is 10 units. The outflow capacity of link 4 and 5 is time-variant to capture the effect of signal (or accident): 0 for time step (5-10), 1 for all other time step. The ratio of free flow speed and shock wave speed is fixed at 1. The value of β is 0.001. The initial state for the network is empty. The total demand is 25 for a departure time period of 30 time steps. Details of the parameter setting are provided in Table 6.1.

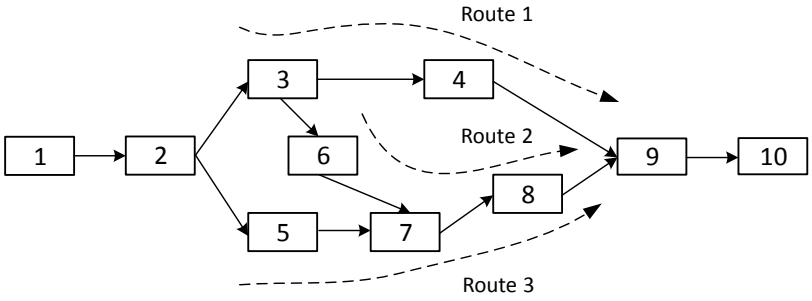

Fig. 6.2. Test network 1 [177]

Table 6.2 presents the value of variables $r^{o,d}(p,\bar{t})$ (i.e., departure rate) and $l^{o,d}(p,\bar{t})$ (i.e., the average travel time cost corresponding to departure rate $r^{o,d,p}(\bar{t})$) under the condition of efficient and fair system state. All the values of $r^{o,d,p}(\bar{t})$ are equal to either 0 or 1, indicating that the departure rate is either 0 or 1. Further, all the values of $l^{o,d,p}(\bar{t})$ are either 0 or 11, indicating that the travel time cost is the same for different departure rates (i.e., the solution is at equilibrium).

Similarly, Table 6.3 presents the value of variables $r^{o,d}(p,\bar{t})$ and $l^{o,d}(p,\bar{t})$ under the system optimal (SO) condition. It is obvious that the values of $l^{o,d,p}(\bar{t})$ of different departure time are not the same, indicating that the travel time of different departure

rates is not at equilibrium. Further, the total system travel time (TSTT) is 248, less than that (275) of an efficient and fair system state.

It is worthwhile to point out that Algorithm 1 converges fast. It takes only one iteration for all the tests in this test network, and no more than two iterations for all the tests in test network 2 of the next section. The fast convergence of Algorithm 1 mainly thanks to the tight lower bound from the LP relaxation formulation.

Table 6.1.
Parameter settings of test network 1

Links	1	2	3	4	5	6	7	8	9	10
L_i	2	2	2	4	2	2	2	2	2	2
N_i	100	10	10	10	10	10	10	10	10	100
Q_i	1	1	1	-	-	1	1	1	1	1

Table 6.2.
Departure rate (i.e., $r^{o,d}(p,\bar{t})$) and average travel time (i.e., $l^{o,d}(p,\bar{t})$) of test network 1 under efficient and fair system state (TSTT: 275)

	$r^{o,d}(p,\bar{t})$			$l^{o,d}(p,\bar{t})$		
Departure time	Route 1	Route 2	Route 3	Route 1	Route 2	Route 3
1	1	0	0	11	0	0
2	1	0	0	11	0	0
3	1	0	0	11	0	0
4	1	0	0	11	0	0
5	0	1	0	0	11	0
6	0	1	0	0	11	0
7	0	1	0	0	11	0
8	0	1	0	0	11	0
9	0	1	0	0	11	0
10	0	1	0	0	11	0
11	0	1	0	0	11	0
12	0	1	0	0	11	0
13	0	1	0	0	11	0
14	0	1	0	0	11	0
15	0	1	0	0	11	0
16	0	1	0	0	11	0
17	1	0	0	11	0	0
18	1	0	0	11	0	0
19	1	0	0	11	0	0
20	1	0	0	11	0	0
21	1	0	0	11	0	0
22	1	0	0	11	0	0
23	1	0	0	11	0	0
24	1	0	0	11	0	0
25	1	0	0	11	0	0

Table 6.3.
Departure rate (i.e., $r^{o,d}(p,\bar{t})$) and average travel time (i.e., $l^{o,d}(p,\bar{t})$) of test network 1 under SO condition (TSTT: 248)

	$r^{o,d}(p,\bar{t})$			$l^{o,d}(p,\bar{t})$		
Departure time	Route 1	Route 2	Route 3	Route 1	Route 2	Route 3
1	1	0	0	7	0	0
2	1	0	0	7	0	0
3	1	0	0	7	0	0
4	1	0	0	7	0	0
5	0	0	1	0	0	10
6	0	0	1	0	0	10
7	0	0	1	0	0	10
8	0	0	1	0	0	10
9	0	0	1	0	0	10
10	0	0	1	0	0	10
11	0	0	1	0	0	10
12	0	0	1	0	0	10
13	0	0	1	0	0	10
14	0	0	1	0	0	10
15	0	0	1	0	0	10
16	0	1	0	0	11	0
17	1	0	0	13	0	0
18	1	0	0	15	0	0
19	1	0	0	10	0	0
20	1	0	0	14	0	0
21	1	0	0	7	0	0
22	1	0	0	10	0	0
23	1	0	0	12	0	0
24	1	0	0	7	0	0
25	1	0	0	11	0	0

6.4.2 Test network 2: [187]'s network

The second test network is from [187] with 13 nodes, 19 links and 4 OD pairs, as shown in Figure 6.3. The settings for the network are as following. The size of the time step is taken at 6 s. The saturation flow is still 1800 vph. The maximum accumulative departure rate Q is set at 3 vehicles/time step. Other parameters are the same as defined in test network 1, unless specified otherwise. The route choices for the network are listed in Table 6.4.

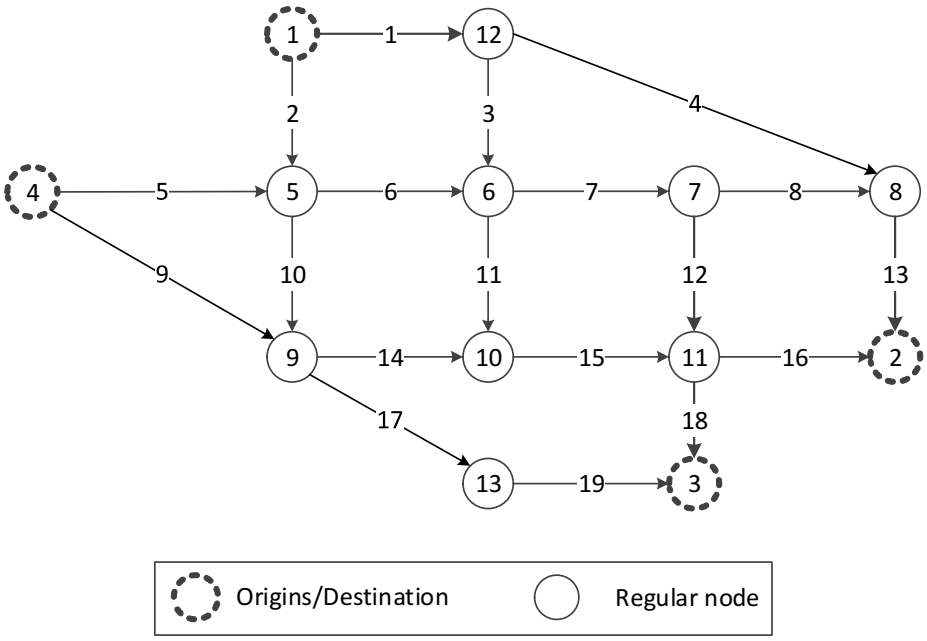

Fig. 6.3. Test network 2 [187]

The purpose of constructing test network 2 is to demonstrate the proposed framework's capability of handling a generalized multi-OD network. In the experiment design, we consider two demand scenarios as presented in Table 6.5. Moreover, we consider that the outflow capacity of link 1, 7, and 10 drops to zero (due to traffic signal or accident) during time step (1∼5), and the outflow capacity of link 4, 6, and 14 drops to zero during time step (10∼15).

Table 6.4.
Route choices of different ODs of test network 2

OD	Route NO.	Sequence of links	OD	Route NO.	Sequence of links
(1,2)	1	1-4-13	(4,2)	1	5-6-7-8-13
	2	1-3-7-8-13		2	5-6-7-12-16
	3	1-3-11-15-16		3	5-6-11-15-16
	4	2-10-14-15-16		4	9-14-15-16
(1,3)	1	1-3-11-15-18	(4,3)	1	5-6-11-15-18
	2	2-6-11-15-18		2	5-10-14-15-18
	3	2-10-14-15-18		3	9-17-19

Table 6.6 and Table 6.7 present the value of departure rate $r^{o,d}(p,\bar{t})$ and average travel time $l^{o,d}(p,\bar{t})$ for demand scenario 2 (results of demand scenario 1 are omitted for the sake of space) under the efficient and fair system state. Note that in this test network, $Q = 3$. From Table 6.6, the summation of values of $r^{o,d}(p,\bar{t})$ over all paths are equal to either 0 or 3, indicating that the accumulative departure rate is either zero or 3. Further, from Table 6.7, all the values of $l^{o,d}(p,\bar{t})$ are either zero or the same for the same OD, indicating that the travel time cost is the same for different departure rates under the same OD (i.e., the solution is at equilibrium).

Table 6.5.
Demand scenarios of test network 2

OD	Demand 1	Demand 2
(1,2)	30	45
(1,3)	9	15
(4,2)	30	45
(4,3)	9	15

Table 6.6.
Departure rate (i.e., $r^{o,d}(p,\bar{t})$) for demand scenario 2 of test network 2 under efficient and fair system state

Departure time	OD(1,2)				OD(1,3)			OD(4,2)				OD(4,3)		
	R1	R2	R3	R4	R1	R2	R3	R1	R2	R3	R4	R1	R2	R3
1	2.17	0.83	0	0	1.12	1.88	0	3	0	0	0	0.78	0	2.22
2	3	0	0	0	3	0	0	3	0	0	0	0	0	3
3	3	0	0	0	3	0	0	3	0	0	0	0	0	3
4	0	3	0	0	3	0	0	1.69	1.31	0	0	0.51	0	2.49
5	1.17	1.83	0	0	3	0	0	3	0	0	0	0	0	3
6	3	0	0	0	0	0	0	3	0	0	0	0	0	0
7	3	0	0	0	0	0	0	3	0	0	0	0	0	0
8	3	0	0	0	0	0	0	3	0	0	0	0	0	0
9	3	0	0	0	0	0	0	3	0	0	0	0	0	0
10	3	0	0	0	0	0	0	3	0	0	0	0	0	0
11	3	0	0	0	0	0	0	3	0	0	0	0	0	0
12	3	0	0	0	0	0	0	3	0	0	0	0	0	0
13	3	0	0	0	0	0	0	3	0	0	0	0	0	0
14	3	0	0	0	0	0	0	3	0	0	0	0	0	0
15	3	0	0	0	0	0	0	3	0	0	0	0	0	0

Table 6.8 and Table 6.9 present the value of departure rate $r^{o,d}(p,\bar{t})$ and average travel time $l^{o,d}(p,\bar{t})$ for demand scenario 2 under the system optimal condition. From Table 6.8, the departure rates (i.e., $r^{o,d}(p,\bar{t})$) are equal to either 0 or 3, indicating that the departure rate is either 0 or 3. Table 6.9 shows that the average travel time (i.e., $l^{o,d}(p,\bar{t})$) are different for different departure rates (i.e., the solution is not at equilibrium). Further, the total system travel time (TSTT) is 2130, less than that (2250) of an efficient and fair system state.

Table 6.7.
Average travel time (i.e., $l^{o,d}(p,\bar{t})$) for demand scenario 2 of test network 2 under efficient and fair system state (TSTT: 2250)

Departure time	OD(1,2)				OD(1,3)			OD(4,2)				OD(4,3)		
	R1	R2	R3	R4	R1	R2	R3	R1	R2	R3	R4	R1	R2	R3
1	18	18	0	0	17	17	0	22	0	0	0	13	0	13
2	18	0	0	0	17	0	0	22	0	0	0	0	0	13
3	18	0	0	0	17	0	0	22	0	0	0	0	0	13
4	0	18	0	0	17	0	0	22	22	0	0	13	0	13
5	18	18	0	0	17	0	0	22	0	0	0	0	0	13
6	18	0	0	0	0	0	0	22	0	0	0	0	0	0
7	18	0	0	0	0	0	0	22	0	0	0	0	0	0
8	18	0	0	0	0	0	0	22	0	0	0	0	0	0
9	18	0	0	0	0	0	0	22	0	0	0	0	0	0
10	18	0	0	0	0	0	0	22	0	0	0	0	0	0
11	18	0	0	0	0	0	0	22	0	0	0	0	0	0
12	18	0	0	0	0	0	0	22	0	0	0	0	0	0
13	18	0	0	0	0	0	0	22	0	0	0	0	0	0
14	18	0	0	0	0	0	0	22	0	0	0	0	0	0
15	18	0	0	0	0	0	0	22	0	0	0	0	0	0

Table 6.8.
Departure rate (i.e., $r^{o,d}(p,\bar{t})$) for demand scenario 2 of test network 2 under SO condition

Departure time	OD(1,2)				OD(1,3)			OD(4,2)				OD(4,3)		
	R1	R2	R3	R4	R1	R2	R3	R1	R2	R3	R4	R1	R2	R3
1	3	0	0	0	0	3	0	0	0	3	0	0	3	0
2	3	0	0	0	3	0	0	3	0	0	0	0	0	3
3	3	0	0	0	3	0	0	0	0	3	0	0	0	3
4	0	3	0	0	3	0	0	0	3	0	0	0	0	3
5	0	3	0	0	3	0	0	3	0	0	0	0	0	3
6	3	0	0	0	0	0	0	3	0	0	0	0	0	0
7	3	0	0	0	0	0	0	3	0	0	0	0	0	0
8	3	0	0	0	0	0	0	3	0	0	0	0	0	0
9	3	0	0	0	0	0	0	3	0	0	0	0	0	0
10	3	0	0	0	0	0	0	3	0	0	0	0	0	0
11	3	0	0	0	0	0	0	3	0	0	0	0	0	0
12	3	0	0	0	0	0	0	3	0	0	0	0	0	0
13	3	0	0	0	0	0	0	3	0	0	0	0	0	0
14	3	0	0	0	0	0	0	3	0	0	0	0	0	0
15	3	0	0	0	0	0	0	3	0	0	0	0	0	0

Table 6.9.
Average travel time (i.e., $l^{o,d}(p,\bar{t})$) for demand scenario 2 of test network 2 under SO condition (TSTT: 2130)

Departure time	OD(1,2)				OD(1,3)			OD(4,2)				OD(4,3)		
	R1	R2	R3	R4	R1	R2	R3	R1	R2	R3	R4	R1	R2	R3
1	22	0	0	0	0	13	0	0	0	12	0	0	22	0
2	10	0	0	0	18	0	0	14	0	0	0	0	0	14
3	11	0	0	0	19	0	0	0	0	12	0	0	0	14
4	0	14	0	0	17	0	0	0	13	0	0	0	0	14
5	0	14	0	0	14	0	0	32	0	0	0	0	0	10
6	21	0	0	0	0	0	0	0	0	18	0	0	0	0
7	24	0	0	0	0	0	0	26	0	0	0	0	0	0
8	12	0	0	0	0	0	0	31	0	0	0	0	0	0
9	21	0	0	0	0	0	0	27	0	0	0	0	0	0
10	15	0	0	0	0	0	0	24	0	0	0	0	0	0
11	10	0	0	0	0	0	0	21	0	0	0	0	0	0
12	10	0	0	0	0	0	0	29	0	0	0	0	0	0
13	15	0	0	0	0	0	0	27	0	0	0	0	0	0
14	12	0	0	0	0	0	0	24	0	0	0	0	0	0
15	14	0	0	0	0	0	0	20	0	0	0	0	0	0

Table 6.10 presents the total system travel time (TSTT) for different values of ε-*tolerance*. When $\varepsilon = 0$, there is no tolerance and the solution is exactly the same as the efficient and fair system state. When $0 < \varepsilon < 2$, the TSTT gradually improves with the increase of tolerance ε. When ε is increased to 2 or greater than 2, the TSTT is the same as the system optimal (SO) solution. The results are in accord with our expectation that the value of ε-*tolerance* governs the relaxation of the equilibrium constraint. The equilibrium constraint is relaxed more with the increase of the ε-*tolerance*. Eventually, when the ε-*tolerance* is increased to a certain threshold, the equilibrium constraint places no effect on the formulation due to the relaxation, and the formulation is reduced to the SO formulation.

Table 6.10.
Efficient and *ε-tolerant* system states

	TSTT (time steps)	
ε-tolerance (time steps)	Demand 1	Demand 2
0	1302	2250
0.5	1267	2175
1	1246	2155
1.5	1236	2140
≥ 2	1227 (SO)	2130 (SO)

6.5 Conclusions

With the advance in communication and computing technologies, personalized travel guidance to drivers is rapidly becoming a reality. To fully utilize the benefit of guidance devices and encourage users to comply with the guidance, there is a pressing need to provide efficient and fair guidance to attain the system state close to system optimal and individual users do not worse off. Addressing the need, this chapter models a transportation system that is both efficient (system optimal) and fair (user equilibrium) within the dynamic traffic assignment environment. The formulation is capable of accounting for dynamic departure time and route choice for a generalized multi-OD network. The *key contribution* is that we propose a linear programming formulation that produces a tight lower bound of an efficient and fair system state, then we develop an efficient iterative algorithm to obtain the exact solution. Firstly, a bi-level optimization formulation based on a link-based traffic flow model is introduced. At the upper level, the objective is to optimize the total system travel time of the traffic flow at the network level (efficient). At the lower level, the objective is to equilibrium the travel cost of individual users (fair). Then the bi-level formulation is relaxed to a linear programming formulation which produces a lower bound of the efficient and fair system state. Based on the lower bound, we further develop an efficient algorithm to obtain the solution of an efficient and fair system state. It is shown that the number of iterations of the algorithm is bounded and the traffic flow output of the algorithm is at equilibrium. In the numerical case studies, we construct two test networks including a single OD network and a multi-OD network. For the tests, the algorithm converges within two iterations, indicating that the LP relaxation formulation produces a tight lower bound on the solution of an efficient and fair system state. Moreover, the results of various tests confirm that the average travel cost of every departure rate is either zero or the same under the same OD. For test work 2, we also test the efficient and ε-*tolerant* system state, it shows that the total system travel time decreases with the increase of the tolerance (less than two

time steps). When the tolerance reaches two time steps or more, the TSTT is the same as the system optimal solution.

There are multiple future research directions of this study:

1. This study is motivated by the need of providing an efficient and fair personalized travel guidance to travelers. However, users' decision making process is a complex process. Users may not necessarily comply with guidance even if the guidance is both efficient and fair. How to capture user's decision making behavior in the formulation will be an interesting topic.

2. We have not investigated the impact of information guidance into the formulation. Providing more information does not necessarily lead to improved system outcome due to the self-interest driven reactions of individual agents. There is a need to understand at a fundamental level how information can be collected, synthesized and disseminated in ways that are easily consumable by a large number of self-interested agents to yield globally fair and efficient outcomes.

3. This study considers users as a homogeneous class. In the real world, users can be classified into multiple classes depending on the transportation mode (e.g., bus, truck, passenger car), various value of time, various tolerance levels of early or late arrival, and so on. Hence it will be more realistic to incorporate the heterogeneity of users into the formulation in the future study.

7. SUMMARY

The connected vehicle (CV) and autonomous vehicle (AV) technology have the potential to greatly improve the transportation system in terms of safety, efficiency, and sustainability. This dissertation aims to develop a systematic tool designated for connected and autonomous vehicles, integrating the simulation of traffic dynamics, traffic control strategies, and impact analysis at the network level of the next generation transportation system.

Part I of the dissertation is devoted to the traffic flow modeling of the connected vehicles and autonomous vehicles. This task is the foundation step for transportation planning, optimized network design, efficient traffic control strategies, etc, for the next generation transportation system. Chapter 2 proposes a cell-based simulation approach to model the proactive driving behavior of connected vehicles. Firstly, a state variable of connected vehicles is introduced to track the trajectory of connected vehicles. Then the exit flow of cells containing connected vehicles is adjusted to simulate the proactive driving behavior, such that the traffic light is green when the connected vehicle arrives at the signalized intersection. Extensive numerical simulation results consistently show that the presence of connected vehicles contributes significantly to the smoothing of traffic flow and vehicular emission reductions in the network. Chapter 3 proposes an optimal estimation approach to calibrate connected vehicles' car-following behavior in a mixed traffic environment. Particularly, the state-space system dynamics is captured by the simplified car-following model with disturbances, where the trajectory of non-connected vehicles are considered as unknown states and the trajectory of connected vehicles are considered as measurements with errors. Objective of the reformulation is to obtain an optimal estimation of states and model parameters simultaneously. It is shown that the customized state-space model is identifiable with the mild assumption that the disturbance covariance

of the state update process is diagonal. Then a modified Expectation-Maximization (EM) algorithm based on Kalman smoother is developed to solve the optimal estimation problem. The performance of the EM algorithm is validated through simulation data.

Part II of the dissertation contributes to proposing efficient traffic control strategies to better off the next generation transportation system. This task pushes the next generation transportation system to a better performance state in terms of traffic safety, travel time saving, vehicular emission reduction, etc. Chapter 4 develops a novel reinforcement learning algorithm for the challenging coordinated signal control problem. Traffic signals are modeled as intelligent agents interacting with the stochastic traffic environment. The model is built on the framework of coordinated reinforcement learning. The Junction Tree Algorithm (JTA) based reinforcement learning is proposed to obtain an exact inference of the best joint actions for all the coordinated intersections. The algorithm is implemented and tested with a network containing 18 signalized intersections in VISSIM. Results show that the JTA based algorithm outperforms independent learning (Q-learning), real-time adaptive learning, and fixed timing plans in terms of average delay, number of stops, and vehicular emissions at the network level. Chapter 5 develops a novel linear programming formulation for autonomous intersection control (LPAIC) accounting for traffic dynamics within a connected vehicle environment. Firstly, a lane based bi-level optimization model is introduced to propagate traffic flows in the network, accounting for dynamic departure time, dynamic route choice, and autonomous intersection control in the context of system optimum network model. Then the bi-level optimization model is transformed to the linear programming formulation by relaxing the nonlinear constraints with a set of linear inequalities. One special feature of the LPAIC formulation is that the entries of the constraint matrix has only values in -1, 0, 1. Moreover, it is proved that the constraint matrix is totally unimodular, the optimal solution exists and contains only integer values. Further, it shows that traffic flows from different lanes pass through the conflict points of the intersection safely and there are no

holding flows in the solution. Three numerical case studies are conducted to demonstrate the properties and effectiveness of the LPAIC formulation to solve autonomous intersection control.

Part III of the dissertation moves on to the impact analysis of connected vehicles and autonomous vehicles at the network level. This task assesses the positive and negative impacts of the system and provides guidance on transportation planning, traffic control, transportation budget spending, etc. In this part, the impact of different penetration rates of connected vehicle and autonomous vehicles is revealed on the network efficiency of a transportation system. Chapter 6 sets out to model an efficient and fair transportation system accounting for both departure time choice and route choice of a general multi OD network within a dynamic traffic assignment environment. Firstly, a bi-level optimization formulation is introduced based on the link-based traffic flow model. The upper level of the formulation minimizes the total system travel time, whereas the lower level captures traffic flow propagation and the user equilibrium constraint. Then the bi-level formulation is relaxed to a linear programming formulation that produces a lower bound of an efficient and fair system state. An efficient iterative algorithm is proposed to obtain the exact solution. It is shown that the number of iterations is bounded, and the output traffic flow solution is efficient and fair. Finally, two numerical cases (including a single OD network and a multi-OD network) are conducted to demonstrate the performance of the algorithm. The results consistently show that the travel time of different departure rates of the same OD pair are identical and the algorithm converges within two iterations across all test scenarios.

Along the line of this dissertation, there are a number of interesting research directions for future research.

- In part I (traffic flow modeling), we have only simulated one type of proactive speed adjustment scheme (i.e., the connected vehicle decreases speed to arrive the signalized intersection exactly at the end of the red traffic light). It is worthwhile to investigate other types of speed adjustment scheme as well. Further,

we have assumed that the traffic flow (both connected and non-connected vehicles) propagates on determined routes. However, as connected vehicles are more informed about the traffic situation in the downstream network, they may alternate routes dynamically during the trip. The most important feature of connected vehicles lies in the exchanging of short range and real time traffic information, based on which connected vehicles can alter routes or departure time. Incorporating both the cooperative driving behavior and the route choice behavior of connected vehicles will be an interesting topic.

- In part II (traffic control strategies), the CV environment can be modeled with more details using wireless communications simulation tools. This would help to assess the resilience and stability of the control schemes with variation in communication strengths. Further, the proposed LPAIC formulation is limited to the area of system optimum. How to adjust the formulation to account for user equilibrium (UE) behavior is an important extension that deserves future study. Last but not the least, it is worthwhile to address the lane changing issue. Lane changing behavior is realistic and necessary in traffic flow modeling. However, we are unable to capture it in the proposed formulation due to the complexity and nonlinear nature of the lane changing constraint. The LPAIC formulation will be more complete and powerful if there is a way to transform the nonlinear constraint of lane changing to a linear form.

- In part III (impact analysis), the study is motivated by the need of providing an efficient and fair personalized travel guidance to travelers. However, users' decision making process is a complex process. Users may not necessarily comply with guidance even if the guidance is both efficient and fair. How to capture user's decision making behavior in the formulation will be an interesting topic.

BIBLIOGRAPHY

Bibliography

[1] NHTSA, "U.S. Department of Transportation Issues Advance Notice of Proposed Rulemaking to Begin Implementation of Vehicle-to-Vehicle Communications Technology," 2014.

[2] A. Broggi, "IEEE News Releases," 2012.

[3] NHTSA, "National Highway Traffic Safety Administration. Preliminary Statement of Policy Concerning Automated Vehicles." 2013.

[4] RITA, "Connected Vehicle Research in the United States," 2014.

[5] H.-Y. Huang, P.-E. Luo, M. Li, D. Li, X. Li, W. Shu, and M.-Y. Wu, "Performance Evaluation of SUVnet With Real-Time Traffic Data," *IEEE Transactions on Vehicular Technology*, vol. 56, no. 6, pp. 3381–3396, 2007.

[6] C. Lochert, A. Barthels, A. Cervantes, M. Mauve, and M. Caliskan, "Multiple simulator interlinking environment for IVC," in *Proceedings of the 2nd ACM international workshop on Vehicular ad hoc networks - VANET '05*. New York, USA: ACM Press, Sep. 2005, p. 87.

[7] PTV, "PTV Vision software suite (VISUM/VISSIM)." *PTV AG Traffic Mobility Logistics.*, 2005.

[8] C. Sommer, R. German, and F. Dressler, "Bidirectionally Coupled Network and Road Traffic Simulation for Improved IVC Analysis," *IEEE Transactions on Mobile Computing*, vol. 10, no. 1, pp. 3–15, Jan. 2011.

[9] A. Varga, "The OMNeT++ Discrete Event Simulation System," *Proc. European Simulation Multiconf. (ESM 01)*, 2001.

[10] D. Krajzewicz, G. Hertkorn, C. Rossel, and P. Wagner, "SUMO (Simulation of Urban MObility); An Open-Source Traffic Simulation," *Proc. Fourth Middle East Symp. Simulation and Modelling (MESM 02)*, pp. 183–187, 2002.

[11] F. Knorr and M. Schreckenberg, "Influence of inter-vehicle communication on peak hour traffic flow," *Physica A: Statistical Mechanics and its Applications*, vol. 391, no. 6, pp. 2225–2231, Mar. 2012.

[12] G. Kliot, "Technion extensions of the JiST/SWANS simulator," 2010. [Online]. Available: http://www.cs.technion.ac.il/ gabik/Jist-Swans/

[13] S. I. Guler, M. Menendez, and L. Meier, "Using connected vehicle technology to improve the efficiency of intersections," *Transportation Research Part C: Emerging Technologies*, vol. 46, pp. 121–131, 2014.

[14] N. Goodall, B. Smith, and B. Park, "Traffic signal control with connected vehicles," *Transportation Research Record: Journal of the Transportation Research Board*, no. 2381, pp. 65–72, 2013.

[15] NHTSA, "National Motor Vehicle Crash Causation Survey. U.S. Department of Transportation, Report DOT HS 811 059," 2008.

[16] ——, "Traffic Safety Facts 2012: Alcohol-Impaired Driving. Dept of Transportation (US), National Highway Traffic Safety Administration (NHTSA). Available at URL: http://www-nrd.nhtsa.dot.gov/Pubs/811870.pdf. Access date: 11/17/2014." 2012.

[17] A. Ceder, "Relationships between road accidents and hourly traffic flowii: Probabilistic approach," *Accident Analysis & Prevention*, vol. 14, no. 1, pp. 35–44, 1982.

[18] D. Lord, A. Manar, and A. Vizioli, "Modeling crash-flow-density and crash-flow-v/c ratio relationships for rural and urban freeway segments," *Accident Analysis & Prevention*, vol. 37, no. 1, pp. 185–199, 2005.

[19] C. Wang, M. A. Quddus, and S. G. Ison, "Impact of traffic congestion on road accidents: a spatial analysis of the m25 motorway in england," *Accident Analysis & Prevention*, vol. 41, no. 4, pp. 798–808, 2009.

[20] Z. Zheng, S. Ahn, and C. M. Monsere, "Impact of traffic oscillations on freeway crash occurrences," *Accident Analysis & Prevention*, vol. 42, no. 2, pp. 626–636, 2010.

[21] D. C. Gazis, R. Herman, and R. B. Potts, "Car-Following Theory of Steady-State Traffic Flow," *Operations Research*, vol. 7, no. 4, pp. 499–505, Aug. 1959.

[22] P. Gipps, "A behavioural car-following model for computer simulation," *Transportation Research Part B: Methodological*, vol. 15, no. 2, pp. 105–111, Apr. 1981.

[23] M. Brackstone and M. McDonald, "Car-following: a historical review," *Transportation Research Part F: Traffic Psychology and Behaviour*, vol. 2, no. 4, pp. 181–196, Dec. 1999.

[24] G. Newell, "A simplified car-following theory: a lower order model," *Transportation Research Part B: Methodological*, vol. 36, no. 3, pp. 195–205, Mar. 2002.

[25] S. T. Waller, M. Ng, E. Ferguson, N. Nezamuddin, and D. Sun, "Speed harmonization and peak-period shoulder use to manage urban freeway congestion," 2009.

[26] A. Talebpour, H. S. Mahmassani, and S. H. Hamdar, "Speed harmonization: effectiveness evaluation under congested conditions," *Transportation Research Record: Journal of the Transportation Research Board*, vol. 2391, no. 1, pp. 69–79, 2013.

[27] F. Zhu and S. V. Ukkusuri, "Accounting for dynamic speed limit control in a stochastic traffic environment: a reinforcement learning approach," *Transportation Research Part C: emerging technologies*, vol. 41, pp. 30–47, 2014.

[28] E. Van den Hoogen and S. Smulders, "Control by variable speed signs: Results of the dutch experiment," 1994.

[29] P. Rämä, "Effects of weather-controlled variable speed limits and warning signs on driver behavior," *Transportation Research Record: Journal of the Transportation Research Board*, no. 1689, pp. 53–59, 1999.

[30] K.-P. Kang, G.-L. Chang, and N. Zou, "Optimal dynamic speed-limit control for highway work zone operations," *Transportation Research Record: Journal of the Transportation Research Board*, no. 1877, pp. 77–84, 2004.

[31] R. C. Carlson, I. Papamichail, M. Papageorgiou, and A. Messmer, "Optimal motorway traffic flow control involving variable speed limits and ramp metering," *Transportation Science*, vol. 44, no. 2, pp. 238–253, 2010.

[32] A. Hegyi, B. De Schutter, and H. Hellendoorn, "Model predictive control for optimal coordination of ramp metering and variable speed limits," *Transportation Research Part C: Emerging Technologies*, vol. 13, no. 3, pp. 185–209, 2005.

[33] K. Jerath, V. V. Gayah, and S. N. Brennan, "Influential subspaces of connected vehicles in highway traffic," in *Symposium Celebrating 50 Years of Traffic Flow Theory, August 2014, Portland, OR*, 2014.

[34] C. F. Daganzo, "The cell transmission model: A dynamic representation of highway traffic consistent with the hydrodynamic theory," *Transportation Research Part B: Methodological*, vol. 28, no. 4, pp. 269–287, 1994.

[35] ——, "The cell transmission model, part ii: network traffic," *Transportation Research Part B: Methodological*, vol. 29, no. 2, pp. 79–93, 1995.

[36] I. Yperman, S. Logghe, and B. Immers, "The link transmission model: An efficient implementation of the kinematic wave theory in traffic networks," in *Proceedings of the 10th EWGT Meeting*, 2005.

[37] F. Zhu and S. V. Ukkusuri, "A linear programming formulation for autonomous intersection control within a dynamic traffic assignment and connected vehicle environment," *Transportation Research Part C: Emerging Technologies*, vol. 55, pp. 363–378, 2015.

[38] W.-L. Jin, "Continuous formulations and analytical properties of the link transmission model," *Transportation Research Part B: Methodological*, vol. 74, pp. 88–103, 2015.

[39] M. J. Lighthill and G. B. Whitham, "On kinematic waves. ii. a theory of traffic flow on long crowded roads," in *Proceedings of the Royal Society of London A: Mathematical, Physical and Engineering Sciences*, vol. 229, no. 1178. The Royal Society, 1955, pp. 317–345.

[40] P. I. Richards, "Shock waves on the highway," *Operations Research*, vol. 4, no. 1, pp. 42–51, 1956.

[41] H. K. Lo and W. Szeto, "A cell-based variational inequality formulation of the dynamic user optimal assignment problem," *Transportation Research Part B: Methodological*, vol. 36, no. 5, pp. 421–443, 2002.

[42] W. Szeto and H. K. Lo, "A cell-based simultaneous route and departure time choice model with elastic demand," *Transportation Research Part B: Methodological*, vol. 38, no. 7, pp. 593–612, 2004.

[43] L. Han, S. Ukkusuri, and K. Doan, "Complementarity formulations for the cell transmission model based dynamic user equilibrium with departure time choice, elastic demand and user heterogeneity," *Transportation Research Part B: Methodological*, vol. 45, no. 10, pp. 1749–1767, 2011.

[44] S. V. Ukkusuri, L. Han, and K. Doan, "Dynamic user equilibrium with a path based cell transmission model for general traffic networks," *Transportation Research Part B: Methodological*, vol. 46, no. 10, pp. 1657–1684, 2012.

[45] H. K. Lo, "A novel traffic signal control formulation," *Transportation Research Part A: Policy and Practice*, vol. 33, no. 6, pp. 433–448, 1999.

[46] H. K. Lo, E. Chang, and Y. C. Chan, "Dynamic network traffic control," *Transportation Research Part A: Policy and Practice*, vol. 35, no. 8, pp. 721–744, 2001.

[47] S. V. Ukkusuri, G. Ramadurai, and G. Patil, "A robust transportation signal control problem accounting for traffic dynamics," *Computers & Operations Research*, vol. 37, no. 5, pp. 869–879, 2010.

[48] C. Wong, S. Wong, and H. K. Lo, "A spatial queuing approach to optimize coordinated signal settings to obviate gridlock in adjacent work zones," *Journal of Advanced Transportation*, vol. 44, no. 4, pp. 231–244, 2010.

[49] Y. Zhao and K. M. Kockelman, "The propagation of uncertainty through travel demand models: an exploratory analysis," *The Annals of Regional Science*, vol. 36, no. 1, pp. 145–163, 2002.

[50] S. Krishnamurthy and K. M. Kockelman, "Propagation of uncertainty in transportation land use models: Investigation of dram-empal and utpp predictions in austin, texas," *Transportation Research Record: Journal of the Transportation Research Board*, vol. 1831, no. 1, pp. 219–229, 2003.

[51] B. W. Siu and H. K. Lo, "Doubly uncertain transportation network: degradable capacity and stochastic demand," *European Journal of Operational Research*, vol. 191, no. 1, pp. 166–181, 2008.

[52] M. Ng, K. Kockelman, and S. Waller, "Relaxing the multivariate normality assumption in the simulation of transportation system dependencies: an old technique in a new domain," *Transportation Letters*, vol. 2, no. 2, pp. 63–74, 2010.

[53] A. Sumalee, R. Zhong, T. Pan, and W. Szeto, "Stochastic cell transmission model (sctm): A stochastic dynamic traffic model for traffic state surveillance and assignment," *Transportation Research Part B: Methodological*, vol. 45, no. 3, pp. 507–533, 2011.

[54] H. Frey, A. Unal, J. Chen, S. Li, and C. Xuan, "Methodology for developing modal emission rates for epas multi-scale motor vehicle & equipment emission system," *Ann Arbor, Michigan: US Environmental Protection Agency*, 2002.

[55] H. C. Frey, A. Unal, N. M. Rouphail, and J. D. Colyar, "On-road measurement of vehicle tailpipe emissions using a portable instrument," *Journal of the Air & Waste Management Association*, vol. 53, no. 8, pp. 992–1002, 2003.

[56] M. C. Coelho, H. C. Frey, N. M. Rouphail, H. Zhai, and L. Pelkmans, "Assessing methods for comparing emissions from gasoline and diesel light-duty vehicles based on microscale measurements," *Transportation Research Part D: Transport and Environment*, vol. 14, no. 2, pp. 91–99, 2009.

[57] USDOT, *Connected Vehicle Test Beds*. U.S. Department of Transportation Intelligent Transportation Systems Joint Program Office (JPO), 2015. [Online]. Available: http://www.its.dot.gov/testbed.htm Date accessed: 2015/4/2

[58] H. Deng and H. M. Zhang, "Driver Anticipation in Car Following," *Transportation Research Record: Journal of the Transportation Research Board*, vol. 2316, pp. 31–37, 2012.

[59] H. Yeo and A. Skabardonis, "Understanding stop-and-go traffic in view of asymmetric traffic theory," in *18th Int. Symp. Traffic Theory and Transportation*, W. H. K. Lam, S. C. Wong, and H. K. Lo, Eds., vol. 1. Hong Kong: Springer, 2009, pp. 99–116.

[60] J. Monteil, R. Billot, D. Rey, and N.-E. E. Faouzi, "Distributed and Centralized Approaches for Cooperative Road Traffic Dynamics," *Procedia - Social and Behavioral Sciences*, vol. 48, pp. 3198–3208, Jan. 2012.

[61] J. Monteil, R. Billot, J. Sau, F. Armetta, S. Hassas, and N.-E. El Faouzi, "Cooperative Highway Traffic: Multiagent Modeling and Robustness Assessment of Local Perturbations," *Transportation Research Record: Journal of the Transportation Research Board*, vol. 2391, pp. 1–10, 2013.

[62] W. Helly, "Simulation of bottlenecks in single-lane traffic flow," in *Theory of Traffic Flow Symposium.* Elsevier Publishing Company, 1961, pp. 207–238.

[63] S. Ossen and S. Hoogendoorn, "Car-following behavior analysis from microscopic trajectory data," *Transportation Research Record: Journal of the Transportation Research Board*, no. 1934, pp. 13–21, 2005.

[64] A. Kesting and M. Treiber, "Calibrating car-following models by using trajectory data: Methodological study," *Transportation Research Record: Journal of the Transportation Research Board*, no. 2088, pp. 148–156, 2008.

[65] C. Chen, L. Li, J. Hu, and C. Geng, "Calibration of mitsim and idm car-following model based on ngsim trajectory datasets," in *Vehicular Electronics and Safety (ICVES), 2010 IEEE International Conference on.* IEEE, 2010, pp. 48–53.

[66] J. Kim and H. Mahmassani, "Correlated parameters in driving behavior models: car-following example and implications for traffic microsimulation," *Transportation Research Record: Journal of the Transportation Research Board*, no. 2249, pp. 62–77, 2011.

[67] M. Treiber and A. Kesting, "Validation of traffic flow models with respect to the spatiotemporal evolution of congested traffic patterns," *Transportation research part C: emerging technologies*, vol. 21, no. 1, pp. 31–41, 2012.

[68] J. Monteil, R. Billot, J. Sau, C. Buisson, and N.-E. El Faouzi, "Calibration, estimation, and sampling issues of car-following parameters," *Transportation Research Record: Journal of the Transportation Research Board*, no. 2422, pp. 131–140, 2014.

[69] P. J. Jin, D. Yang, and B. Ran, "Reducing the error accumulation in car-following models calibrated with vehicle trajectory data," *Intelligent Transportation Systems, IEEE Transactions on*, vol. 15, no. 1, pp. 148–157, 2014.

[70] V. Punzo, M. Montanino, and B. Ciuffo, "Do we really need to calibrate all the parameters? variance-based sensitivity analysis to simplify microscopic traffic flow models," *Intelligent Transportation Systems, IEEE Transactions on*, vol. 16, no. 1, pp. 184–193, 2015.

[71] P. J. Jin, D. Yang, B. Ran, M. Cebelak, and C. M. Walton, "Bidirectional Control Characteristics of General Motors and Optimal Velocity Car-Following Models: Implications for Coordinated Driving in a Connected Vehicle Environment," *Transportation Research Record: Journal of the Transportation Research Board*, vol. 2381, pp. 110–119, 2013.

[72] V. Punzo, M. T. Borzacchiello, and B. Ciuffo, "On the assessment of vehicle trajectory data accuracy and application to the next generation simulation (ngsim) program data," *Transportation Research Part C: Emerging Technologies*, vol. 19, no. 6, pp. 1243–1262, 2011.

[73] T. Tang, W. Shi, H. Shang, and Y. Wang, "A new car-following model with consideration of inter-vehicle communication," *Nonlinear Dynamics*, vol. 76, no. 4, pp. 2017–2023, Feb. 2014.

[74] J. Sangster, H. Rakha, and J. Du, "Application of Naturalistic Driving Data to Modeling of Driver Car-Following Behavior," *Transportation Research Record: Journal of the Transportation Research Board*, vol. 2390, pp. 20–33, 2013.

[75] S. Ahn, M. J. Cassidy, and J. Laval, "Verification of a simplified car-following theory," *Transportation Research Part B: Methodological*, vol. 38, no. 5, pp. 431–440, Jun. 2004.

[76] J. A. Laval and L. Leclercq, "A mechanism to describe the formation and propagation of stop-and-go waves in congested freeway traffic." *Philosophical transactions. Series A, Mathematical, physical, and engineering sciences*, vol. 368, no. 1928, pp. 4519–41, Oct. 2010.

[77] D. Chen, J. Laval, Z. Zheng, and S. Ahn, "A behavioral car-following model that captures traffic oscillations," *Transportation Research Part B: Methodological*, vol. 46, no. 6, pp. 744–761, Jul. 2012.

[78] M. J. Lighthill and G. B. Whitham, "On Kinematic Waves. II. A Theory of Traffic Flow on Long Crowded Roads," *Proceedings of the Royal Society of London.Series A, Mathematical and Physical Sciences*, vol. 229, pp. 317–345, 1955.

[79] P. I. Richards, "Shock Waves on the Highway," *Operations research*, vol. 4, pp. 42–51, 1956.

[80] K. S. Arun and S. Y. Kung, "Balanced Approximation of Stochastic Systems," *SIAM Journal on Matrix Analysis and Applications*, vol. 11, no. 1, pp. 42–68, Jan. 1990.

[81] P. Van Overschee and B. De Moor, *Subspace Identification for Linear Systems*. Boston, MA: Springer US, 1996.

[82] A. Dempster, N. Laird, and D. Rubin, "Maximum likelihood from incomplete data via the EM algorithm," *Journal of the Royal Statistical Society. Series B (Methodological)*, vol. 39, no. 1, pp. 1–38, 1977.

[83] X. Zhan and S. V. Ukkusuri, "Probabilistic urban link travel time estimation model using large-scale taxi trip data," in *Transportation Research Board 94th Annual Meeting*, no. 15-4054, 2015.

[84] R. H. Shumway and D. S. Stoffer, "An approach to time series smoothing and forecasting using the em algorithm," *Journal of Time Series Analysis*, vol. 3, no. 4, pp. 253–264, Jul. 1982.

[85] ——, "Dynamic Linear Models With Switching," *Journal of the American Statistical Association*, vol. 86, no. 415, pp. 763–769, Sep. 1991.

[86] R. E. Kalman, "A new approach to linear filtering and prediction problems," *Journal of Fluids Engineering*, vol. 82, no. 1, pp. 35–45, 1960.

[87] R. G. Brown, P. Y. Hwang *et al.*, *Introduction to random signals and applied Kalman filtering*. Wiley New York, 1992, vol. 3.

[88] FHWA, *Test Data Set for Michigan (August, 2008)*. U.S. Department of Transportation Intelligent Transportation Systems Joint Program Office (JPO), 2008. [Online]. Available: https://www.its-rde.net/ Date accessed: 2015/4/2

[89] ——, "Congestion reduction toolbox," *U.S. Department of Transportation Federal Highway Administration*, vol. Accessible via www.fhwa.dot.gov/congestion/toolbox, 2011.

[90] NTOC, "2012 national traffic signalreport card: Technical report," *The National Transportation Operations Coalition*, 2012.

[91] P. B. Hunt, D. I. Robertson, R. D. Bretherton, and M. C. Royle, "The scoot on-line traffic signal optimisation technique," *Traffic Engineering and Control*, vol. 23, no. 4, pp. p. 190–192, 1982.

[92] P. R. Lowrie, "Scats:the sydney coordinated adaptive traffic system principles, methodology, algorithms." *Proceedings of the IEE international conference on road traffic signaling*, pp. 66–70, 1982.

[93] J. Farges, J. Henry, and J. Tufal, "The prodyn real-time traffic algorithm." *Proceedings of the fourth IFAC symposium on transportation systems*, pp. 307–312, 1983.

[94] N. H. Gartner, "Opac: A demand-responsivestrategy for traffic signal control," *Transportation Research Record*, no. 906, pp. p. 75–81, 1983.

[95] P. Mirchandani and L. Head, "A real-time traffic signal control system: architecture, algorithms, and analysis," *Transportation Research Part C: Emerging Technologies*, vol. 9, no. 6, pp. 415–432, 2001.

[96] V. Mauro and D. Taranto, "Utopia," *Proceedings of the sixth IFAC/IFIP/IFORS symposium on control, computers, communications on transportation*, pp. 245–252, 1989.

[97] F. Boillot, S. Midenet, and J.-C. Pierrele, "The real-time urban traffic control system cronos: Algorithm and experiments," *Transportation Research Part C: Emerging Technologies*, vol. 14, no. 1, pp. 18–38, 2006.

[98] C. Diakaki, M. Papageorgiou, and K. Aboudolas, "A multivariable regulator approach to traffic-responsive network-wide signal control," *Control Engineering Practice*, vol. 10, no. 2, pp. 183–195, 2002.

[99] G. F. Newell, "The rolling horizon scheme of traffic signal control," *Transportation Research Part A: Policy and Practice*, vol. 32, no. 1, pp. 39–44, 1998.

[100] A. Hegyi, B. De Schutter, and H. Hellendoorn, "Model predictive control for optimal coordination of ramp metering and variable speed limits," *Transportation Research Part C: Emerging Technologies*, vol. 13, no. 3, pp. 185–209, 2005.

[101] K. Aboudolas, M. Papageorgiou, and E. Kosmatopoulos, "Store-and-forward based methods for the signal control problem in large-scale congested urban road networks," *Transportation Research Part C: Emerging Technologies*, vol. 17, no. 2, pp. 163–174, 2009.

[102] H. K. Lo, "A cell-based traffic control formulation: strategies and benefits of dynamic timing plans," *Transportation Science*, vol. 35, no. 2, pp. 148–164, 2001.

[103] W.-H. Lin and C. Wang, "An enhanced 01 mixed-integer lp formulation for traffic signal control," *IEEE Transactions on Intelligent Transportation Systems*, vol. 5, no. 4, pp. 238–245, 2004.

[104] C. Beard, , and A. K. Ziliaskopoulos., "System optimal signal optimization formulation," *Transportation Research Record*, vol. 1978, pp. 102–112, 2006.

[105] Y. Pavlis and W. Recker, "A mathematical logic approach for the transformation of the linear conditional piecewise functions of dispersion-and-store and cell transmission traffic flow models into linear mixed-integer form," *Transportation Science*, vol. 43, no. 1, pp. 98–116, 2009.

[106] A. H. M. Aziz and S. V. Ukkusuri, "Unified framework for dynamic traffic assignment and signal control with cell transmission model," *Transportation Research Record*, vol. 2311, pp. 73–84, 2012.

[107] B. Abdulhai, R. Pringle, and G. J. Karakoulas, "Reinforcement learning for true adaptive traffic signal control," *Journal of Transportation Engineering*, vol. 129, no. 3, pp. 278–285, 2003.

[108] A. L. C. Bazzan, "A distributed approach for coordination of traffic signal agents," *Autonomous Agents and Multi-Agent Systems*, vol. 10, no. 2, pp. 131–164, 2005.

[109] A. L. C. Bazzan, D. de Oliveira, and B. C. da Silva, "Learning in groups of traffic signals," *Engineering Applications of Artificial Intelligence*, vol. 23, no. 4, pp. 560–568, 2010.

[110] J. C. Medina and R. F. Benekohal, "Traffic signal control using reinforcement learning and the max-plus algorithm as a coordinating strategy," *Intelligent Transportation Systems (ITSC), 2012 15th International IEEE Conference on*, pp. 596–601, 2012.

[111] S. El-Tantawy and B. Abdulhai, "Towards multi-agent reinforcement learning for integrated network of optimal traffic controllers (marlin-otc)," *Transportation Letters: the International Journal of Transportation Research*, vol. 2, no. 2, pp. 89–110, 2010.

[112] S. Mikami and Y. Kakazu, "Genetic reinforcement learning for cooperative traffic signal control," *Evolutionary Computation, 1994. IEEE World Congress on Computational Intelligence., Proceedings of the First IEEE Conference on*, vol. 1, pp. 223–228, 1994.

[113] J. France and A. A. Ghorbani, "A multiagent system for optimizing urban traffic," *Intelligent Agent Technology, 2003. IAT 2003. IEEE/WIC International Conference on*, pp. 411–414, 2003.

[114] M. Wiering, J. Vreeken, J. van Veenen, and A. Koopman, "Simulation and optimization of traffic in a city," *Intelligent Vehicles Symposium, 2004 IEEE*, pp. 453–458, 2004.

[115] D. d. Oliveira, A. L. C. Bazzan, and V. Lesser, "Using cooperative mediation to coordinate traffic lights: a case study," *Proceedings of the fourth international joint conference on Autonomous agents and multiagent systems*, pp. 463–470, 2005.

[116] D. Oliveira and A. C. Bazzan, "Traffic lights control with adaptive group formation based on swarm intelligence," *Ant Colony Optimization and Swarm Intelligence*, vol. 4150, pp. 520–521, 2006.

[117] T. Hu and L. Chen, "Traffic signal optimization with greedy randomized tabu search algorithm," *Journal of Transportation Engineering*, vol. 138, no. 8, pp. 1040–1050, 2012.

[118] Y. Li, J. Yang, X. Guo, and M. M. Abbas, "Urban traffic signal control network partitioning using self-organizing maps," *Transportation Research Board 90th Annual MeetingTransportation Research Board*, p. 20p, 2011.

[119] J. R. Kok and N. Vlassis, "Collaborative Multiagent Reinforcement Learning by Payoff Propagation," *The Journal of Machine Learning Research*, vol. 7, pp. 1789–1828, Dec. 2006.

[120] L. Kuyer, S. Whiteson, B. Bakker, and N. Vlassis, *Machine Learning and Knowledge Discovery in Databases*, ser. Lecture Notes in Computer Science, W. Daelemans, B. Goethals, and K. Morik, Eds. Berlin, Heidelberg: Springer Berlin Heidelberg, Sep. 2008, vol. 5211.

[121] M. Wainwright, T. Jaakkola, and A. Willsky, "Tree consistency and bounds on the performance of the max-product algorithm and its generalizations," *Statistics and Computing*, vol. 14, no. 2, pp. 143–166, Apr. 2004.

[122] J. C. Medina and R. F. Benekohal, "Traffic signal control using reinforcement learning and the max-plus algorithm as a coordinating strategy," pp. 596–601, 2012.

[123] S. Huang, A. W. Sadek, and Y. Zhao, "Assessing the mobility and environmental benefits of reservation-based intelligent intersections using an integrated simulator," *Intelligent Transportation Systems, IEEE Transactions on*, vol. PP, no. 99, pp. 1–14, 2012.

[124] J. Kwak, B. Park, and J. Lee, "Evaluating the impacts of urban corridor traffic signal optimization on vehicle emissions and fuel consumption," *Transportation Planning and Technology*, vol. 35, no. 2, pp. 145–160, 2012.

[125] C. M. Bishop, *Pattern Recognition and Machine Learning (Information Science and Statistics)*. Springer, 2007.

[126] R. S. Sutton and A. G. Barto, *Reinforcement learning: An introduction*. Cambridge Univ Press, 1998, vol. 1.

[127] A. Gosavi, *Simulation-Based Optimization: Parametric Optimization Techniques & Reinforcement Learning*. Springer, 2003.

[128] M. I. Jordan, "Graphical models," *Statistical Science*, vol. 19, no. 1, 2004.

[129] V. PTV America, "5.4 user manual," *PTV Vision*, 2012.

[130] EPA, "Motor vehicle emission simulator: User guide for moves2010b," *Environmental Protection Agency*, no. EPA-420-B-12-001b, June 2012.

[131] R. Wunderlich, I. Elhanany, and T. Urbanik, "A Novel Signal-Scheduling Algorithm With Quality-of-Service Provisioning for an Isolated Intersection," *IEEE Transactions on Intelligent Transportation Systems*, vol. 9, no. 3, pp. 536–547, Sep. 2008.

[132] B. Arem van, C. J. Driel van, and R. Visser, "The Impact of Cooperative Adaptive Cruise Control on Traffic-Flow Characteristics," *IEEE Transactions on Intelligent Transportation Systems*, vol. 7, no. 4, pp. 429–436, Dec. 2006.

[133] K. Dresner and P. Stone, "A multiagent approach to autonomous intersection management," *Journal of Artificial Intelligence Research*, vol. 31, no. 1, pp. 591–656, Jan. 2008.

[134] D. Fajardo, T.-C. Au, S. T. Waller, P. Stone, and D. Yang, "Automated Intersection Control," *Transportation Research Record: Journal of the Transportation Research Board*, vol. 2259, no. -1, pp. 223–232, Dec. 2011.

[135] C. Wuthishuwong and A. Traechtler, "Vehicle to infrastructure based safe trajectory planning for Autonomous Intersection Management," in *2013 13th International Conference on ITS Telecommunications (ITST)*. IEEE, Nov. 2013, pp. 175–180.

[136] M. Hausknecht, T.-C. Au, and P. Stone, "Autonomous Intersection Management: Multi-Intersection Optimization," *IEEE/RSJ International Conference on Intelligent Robots and Systems*, pp. 4581–4586, 2011.

[137] J. Lee and B. Park, "Development and Evaluation of a Cooperative Vehicle Intersection Control Algorithm Under the Connected Vehicles Environment," *IEEE Transactions on Intelligent Transportation Systems*, vol. 13, no. 1, pp. 81–90, Mar. 2012.

[138] J. Lee, B. B. Park, K. Malakorn, and J. J. So, "Sustainability assessments of cooperative vehicle intersection control at an urban corridor," *Transportation Research Part C: Emerging Technologies*, vol. 32, pp. 193–206, Jul. 2013.

[139] C. F. Daganzo, "The cell transmission model: A dynamic representation of highway traffic consistent with the hydrodynamic theory," *Transportation Research Part B: Methodological*, vol. 28, pp. 269–287, 1994.

[140] ——, "The cell transmission model, part II: Network traffic," *Transportation Research Part B: Methodological*, vol. 29, pp. 79–93, 1995.

[141] H. K. Lo and W. Szeto, "A cell-based variational inequality formulation of the dynamic user optimal assignment problem," *Transportation Research Part B: Methodological*, vol. 36, no. 5, pp. 421–443, Jun. 2002.

[142] W. Y. Szeto and H. K. Lo, "A cell-based simultaneous route and departure time choice model with elastic demand," *Transportation Research Part B-Methodological*, vol. 38, pp. 593–612, 2004.

[143] S. T. Waller and A. K. Ziliaskopoulos, "A Combinatorial user optimal dynamic traffic assignment algorithm," *Annals of Operations Research*, vol. 144, no. 1, pp. 249–261, May 2006.

[144] L. S. Han, S. Ukkusuri, and K. Doan, "Complementarity formulations for the cell transmission model based dynamic user equilibrium with departure time choice, elastic demand and user heterogeneity," *Transportation Research Part B-Methodological*, vol. 45, pp. 1749–1767, 2011.

[145] S. V. Ukkusuri, L. Han, and K. Doan, "Dynamic user equilibrium with a path based cell transmission model for general traffic networks," *Transportation Research Part B: Methodological*, vol. 46, no. 10, pp. 1657–1684, Dec. 2012.

[146] I. Yperman, C. M. J. Tampere, and B. Immers, "A Kinematic Wave Dynamic Network Loading Model Including Intersection Delays," in *Transportation Research Board 86th Annual Meeting*, 2007.

[147] F. Zhu and S. V. Ukkusuri, "Accounting for dynamic speed limit control in a stochastic traffic environment: A reinforcement learning approach," *Transportation Research Part C: Emerging Technologies*, vol. 41, pp. 30–47, Apr. 2014.

[148] W. Jin and H. Zhang, "On the distribution schemes for determining flows through a merge," *Transportation Research Part B: Methodological*, vol. 37, no. 6, pp. 521–540, Jul. 2003.

[149] M. C. J. Bliemer, "Dynamic Queuing and Spillback in Analytical Multiclass Dynamic Network Loading Model," *Transportation Research Record: Journal of the Transportation Research Board*, vol. 2029, no. 2029, pp. 14–21, 2007.

[150] T. L. Friesz, K. Han, P. A. Neto, A. Meimand, and T. Yao, "Dynamic user equilibrium based on a hydrodynamic model," *Transportation Research Part B: Methodological*, vol. 47, pp. 102–126, Jan. 2013.

[151] J. Lebacque and M. Khoshyaran, "First Order Macroscopic Traffic Flow Models for Networks in the Context of Dynamic Assignment," *Transportation Planning-Applied Optimization*, vol. 64, pp. 119–140, 2002.

[152] C. M. Tampère, R. Corthout, D. Cattrysse, and L. H. Immers, "A generic class of first order node models for dynamic macroscopic simulation of traffic flows," *Transportation Research Part B: Methodological*, vol. 45, no. 1, pp. 289–309, Jan. 2011.

[153] A. K. Ziliaskopoulos, "A Linear Programming Model for the Single Destination System Optimum Dynamic Traffic Assignment Problem," *Transportation Science*, vol. 34, no. 1, pp. 37–49, Feb. 2000.

[154] S. Peeta and A. Ziliaskopoulos, "Foundations of Dynamic Traffic Assignment: The Past, the Present and the Future," *Networks and Spatial Economics*, vol. 1, no. 3, pp. 233 – 265, 2001.

[155] Y. M. Nie, "A cell-based MerchantNemhauser model for the system optimum dynamic traffic assignment problem," *Transportation Research Part B: Methodological*, vol. 45, no. 2, pp. 329–342, Feb. 2011.

[156] J. K. Ho, "A Successive Linear Optimization Approach to the Dynamic Traffic Assignment Problem," *Transportation Science*, vol. 14, pp. 295–305, 1980.

[157] H. Zheng and Y. C. Chiu, "A Network Flow Algorithm for the Cell-Based Single-Destination System Optimal Dynamic Traffic Assignment Problem," *Transportation Science*, vol. 45, pp. 121–137, 2011.

[158] K. Doan and S. V. Ukkusuri, "On the holding-back problem in the cell transmission based dynamic traffic assignment models," *Transportation Research Part B*, vol. 46, no. 9, pp. 1218 – 1238, 2012.

[159] F. Zhu and S. V. Ukkusuri, "A cell based dynamic system optimum model with non-holding back flows," *Transportation Research Part C: Emerging Technologies*, vol. 36, pp. 367–380, Nov. 2013.

[160] W. H. Lin and C. H. Wang, "An enhanced 0-1 mixed-integer LP formulation for traffic signal control," *IEEE Transactions on Intelligent Transportation Systems*, vol. 5, no. 4, pp. 238–245, 2004.

[161] H. K. Lo, "A novel traffic signal control formulation," *Transportation Research Part A: Policy and Practice*, vol. 33, pp. 433–448, 1999.

[162] S. V. Ukkusuri, G. Ramadurai, and G. Patil, "A robust transportation signal control problem accounting for traffic dynamics," *Computers & Operations Research*, vol. 37, pp. 869–879, 2010.

[163] A. Schrijver, *Theory of Linear and Integer Programming.* John Wiley & Sons, 1998.

[164] J. Matousek and B. Gärtner, *Understanding and Using Linear Programming.* Springer, 2006.

[165] G. B. Dantzig and M. N. Thapa, *Linear Programming 2: Theory and Extensions.* Springer, 2003.

[166] D. K. Merchant and G. L. Nemhauser, "A model and an algorithm for the dynamic traffic assignment problems," *Transportation science*, vol. 12, no. 3, pp. 183–199, 1978.

[167] ——, "Optimality conditions for a dynamic traffic assignment model," *Transportation Science*, vol. 12, no. 3, pp. 200–207, 1978.

[168] M. Carey, "Optimal time-varying flows on congested networks," *Operations research*, vol. 35, no. 1, pp. 58–69, 1987.

[169] M. Carey and A. Srinivasan, "Externalities, average and marginal costs, and tolls on congested networks with time-varying flows," *Operations Research*, vol. 41, no. 1, pp. 217–231, 1993.

[170] M. Ghali and M. Smith, "A model for the dynamic system optimum traffic assignment problem," *Transportation Research Part B: Methodological*, vol. 29, no. 3, pp. 155–170, 1995.

[171] S. Peeta and H. S. Mahmassani, "System optimal and user equilibrium time-dependent traffic assignment in congested networks," *Annals of Operations Research*, vol. 60, no. 1, pp. 81–113, 1995.

[172] Z. S. Qian, W. Shen, and H. Zhang, "System-optimal dynamic traffic assignment with and without queue spillback: Its path-based formulation and solution via approximate path marginal cost," *Transportation research part B: methodological*, vol. 46, no. 7, pp. 874–893, 2012.

[173] K. Doan and S. V. Ukkusuri, "Dynamic system optimal model for multi-od traffic networks with an advanced spatial queuing model," *Transportation Research Part C: Emerging Technologies*, vol. 51, pp. 41–65, 2015.

[174] B.-W. Wie, T. L. Friesz, and R. L. Tobin, "Dynamic user optimal traffic assignment on congested multidestination networks," *Transportation Research Part B: Methodological*, vol. 24, no. 6, pp. 431–442, 1990.

[175] T. L. Friesz, D. Bernstein, T. E. Smith, R. L. Tobin, and B. Wie, "A variational inequality formulation of the dynamic network user equilibrium problem," *Operations Research*, vol. 41, no. 1, pp. 179–191, 1993.

[176] S. T. Waller and A. K. Ziliaskopoulos, "A combinatorial user optimal dynamic traffic assignment algorithm," *Annals of Operations Research*, vol. 144, no. 1, pp. 249–261, 2006.

[177] A. K. Ziliaskopoulos, "A linear programming model for the single destination system optimum dynamic traffic assignment problem," *Transportation Science*, vol. 34, no. 1, pp. 37–49, 2000.

[178] S. Peeta and A. K. Ziliaskopoulos, "Foundations of dynamic traffic assignment: The past, the present and the future," *Networks and Spatial Economics*, vol. 1, no. 3-4, pp. 233–265, 2001.

[179] Y. M. Nie, "A cell-based merchant–nemhauser model for the system optimum dynamic traffic assignment problem," *Transportation Research Part B: Methodological*, vol. 45, no. 2, pp. 329–342, 2011.

[180] J. K. Ho, "A successive linear optimization approach to the dynamic traffic assignment problem," *Transportation Science*, vol. 14, no. 4, pp. 295–305, 1980.

[181] F. Zhu and S. V. Ukkusuri, "A cell based dynamic system optimum model with non-holding back flows," *Transportation Research Part C: Emerging Technologies*, vol. 36, pp. 367–380, 2013.

[182] S. V. Ukkusuri and S. T. Waller, "Linear programming models for the user and system optimal dynamic network design problem: formulations, comparisons and extensions," *Networks and Spatial Economics*, vol. 8, no. 4, pp. 383–406, 2008.

[183] J. R. Correa, A. S. Schulz, and N. E. S. Moses, "Computational complexity, fairness, and the price of anarchy of the maximum latency problem," in *Proceedings of the 10th International Integer Programming and Combinatorial Optimization Conference*, vol. 3064, 2004, pp. 59–73.

[184] J. R. Correa, A. S. Schulz, and N. E. Stier-Moses, "Fast, fair, and efficient flows in networks," *Operations Research*, vol. 55, no. 2, pp. 215–225, 2007.

[185] O. Jahn, R. H. Möhring, A. S. Schulz, and N. E. Stier-Moses, "System-optimal routing of traffic flows with user constraints in networks with congestion," *Operations research*, vol. 53, no. 4, pp. 600–616, 2005.

[186] I. Yperman, "The link transmission model for dynamic network loading," *Open Access Publ. from Kathol. Univ. Leuven.*, 2007.

[187] S. Nguyen and C. Dupuis, "An efficient method for computing traffic equilibria in networks with asymmetric transportation costs," *Transportation Science*, vol. 18, no. 2, pp. 185–202, 1984.

[188] H. A. Simon, "Bounded rationality and organizational learning," *Organization science*, vol. 2, no. 1, pp. 125–134, 1991.

[189] W. Szeto, Y. Wang, and K. Han, "Bounded rationality in dynamic traffic assignment," *Bounded Rational Choice Behaviour: Applications in Transport*, p. 163, 2015.

VITA

VITA

Feng Zhu was born in Gaozhou, a beautiful town of southern China. He finished his Bachelor of Engineering degree at Sun Yat-sen University, China in 2009 (graduated summa cum laude). Later he received the degree of Master of Philosophy in Civil Engineering at Hong Kong University of Science and Technology in 2011. Feng Zhu joined the PhD program in Transportation Infrastructure Engineering in the Lyles School of Civil Engineering at Purdue University in Fall 2011 and received the PhD degree in August, 2016. He worked as a research assistant in the Interdisciplinary Transportation Modeling and Analytics Lab at Purdue. During the PhD study at Purdue, he has published over 16 peer-review journal and conference papers in the areas of sustainable transportation, connected vehicles, traffic control and optimization, big data analytics, and agent-based traffic simulations.